

**SELF-ASSEMBLED PEPTIDE GELS
FOR 3D CELL CULTURE**

A Thesis Submitted to the University of Manchester for the Degree of
Doctor of Philosophy
in the Faculty of Engineering and Physical Sciences

2010

CLAIRE TANG

SCHOOL OF MATERIALS

List of Contents

List of Figures	5
List of Tables	8
List of Abbreviations	9
Abstract	10
Declaration	11
Copyright	11
Dedication	12
The Author	13
Acknowledgement	14
CHAPTER 1 — INTRODUCTION	15
CHAPTER 2 — LITERATURE REVIEW	17
2.1. TISSUE ENGINEERING	17
2.1.1. Definition of Tissue Engineering	17
2.1.2. Extracellular Matrix	17
2.1.3. 2D Versus 3D Scaffolds	18
2.1.4. Scaffold Design	19
2.2. SELF-ASSEMBLY	20
2.2.1. Self-Assembly and Forces Involved	21
2.2.2. Self-Assembled Hydrogels	22
2.3. HYDROGELS FOR TISSUE ENGINEERING	23
2.3.1. Natural Polymers	23
2.3.2. Synthetic Polymers	24
2.3.3. <i>De Novo</i> Designed Peptides	25
2.3.3.1. <i>Peptides and Proteins</i>	25
2.3.3.2. <i>Cyclic Peptide Based Systems</i>	29
2.3.3.3. <i>α-Helices and Coiled-Coils Based Systems</i>	30
2.3.3.4. <i>β-Sheets and β-Hairpins Based Systems</i>	31
2.3.3.5. <i>Amphiphile Based Systems</i>	36
2.3.3.6. <i>Aromatic Interactions Based Systems</i>	37
2.4. SUMMARY AND OBJECTIVES	42
2.5. REFERENCES	44
CHAPTER 3 — MATERIALS AND METHODS	50
3.1. MATERIALS	50
3.1.1. Raw Materials	50
3.1.2. Sample Preparation	50
3.2. METHODS	51
3.2.1. Reverse Phase High Performance Liquid Chromatography	51
3.2.1.1. <i>Theory</i>	51

3.2.1.2. <i>Experimental Procedure</i>	52
3.2.2. Potentiometry	52
3.2.2.1. <i>Theory</i>	52
3.2.1.2. <i>Experimental Procedure</i>	54
3.2.1.3. <i>'Titration' Experiments</i>	54
3.2.3. Transmission Electron Microscopy	55
3.2.3.1. <i>Theory</i>	55
3.2.3.2. <i>Experimental procedure</i>	56
3.2.4. X-Ray Scattering	56
3.2.4.1. <i>Theory</i>	56
3.2.4.2. <i>Experimental Procedure</i>	59
3.2.5. Fourier Transform Infrared Spectroscopy	59
3.2.5.1. <i>Theory</i>	59
3.2.5.2. <i>Experimental Procedure</i>	61
3.2.6. Fluorescence Spectroscopy	62
3.2.6.1. <i>Theory</i>	62
3.2.6.2. <i>Experimental Procedure</i>	63
3.2.7. Rheology	64
3.2.7.1. <i>Theory</i>	64
3.2.7.2. <i>Experimental Procedure</i>	66
3.3. REFERENCES	67

CHAPTER 4 — SOLUTION BEHAVIOUR INVESTIGATION FOR THE DEVELOPMENT OF A CONTROLLED SAMPLE PREPARATION METHOD

METHOD	68
4.1. ABSTRACT	68
4.2. INTRODUCTION AND OBJECTIVES	68
4.3. RESULTS AND DISCUSSION	69
4.3.1. Preliminary Study: Sequential pH Change Method	69
4.3.2. Towards a Controlled Sample Preparation Method	72
4.3.2.1. <i>Sodium Hydroxide and Fmoc Loss</i>	72
4.3.2.2. <i>Solution Behaviour</i>	73
4.3.2.3. <i>Optimised Sequential pH Change Method for Gel Formation</i>	79
4.4. CONCLUSION	81
4.5. REFERENCES	82

CHAPTER 5 — EFFECT OF HYDROPHOBIC AROMATIC MOIETIES ON THE SELF-ASSEMBLY OF FMOC-DIPEPTIDES

5.1. ABSTRACT	83
5.2. INTRODUCTION AND OBJECTIVES	83
5.3. RESULTS AND DISCUSSION	84
5.3.1. Fmoc-FF	84
5.3.1.1. <i>Proposed Molecular Model</i>	84

5.3.1.2. <i>pH Study</i>	87
5.3.1.3. <i>Concentration Study</i>	94
5.3.1.4. <i>Summary</i>	96
5.3.2. Fluorescent Molecular Behaviour	97
5.3.3. Fmoc-FG	100
5.3.3.1. <i>pH Study</i>	100
5.3.3.2. <i>Temperature Study at pH ~ 4.5</i>	104
5.3.4. Fmoc-GG pH study	106
5.3.5. Fmoc-GF pH study	109
5.3.6. Summary	111
5.4. CONCLUSION	113
5.5. REFERENCES	114

CHAPTER 6 — EFFECT OF HYDROPHOBIC ALKYL CHAINS IN THE SELF-ASSEMBLY OF FMOC-DIPEPTIDES 116

6.1. ABSTRACT	116
6.2. INTRODUCTION AND OBJECTIVES	116
6.3. RESULTS AND DISCUSSION	117
6.3.1. Solution Behaviour	117
6.3.2. Fluorescent Molecular Behaviour	121
6.3.3. Fmoc-LL pH study	124
6.3.4. Fmoc-LG	128
6.3.4.1. <i>pH Study</i>	128
6.3.4.2. <i>Temperature Study at pH ~ 4.7</i>	131
6.3.5. Fmoc-GL pH study	133
6.3.6. Summary	135
6.4. CONCLUSION	136
6.5. REFERENCES	137

CHAPTER 7 — CONCLUSIONS AND FUTURE WORK 138

7.1. CONCLUSIONS	138
7.2. FUTURE WORK	140

APPENDICES 141

APPENDIX A: HPLC Chromatograms of Commercial Fmoc-Dipeptides	141
APPENDIX B: Dynamic Amplitude Sweeps of Fmoc-Dipeptide Hydrogels	143
APPENDIX C: FT-IR Spectra of Thin Films of Fmoc-FF	144
APPENDIX D: FT-IR Spectra of Commercial Fmoc-Dipeptides	144
APPENDIX E: Fluorescence Spectra of Fmoc-Dipeptides	146
APPENDIX F: AFM Micrographs of Fmoc-GF	147

List of Figures

2.1. General structure of an amino acid at physiological pH	25
2.2. Amid bond formation between two amino acids at physiological pH	27
2.3. Schematic representations of a α -helix, a parallel β -sheet and an antiparallel β -sheet	27
2.4. Ionic equilibrium reactions of an amino acid in aqueous solution depending on the pH	28
2.5. Cyclic D,L- α -octapeptide self-assembling into a tubular structure and schematic representation of the antimicrobial activity of the peptides within a lipid bilayer	29
2.6. Schematic representation of a coiled-coil fibre and a helical wheel of coiled-coil with heptad repeats showing interhelical interactions	30
2.7. Formation of higher order intermolecular β -sheet structures from the self-assembly of chiral rod-like molecules	33
2.8. Schematic representation of peptides folding into β -hairpins in response to an external stimulus and subsequent self-assembly of the structures into fibrillar hydrogels	35
2.9. Schematic representation of peptide amphiphiles self-assembling into a cylindrical micelle and a nanotube or a nanovesicle	37
2.10. Molecular structures and schematic representations of a Nap-peptide involved in an enzymatic dephosphorylation and phosphorylation and of Fmoc-amino acids and dipeptides forming tripeptides, which self-assemble into hydrogels	40
3.1. Schematic representation of a combination pH electrode	53
3.2. Schematic representation of an electron microscope	56
3.3. Schematic representation of X-rays scattering according to Bragg's law	58
3.4. Schematic representation of a multiple bounce ATR-FTIR crystal-sample setup	61
3.5. Simplified version of the Jablonski diagram	62
3.6. Layout of the different components of a typical fluorescence spectrometer	63
3.7. Schematic representation of shear stress applied on a material	64
3.8. Wave-forms for oscillatory stress input and strain output for a viscoelastic material	65
4.1. Equilibrium between Fmoc-dipeptide neutral (acid) and ionised (conjugated base) forms and notation	68
4.2. Macroscopic appearance of Fmoc-dipeptide hydrogels and precipitate formed by sequential pH change	69
4.3. Dynamic frequency sweep of Fmoc-dipeptides hydrogels formed by sequential pH change and schematic representation of fibrillar networks	70
4.4. Cleavage of the Fmoc group from an Fmoc-dipeptide	72
4.5. HPLC chromatogram of a diluted solution of Fmoc-FF at pH 10.5 as a function of time	72

4.6. 'Titration' curves (pH vs. moles of added HCl) of water, Fmoc-FF, Fmoc-FG, Fmoc-GG and Fmoc-GF samples	74
4.7. n_{HCl} vs. $n_{Fmoc-FF}$ for samples at different pH values	76
4.8. n_{HCl} vs. $n_{Fmoc-dipeptide-COOH}$ for Fmoc-FG, Fmoc-GG and Fmoc-GF	78
4.9. Transition pH values versus concentration of the Fmoc-dipeptides and transition pH values versus Log P values of the Fmoc-dipeptides	78
4.10. Macroscopic appearance of Fmoc-dipeptides hydrogels and precipitate formed by the optimised sequential pH change	80
4.11. Storage modulus of Fmoc-FF, Fmoc-FG and Fmoc-GG and WAXS spectrum of Fmoc FF hydrogels prepared using the optimised and the previously reported method	80
5.1. Proposed model structure of Fmoc-FF	85
5.2. WAXS spectra of Fmoc-FF at pH ~ 7.5	86
5.3. Schematic representation of cylinders in a lamellar and a hexagonal packing	86
5.4. FT-IR spectra of Fmoc-FF	88
5.5. TEM micrographs of Fmoc-FF	88
5.6. Cross sections of the fibril previously described and schematic representation of a view down the length of a fibre	90
5.7. WAXS spectra of Fmoc-FF	91
5.8. Dynamic frequency sweep of Fmoc-FF	92
5.9. Proposed self-assembly mechanism of Fmoc-FF	92
5.10. FT-IR spectra and TEM micrographs of Fmoc-FF at 5 mmol L ⁻¹	95
5.11. Dynamic frequency sweep of Fmoc-FF hydrogels at 5 mmol L ⁻¹	96
5.12. Normalised fluorescence emission spectra of Fmoc-FF, Fmoc-FG, Fmoc-GG and Fmoc-GF	97
5.13. Red shift of the excimer peak with respect to the monomer peak as a function of pH for Fmoc-FF, Fmoc-FG, Fmoc-GG and Fmoc-GF	98
5.14. Schematic representation of Fmoc-dipeptides π -stacking in a parallel and an antiparallel manner	99
5.15. TEM micrographs of Fmoc-FG	101
5.16. FT-IR spectra of Fmoc-FG	101
5.17. Dynamic frequency sweep of Fmoc-FG	102
5.18. WAXS spectra of Fmoc-FG	103
5.19. Dynamic temperature sweep of Fmoc-FG	105
5.20. TEM micrograph and FT-IR spectrum of non-heated Fmoc-FG	106
5.21. TEM micrographs of Fmoc-GG	106
5.22. FT-IR spectra of Fmoc-GG	107
5.23. Dynamic frequency sweep of Fmoc-GG	107
5.24. WAXS spectra of Fmoc-GG	108

5.25. TEM micrographs of Fmoc-GG hydrogel precipitating slowly after one week	109
5.26. TEM micrographs of Fmoc-GF	109
5.27. FT-IR spectra of Fmoc-GF	110
5.28. WAXS spectra of Fmoc-GF	110
6.1. Equilibrium between Fmoc-dipeptide neutral (acid) and ionised (conjugated base) forms and notation	117
6.2. ‘Titration’ curves (pH vs. moles of added HCl) of water, Fmoc-LL, Fmoc-LG and Fmoc-GL	118
6.3. n_{HCl} vs. $n_{Fmoc-dipeptide-COOH}$ for Fmoc-LL, Fmoc-LG and Fmoc-GL	120
6.4. Transition pH values versus concentration of the Fmoc-dipeptides studied and transition pH values versus Log P values of the Fmoc-dipeptides	121
6.5. Normalised fluorescence emission spectra of Fmoc-LL, Fmoc-LG and Fmoc-GL ..	122
6.6. Red shift of the excimer peak with respect to the monomer peak as a function of pH for Fmoc-LL, Fmoc-LG and Fmoc-GL	123
6.7. FT-IR spectra of Fmoc-LL	125
6.8. TEM micrographs of Fmoc-LL	125
6.9. WAXS spectra of Fmoc-LL	126
6.10. Dynamic frequency sweep of Fmoc-LL	126
6.11. TEM micrographs of Fmoc-LG	128
6.12. FT-IR spectra of Fmoc-LG	129
6.13. WAXS spectra of Fmoc-LG	129
6.14. Dynamic frequency sweep of Fmoc-LG	130
6.15. Dynamic temperature sweep of Fmoc-LG	132
6.16. TEM micrograph and FT-IR spectrum of non-heated Fmoc-LG	133
6.17. TEM micrographs of Fmoc-GL	133
6.18. FT-IR spectra of Fmoc-GL	134
6.19. WAXS spectra of Fmoc-GL	134

List of Tables

2.1. Strength of different non-covalent forces	22
2.2. Properties and conventions associated with standard amino acids	26
2.3. Peptide names and sequences used by Zhang <i>et al.</i>	32
2.4. Peptide names and sequences used by Boden <i>et al.</i>	34
2.5. Peptide names and sequences used by Pochan <i>et al.</i>	36
2.6. Peptide amphiphile names and sequences used by Zhang <i>et al.</i>	37
2.7. Peptide sequences used by the groups of Xu and Ulijn and their pH conditions	41
3.1. Molecular weight, mass and weight percentage corresponding to Fmoc-dipeptide 2 mL samples at 10 mmol L ⁻¹ , and typical heating times	50
3.2. Typical volume of NaOH needed to bring the pH of the solution to 10.5 depending on the concentration of Fmoc-dipeptide	55
3.3. Amide I frequency values generally associated to some secondary structures in water and deuterated water	60
7.1. Summary of the main characteristics of the studied Fmoc-dipeptides	139

List of Abbreviations

This list is not exhaustive. A complete index of amino acids abbreviations is provided in Chapter 2.

2D	Two-dimensional
3D	Three-dimensional
ADP	Adenosine diphosphate
AFM	Atomic force microscopy
ATP	Adenosine triphosphate
ATR	Attenuated total reflectance
Cbz	Benzyloxycarbonyl
CD	Circular dichroism
<i>E</i>	Tensile modulus
ECM	Extracellular matrix
Fmoc	9-fluorenylmethoxycarbonyl
FT	Fourier transform
<i>G</i>	Shear modulus
GAG	Glycosaminoglycan
HCl	Hydrochloric acid
HPLC	High performance liquid chromatography
IR	Infrared
LCST	Lower critical solution temperature
NaOH	Sodium hydroxide
Nap	Naphthalene
PEG	Poly(ethylene glycol)
PHEMA	poly(hydroxyethyl methacrylate)
PNIPAAm	poly(<i>N</i> -isopropylacrylamide)
TEM	Transmission electron microscopy
TFA	Trifluoroacetic acid
UV	Ultraviolet
WAXS	Wide angle X-ray scattering

Abstract

Under specific conditions short peptides modified with an N-terminal fluorenyl-9-methoxycarbonyl (Fmoc) group can self-assemble into hydrogel scaffolds similar in properties to the natural extracellular matrix. Fmoc-diphenylalanine (Fmoc-FF) for instance, has been shown to form hydrogels at physiological pH that have the ability to support 2D and 3D cell culture. The aim of this investigation is to provide further understanding of the self-assembly mechanism of such systems in order to progress towards the establishment of design rules for the preparation of scaffolds with tuneable properties.

First, Fmoc-dipeptides composed of a combination of hydrophobic aromatic residues phenylalanine (F) and glycine (G) were studied with a particular emphasis on the effect of pH variations. The systems were investigated in order to assess what influence the position of such residues in the peptide sequence had on the physical properties of the molecules, and what impact the chemical structure had on the self-assembly behaviour and the gelation properties of the materials. Subsequently, phenylalanine was replaced by leucine (L), a non-aromatic amino acid that had the same relative hydrophobicity in order to determine whether the self-assembly of such molecules is driven by aromatic interactions or hydrophobic effects.

Using potentiometry, the behaviour of the systems in solution has been investigated, revealing that they were all characterised by pK_a shifts of up to six units above the theoretical values. Fmoc-FF exhibited two transitions whereas the other Fmoc-dipeptides only displayed one. These transitions were found to coincide with the formation of distinct self-assembled structures with differing molecular conformations and properties that were characterised using transmission electron microscopy, infrared and fluorescence spectroscopy, X-ray scattering and shear rheometry.

π -stacking of the aromatic moieties was thought to be the driving force of the self-assembly mechanism, generating dimers that corresponded to the building blocks of the supramolecular structures formed. On the other hand, the peptide components were stabilised via hydrogen bonding and could form antiparallel β -sheets depending on the amino acid sequence and the associated influence on the rigidity of the molecules. Below their (first) apparent pK_a transition, Fmoc-FF, Fmoc-LL, Fmoc-FG, Fmoc-LG and Fmoc-GG formed hydrogels, with the mechanical properties and stability varying depending on the amino acid sequence. Fmoc-FF and Fmoc-LL exhibited the lowest storage modulus values ($G' \sim 0.5\text{--}5$ Pa) of the studied systems while Fmoc-LG displayed the highest ($G' \sim 1000\text{--}2100$ Pa). Fmoc-FG and Fmoc-LG had the peculiarity of being obtained upon heating and were found to be particularly stable, as opposed to Fmoc-GG gels which showed a tendency to crystallise. On the microscopic scale, these gels were all associated with the presence of entangled fibrillar networks of different size and morphology, which in some cases could self-assemble further through a lamellar organisation. Again, Fmoc-FG and Fmoc-LG distinguished from the other systems as they were the only Fmoc-dipeptides to show a supramolecular chirality in the form of twisted ribbons under specific pH conditions. In contrast, Fmoc-GF and Fmoc-GL did not form hydrogels below their apparent pK_a due to the formation of sheet-like and spherical structures respectively.

Keywords: self-assembly; dipeptide; hydrogel; nanostructures; design; tuneable properties.

Declaration

No portion of the work referred to in the thesis has been submitted in support of an application for another degree or qualification of this or any other university or other institute of learning.

Copyright

The author of this thesis (including any appendices and/or schedules to this thesis) owns certain copyright or related rights in it (the “Copyright”) and she has given The University of Manchester certain rights to use such Copyright, including for administrative purposes.

Copies of this thesis, either in full or in extracts and whether in hard or electronic copy, may be made **only** in accordance with the Copyright, Designs and Patents Act 1988 (as amended) and regulations issued under it or, where appropriate, in accordance with licensing agreements which the University has from time to time. This page must form part of any such copies made.

The ownership of certain Copyright, patents, designs, trade marks and other intellectual property (the “Intellectual Property”) and any reproductions of copyright works in the thesis, for example graphs and tables (“Reproductions”), which may be described in this thesis, may not be owned by the author and may be owned by third parties. Such Intellectual Property and Reproductions cannot and must not be made available for use without the prior written permission of the owner(s) of the relevant Intellectual Property and/or Reproductions.

Further information on the conditions under which disclosure, publication and commercialisation of this thesis, the Copyright and any Intellectual Property and/or Reproductions described in it may take place is available in the University IP Policy (see <http://www.campus.manchester.ac.uk/medialibrary/policies/intellectual-property.pdf>), in any relevant Thesis restriction declarations deposited in the University Library, The University Library’s regulations (see <http://www.manchester.ac.uk/library/aboutus/regulations>) and in The University’s policy on presentation of Theses.

A mes parents,

The Author

Academic training

2006–2010 Ph.D. in Materials Science, the University of Manchester

2004–2006 MSc. (Hons.) in Chemistry, Université Bordeaux 1

2000–2004 BSc. in Biology and Biochemistry, Université Bordeaux 1

Publications

Tang, C., Ulijn, R.V., and Saiani, A. *Effect of glycine substitution on Fmoc-diphenylalanine self-assembly mechanism*. In preparation.

Tang, C., Smith, A.M., Collins, R.F., Ulijn, R.V., and Saiani, A. *Fmoc-diphenylalanine self-assembly mechanism induces apparent pK_a shifts*. *Langmuir*, **2009**, 25 (16), 9447-9453.

Smith, A.M., Williams, R.J., **Tang, C.**, Coppo, P., Collins, R.F., Turner, M.L., Saiani, A., Ulijn, R.V. *Fmoc-diphenylalanine self-assembles to a hydrogel via a novel architecture based on π - π interlocked β -sheets*. *Advanced Materials*, **2008**, 20 (1), 37-41.

Conference oral presentations

Self-assembly mechanism of short aromatic peptide derivatives in nanostructured hydrogels. Materials Research Society Fall Meeting, Boston, Massachusetts, USA, December 2008.

Rheological and structural characterisation of nanostructured hydrogels from aromatic short peptide derivatives. World Biomaterials Congress, Amsterdam, The Netherlands, May 2008.

Acknowledgement

First I would like to express my gratitude towards both of my supervisors Alberto Saiani, for his time and enthusiasm, and Rein Ulijn for entrusting me with this project. I thank them both for the precious advice they gave me during my PhD. I appreciate the opportunity they offered me to attend conferences and the freedom they allowed me to conduct my research. I am thankful to Ian Hamley and Ian Kinloch for agreeing to act as my examiners. Also I gratefully acknowledge EPSRC for funding this project.

I would like to thank Richard Collins, Polly Crook, Nigel Hodson and Judith Shackleton for their assistance with TEM, FT-IR spectroscopy, AFM and WAXS respectively. I also wish to thank post-docs of the groups for their advice and practical support: Laurent Caron, Apurba Das, Andrew Hirst, Rob Mart, Majeed Shaik, Andrew Smith and Elisabeth Vey.

To my colleagues and friends, past and present members of the Ulijn Group, Polymer & Peptide Group, Webb Group, MIB, E13 office and the Materials Chemists, thank you for helping me to settle in Manchester and your daily contribution to such a nice work environment during these last four years.

Last but not least, I thank my family, my parents and sister in particular for their continuous support throughout my studies. Thanks to my friends in France, Laurence and Vanessa in particular, for being with me in their thoughts. Finally, I would like to thank Martyn for his patience, for being present and for helping me with my English in this manuscript.

— Chapter 1 —

Introduction

Living systems are established around hierarchically organised structures with well defined properties. Most of these supramolecular structures result from the non-covalent association and specific recognition of diverse biomolecules such as proteins, nucleic acids and polysaccharides, which correspond to polymers of amino acids, nucleotides and monosaccharides respectively. Despite the variety of random combinations that could theoretically result from the association of these initial monomers, only a few sequences lead to functional macromolecules. Rules governing the linking of these units into complex particular structures must exist; however unravelling them remains a challenge.

Cells are the structural and functional units of living organisms. Like the biomolecules they produce and interact with, cells take part of a hierarchical organisation and form the complex structures of tissues and organs. Most living organisms are constituted of many different types of cells capable of generating diverse structures with specific functions when subjected to the appropriate environmental conditions.

Inspired by these organised and structured examples, scientific researchers have chosen to mimic Nature to produce nanoscale objects and devices. Significant progress has been made in the last decade and designed nanomaterials with particular properties can now fulfil specific applications in biotechnology (tissue engineering, 3D cell culture, biosensing) and nanotechnology (electronics, templating). By virtue of the diversity of their constitutive amino acids, peptides are often the building blocks of choice and have hence been extensively exploited. Such systems have the ability to spontaneously self-assemble into organised structures by either utilising structural motifs that naturally occur in proteins such as α -helices and β -sheets or exploiting covalently linked ligands such as alkyl chains or aromatic moieties.

A relatively new class of hydrogel scaffolds formed from the self-assembly of short peptides modified with aromatic moieties has recently been developed. The aromatic groups play a key role in the self-assembly process through π - π interactions, while the peptide components are stabilised via hydrogen bonding.

The first part of this thesis is devoted to the fabrication of three-dimensional soft scaffolds with tailored properties for tissue engineering applications. A number of different approaches reported in the literature to achieve this aim will then be reviewed with a careful attention to the design features chosen and the stimulus applied to trigger self-assembly and subsequent gelation of the peptide systems.

In Chapter 4, we will focus on a class of short aromatic peptide derivatives – dipeptides possessing an N-terminal fluorenyl-9-methoxycarbonyl group – with a particular focus on the effect of pH variations. Our effort will be concentrated on how reliable and reproducible materials can be methodically prepared.

The peptide derivatives presented in Chapter 5 are constituted of aromatic amino acids. We will assess what influence the position of such amino acid in the peptide sequence has on the physical properties of the molecules, and what impact the chemical structure has on the self-assembly behaviour and the gelation properties of the systems. The effect of such variation on the supramolecular structures generated will be investigated under pH control. The molecular architecture of the self-assemblies will be probed, in particular the arrangement of the peptide components and the interactions between the aromatic groups. The microstructure of the self-assembled objects will be observed and the dynamic mechanical properties of the resulting materials will be assessed.

In order to determine whether aromatic interaction or hydrophobic effect dictate the self-assembly of such materials, in Chapter 6 the aromatic side chains will be replaced by alkyl chains having the same relative hydrophobicity. Investigation of the systems at the molecular, microscopic and macroscopic levels will be undertaken using the same methodology. As a result of this analysis, design rules will be proposed.

— Chapter 2 —

Literature Review

2.1. TISSUE ENGINEERING

2.1.1. Definition of Tissue Engineering

Tissue engineering is a discipline that focuses on tissue and organ replacement, repair and regeneration using engineering and biological principles [1,2]. The process consists of isolating specific cells (differentiated or undifferentiated i.e. stem cells) from biopsies of patients and making the tissue grow either *in vitro* or *in vivo* in order to form tailor-made tissues with appropriate size and shape [3,4].

Use of isolated cells or tissue-inducing substances to replace defective cells or promote tissue growth respectively are strategies which are generally considered for small and well contained damages [5]. A less restrictive approach lies in the use of artificial scaffolds mimicking the natural environment (the extracellular matrix) for tissue growth to guide cells and facilitate the formation of functional tissues.

Tissue engineering can also be used for non-clinical applications. In this case, cells are cultured *in vitro* in a three-dimensional environment (for more details, see Section 2.1.3) in order to produce multicellular structures, which can subsequently be employed for drug development and testing, or simply exploited for fundamental cell studies [4].

2.1.2. Extracellular Matrix

In vivo, cells secrete macromolecules such as proteins and carbohydrates that organise, and make up a complex network called the extracellular matrix (ECM). This matrix surrounds the cells and acts as a supporting scaffold as it bears most the environmental mechanical stress that tissues are subjected to [6].

The matrix composition varies depending on the type and functional requirements of each tissue. Nevertheless the ECM is mainly composed of proteoglycans and polysaccharide chains of the glycosaminoglycan (GAG) class that form a gel-like substance which provides resistance and mechanical support to tissues [6]. Two types of fibrous proteins are embedded in this polysaccharide gel: the first has a structural role (e.g. collagen or elastin),

whereas the second has an adhesive function and promotes the attachment of cells to the matrix (e.g. fibronectin or laminin).

Collagen is a major extracellular fibrous protein. Numerous types of collagen fibres exist but all consist of three polypeptide chains, which coil around each other to make up a triple helix – a characteristic structural feature of collagen. As a result this supramolecular structure provides tensile strength to the matrix [7]. Collagen molecules typically self-assemble into bundles of 50 to 500 nm diameter [8].

The surface of cells is typically decorated with different classes of receptors including integrins. In addition to convey information between cells and their environment (essential to direct cell traffic and differentiation), these adhesion receptors provide specific attachment points between cells and, when interacting with surrounding fibrous proteins, with the ECM to ensure the anchorage of the cells to the matrix [7,9]. Binding of integrins to the ECM molecules (i.e. cell attachment to the matrix) is made through recognition sequences. Arg-Gly-Asp (RGD), a common motif present in many of the extracellular proteins, was the first to be identified [4]. Small variations on the tripeptide such as the addition of a methyl in the amino acid side chains (leading to sequences like Arg-Ala-Asp or Arg-Gly-Glu) were found to eliminate the action of the motif, showing the importance that the exactitude of this key sequence has upon interaction between cells and the ECM [9].

In other words, the ECM is not only used as a scaffold to stabilise the physical structure of tissues but also plays a role in cell migration, proliferation, functionalisation and regulation. Since the ECM matrix is porous, it enables cell migration and the diffusion of various elements essential to their development like nutrients, metabolites, hormones, growth factors and oxygen [6].

2.1.3. 2D Versus 3D Scaffolds

Although within tissues, cells naturally grow in a three-dimensional (3D) environment, *in vitro* cell culture is commonly carried out in two-dimensional (2D) systems such as culture dishes, multi-well plates or glass slides coated with substrates. Use of these methods implies that cells are being mixed into culture media and seeded on top of the prefabricated scaffolds. As a result, cells are cultured onto the surface of the support. In 3D cell culture, introduction of cell suspensions into culture media is part of the scaffold preparation process. Suspended cells can be mixed with liquid hydrogel precursors for instance. Cells

are therefore integrated into the mixture during gelation and surrounded by the scaffold after its formation [10].

As they offer more realistic conditions for cell culture, 3D scaffolds are more appropriate ECM mimics than 2D supports in guiding cells to form functional tissues. In such biomaterials, cells do not need to adapt to an unnatural environment, which reduces stress and subsequent alteration of cell metabolism, gene expression or production of extracellular matrix proteins [11]. Importantly, 3D materials also allow diffusion of solute molecules from the aqueous medium through the network, which is necessary to cell development.

2.1.4. Scaffold Design

Ideal multi-purpose scaffolds are difficult to design since each tissue requires a specific matrix with defined characteristics. However besides being biocompatible, materials used in tissue engineering applications must conform to at least certain biochemical and physical criteria.

The general **architecture** of the material must comply with the nanoscale dimensions of natural ECM in order to respect the local microenvironment surrounding cells and allow realistic interaction with the matrix. Compared to microscale scaffolds, the dimensions of which are similar to those of cells and causes their flattening and spreading as if cultured on a plane surface, nanoscale substrates enable cell adhesion within a 3D structure [12]. The scaffold **surface** should be easily modified with cell adhesion ligands and also large enough in order to enhance initial cell attachment and subsequent proliferation, migration and differentiation [5].

High **porosity** and adequate pore size are essential to allow transport of oxygen and nutrients and removal of metabolic waste to and from the cell without risking pore occlusion [13]. On the other hand, pore radii should be restricted to the micron scale in order to limit the diffusion rate of biomolecules [11]. Pore size also depends on the type of tissue to regenerate. Use of scaffolds with pore size of 20 to 125 μm have been reported for adult mammalian skin regeneration for instance while larger pore size ranging from 45 to 150 μm and 200 to 500 μm have been employed to support bone and liver tissue formation respectively [14].

The material must present suitable **mechanical strength** to resist environmental stresses and maintain sufficient structural integrity until its degradation allows the replacement

tissue to complete its formation. In addition to the support provided for cell growth, scaffolds also influence differentiation of the stem cells depending on their mechanical properties. For instance, human mesenchymal stem cells were found to differentiate into distinct cell types by modulating the elasticity* of the material used. Neurone-like lineages were obtained with relatively soft ($E' \sim 1$ kPa) matrices, muscle lineages with moderate ($E' \sim 10$ kPa) matrices and bone lineages with rigid ($E' \sim 100$ kPa) matrices [15].

Biodegradability, preferably in physiological conditions and at a controlled rate, is generally required in order to avoid material-induced inflammation reaction or immune response from the host body. It can either be completed by hydrolysis, dissolution or upon enzymatic action, and should give rise to innocuous by-products [3].

Different technologies have been developed in order to mimic the ECM, particularly the nanofibrous and porous aspect of the collagen matrix, its main component. In order to routinely produce such type of scaffold three techniques have proven to be relatively efficient: electrospinning, phase separation and self-assembly [12,16,17]. Nanofibres with various diameters lying within the ECM collagen range were generated depending on the method used. Under specific conditions, phase separation methods enabled the production of fibres with diameters similar to natural ECM collagen [18,19], whereas electrospinning led to the formation of fibres with larger diameter (ranging from nanometres to a few micrometres) [17,20,21]. Thinner fibrils (typically less than 10 nm) were obtained by self-assembly although these commonly aggregate into bundles of fibres [22]. All of these techniques allow design of fibrillar networks with suitable dimensions, however they each present limitations as for the production of 3D scaffolds. Lack of control on the internal pore size and use of toxic solvents constitute some of the major issues to be addressed. Self-assembly can be conducted in aqueous solvents, which is a particular advantage in order to avoid organic solvent residues in the final scaffold. Here we will therefore focus on this approach, which has received considerable attention in biomaterials research during the past ten years.

2.2. SELF-ASSEMBLY

Self-assembly is an autonomous process that naturally occurs in nature to create ordered and functional molecular architectures from un- or less ordered building blocks (bottom-up approach). The structures generated by self-assembly are usually in an equilibrium or

* The elasticity referred to here corresponds to the tensile elastic modulus E' . Although the values cannot be directly compared to the shear elastic modulus G' (values reported in the results chapters), it gives an indication of the material's strength.

metastable state. This spontaneous phenomenon is based on the balance between different types of attractive and repulsive non-covalent or weak covalent forces, which are created between neighbouring molecules (intermolecular interactions) and within molecules (intramolecular interactions) [23,24].

2.2.1. Self-Assembly and Forces Involved

Hydrogen bonds form between hydrogen donors (hydrogen covalently linked to electronegative atoms such as oxygen or nitrogen) and hydrogen acceptors or electronegative atoms. Hydrogen bonding is a directional force, which perfect geometry implies the alignment of the three atoms involved in it (i.e. the hydrogen and the two electronegative atoms which share it), resulting in the formation of a strong bond [7]. In organic systems and in peptides in particular hydrogen bonds commonly involve nitrogen and oxygen atoms. In this case the donor and the acceptor are typically $\sim 3 \text{ \AA}$ apart.

Electrostatic interactions occur between polar charged groups. Opposite and same charges attract and repel each other respectively. Attractive electrostatic interactions are also directional as their axes lead from the positive to the negative charge. Such forces can be particularly strong in vacuum (Table 2.1), however their strength can be reduced by up to two orders of magnitude in polar media [25]. The presence of salts in solution is also known to weaken electrostatic interactions as salt molecules act as counter-ions screening the charges of the compounds [6].

In solution molecules tend to gather according to their affinity to the solvent. Hence in a polar solvent, **hydrophobic interactions** occur between groups such as hydrocarbon chains and aromatic moieties in order to minimize their contact with the polar environment. This type of interaction is less geometrically constrained.

Aromatic **π - π interactions** arise from the attraction of π -electron clouds present on the surfaces of aromatic groups, enabling them to stack on top of each other. Due to the arrangement of the aromatic moieties this type of interaction is directional. In a face-to-face arrangement centroids of aromatic groups are $\sim 3.5 \text{ \AA}$ apart on average [26].

Van der Waals forces are created in a non-directional manner between two atoms that are in close proximity. The electron cloud surrounding them creates temporary electric dipoles, resulting in the attraction of the two nuclei [7]. However, this attraction is limited as two atoms will repel each other when the distance between them equals the sum of their Van der Waals radii. The Van der Waals radii of hydrogen, carbon, nitrogen and oxygen (the

most common atoms present in organic systems) are 1.2, 2.0, 1.5 and 1.4 Å respectively [6].

Any of the above-mentioned forces, or combinations thereof, can drive the self-assembly process. In comparison to covalent bonds (100–400 kJ mol⁻¹) these forces are weak (Table 2.1), however when acting cooperatively they can generate stable supramolecular assemblies.

Table 2.1. Strength of different non-covalent forces [26].

Type of non-covalent force	Strength / kJ mol ⁻¹
Hydrogen bonding	10–65
Electrostatic	250
Hydrophobic	not applicable
π - π	0–50
Van der Waals	<5

Self-assembly allows structures to be built with micro- and nanometre dimensions. Such architectures are of particular interest because of their potential use in a versatile range of applications, including microelectronics, photonics, nanosciences and nanotechnology (nanotubes, nanowires, colloids, sensors). In addition to the development of these applications, self-assembly is crucial for fundamentally understanding biological structures and processes, as well as designing their non-biological mimics [23].

2.2.2. Self-Assembled Hydrogels

Self-assembled fibrillar networks can often trap molecules of solvent in a three-dimensional manner to form gels. This phenomenon is displayed at the macroscopic scale by a system that does not flow when the container is inverted. When the solvent is water, gels are referred to as hydrogels. Hydrogels have high water content as they can absorb up to thousands of times their own dry weight in water. Since it is a metastable state of precipitate, a gel is in equilibrium and can be stable but may also dissolve or precipitate.

Most gels are based on polymeric gelators. Two categories can be distinguished: reversible/physical gels and permanent/chemical gels. **Physical gels** bring into play weak forces such as hydrogen bonds, Van der Waals, hydrophobic and ionic interactions (see Section 2.2.1.) that are reversible and sensitive to environmental physico-chemical changes. In this type of gel, fibres are entangled and can create heterogeneities. **Chemical gels** arise from covalent crosslinking. These gels are therefore irreversible. These links

cannot be dispersed unless the system is entirely degraded. In this case again, gels may not be totally homogeneous as the crosslink density can vary within the sample [13].

2.3. HYDROGELS FOR TISSUE ENGINEERING

As discussed in Section 2.2.2, hydrogels are often regarded as mimics of the cell's natural environment due to their high water content [27]. Hence they are of particular interest for their potential applications in tissue engineering and *in vitro* 3D cell culture [13].

In the last twenty years, two categories of biomaterials have been developed to assist 3D tissue regeneration: synthetic and natural-derivative polymers. In both cases, bioactive molecules can be covalently attached to the substrates in order to induce their degradability or to enhance cell adhesion to the scaffolds [28]. This section presents the most commonly used polymer hydrogels in tissue engineering.

2.3.1. Natural Polymers

Natural polymers such as proteins and polysaccharides have been extensively used in tissue engineering. In addition to their biocompatibility and enzyme-mediated degradability they can generate suitable nanofibre networks for 3D cell culture.

Collagen for instance, a major constituent of the ECM of mammalian tissues, is widely available from the purification of animal tissue collagen. The physical structure of such scaffold can be controlled and tailored to specific cell culture applications. Some studies suggested that varying the polymer concentration could lead to fibrillar networks with different pore radii [29]. Collagen has been successfully employed for tissue regeneration, including reconstruction of liver, skin, blood vessel and small intestine tissues [3], yet due to its origins, collagen can potentially cause pathogen transmission or immune reactions [5]. Denaturation of collagen using thermal or alkaline processes generates gelatine. Due to its ease of gelation, gelatine is an interesting polymer for tissue engineering and has proven to be efficient in tissue repair [30]. However collagen and gelatine gels are weak and often require chemical modifications to improve their mechanical properties [30,31].

Hyaluronate is one of the main glycosaminoglycans found in natural extracellular matrices. Large quantities of hyaluronate can be produced by microbial fermentation, which reduces the risk of animal-derived pathogen transmission. Gels of this anionic polysaccharide are typically characterised by low mechanical properties, however their viscosity can be tuned by chemically altering the polymer structure (e.g. esterification) in order to obtain the

required properties [32]. Hyaluronate hydrogels have found applications in wound healing, artificial skin generation and soft tissue augmentation [3]. Alternatively, marine algal polysaccharides such as alginate or agarose can be used to produce scaffold materials as these polymers present low toxicity due to their origin.

Natural polymer hydrogels have been widely used for tissue engineering approaches. However they present weak mechanical properties in many cases and can contain residual amounts of growth factors or impurities, which is a problem for their use in human tissue regeneration applications [11]. These restrictions have among others motivated the use of synthetic polymers.

2.3.2. Synthetic Polymers

Since they can be produced with tailored properties (e.g. appropriate gelation kinetics or mechanical strength) and offer control over their structural characteristics (e.g. cross-linking density), synthetic polymers constitute attractive materials for tissue engineering.

Poly(ethylene glycol) (PEG) is one of the most commonly used synthetic polymers for tissue engineering approaches. PEG chains can be cross-linked by photopolymerisation allowing the formation of polymeric scaffolds in the presence of cells [33]. However use of cross-linking agents results in toxicity concerns [5]. On the other hand, the main advantage of this polymer is its non-immunogenicity since it is known to be inert to most biomolecules, including proteins [2]. The surface of the scaffold can be chemically modified with specific ligands in order to enhance cell adhesion [34] or induce degradation of the polymer [35] for example. Use of PEG-based hydrogels has been reported to be successful for cartilaginous tissue regeneration [36].

Hydrogels of poly(acrylic acid) and its derivatives are another family of synthetic polymers that has been extensively studied for tissue engineering. One of the most widely used is poly(hydroxyethyl methacrylate) (PHEMA), which has found applications in contact lenses and drug delivery [2,3]. PHEMA hydrogels do not degrade in physiological conditions, however like PEG, the scaffold surface can be chemically altered in order to introduce degradation sites. Another example is poly(*N*-isopropylacrylamide) (PNIPAAm). This polymer is characterised by a lower critical solution temperature (LCST) located around body temperature ($\sim 31^{\circ}\text{C}$ in aqueous solutions) above which the polymeric solution undergoes a reversible phase transition associated to the precipitation or the gelation of the polymer [37]. To modulate the temperature responsiveness of the polymer (e.g. to body temperature) PNIPAAm is usually copolymerised, making it an attractive

candidate for *in vivo* applications. However the use of PNIPAAm is limited by the carcinogenic nature of its monomer – the residues of which could be problematic for tissue engineering approaches – as well as the toxicity of the cross-linkers typically utilised to reduce the polymer solubility in water at low temperature [37]. Neuronal and cartilaginous tissue regeneration has been reported using PHEMA and PNIPAAm derivatives respectively [38,39].

Despite the versatility of copolymers and cross-linkers available to tune their characteristics to the required properties, some synthetic polymers remain potentially harmful for tissue engineering applications. Components involved in the production of these materials can indeed be toxic in some cases, making hydrogels prepared from not entirely pure polymers inadequate for such applications.

Polypeptides constitute a compromise between natural and synthetic polymers. This class of biomaterials can be generated synthetically to mimic the behaviour of natural proteins and may lead to hydrogel formation. The following section reviews examples of peptide-based self-assembling systems designed to create nanostructured architectures with potential applications in tissue engineering.

2.3.3. *De Novo* Designed Peptides

This section will begin with a brief definition of peptides and proteins. Different examples from the literature describing peptides designed to generate homogeneous, reproducible fibrous networks in a controlled manner will then be outlined.

2.3.3.1. *Peptides and Proteins*

Proteins and (poly)peptides are molecules composed of linear sequences of amino acids covalently linked with one another. With exception of proline, all amino acids have a common structural feature (Figure 2.1): they all contain both an amino and a carboxylic function, fixed on one carbon atom, so-called α -carbon (C_α). However, they all differ from each other by the nature of their lateral residue (R), which is also attached on the α -carbon.

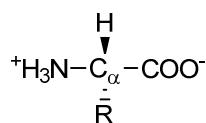
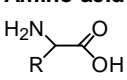
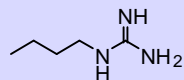
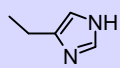
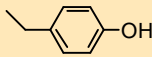
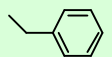
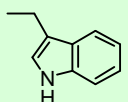
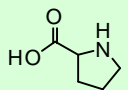


Figure 2.1. General structure of an amino acid at physiological pH.

Table 2.2 shows the 20 standard naturally occurring amino acids. Depending on the nature of the lateral residue, they can either be nonpolar, uncharged polar or ionisable polar. Most

are chiral and L-enantiomers, however there are exceptions: glycine and cysteine. The former is non-chiral as its residue is a hydrogen atom, while the latter is a D-enantiomer because of the priority of the sulphur atom over the nitrogen atom according to Cahn Ingold-Prelog rule [7].

Table 2.2. Properties and conventions associated with standard amino acids. Negatively charged, positively charged, uncharged polar and nonpolar residues are represented in red, blue, yellow and green respectively (adapted from [7,40]). In the case of proline, the molecule represented here is the full amino acid as there is no side chain as the amine function is included in a cycle of five atoms.

Amino acid 	Code	Side chain R	Side chain hydrophobicity	pK ₁ (-COOH)	pK ₂ (-NH ₃ ⁺)	pK _R (R group)	pI
Aspartate	Asp (D)	-CH ₂ -COOH	-55	1.88	9.60	3.65	2.77
Glutamate	Glu (E)	-(CH ₂) ₂ -COOH	-31	2.19	9.67	4.25	3.22
Lysine	Lys (K)	-(CH ₂) ₄ -NH ₂	-23	2.18	8.95	10.53	9.74
Arginine	Arg (R)		-14	2.17	9.04	12.48	10.76
Histidine	His (H)		8	1.82	9.17	6.00	7.59
Asparagine	Asn (N)	-CH ₂ -CO-NH ₂	-28	2.02	8.80	-	5.41
Glutamine	Gln (Q)	-(CH ₂) ₂ -CO-NH ₂	-10	2.17	9.13	-	5.65
Serine	Ser (S)	-CH ₂ -OH	-5	2.21	9.15	-	5.68
Threonine	Thr (T)	-CH(CH ₃)-OH	13	2.11	9.62	-	5.87
Tyrosine	Tyr (Y)		63	2.20	9.11	10.07	5.66
Glycine	Gly (G)	-H	0	2.34	9.60	-	5.97
Alanine	Ala (A)	-CH ₃	41	2.34	9.69	-	6.01
Valine	Val (V)	-CH(CH ₃) ₂	76	2.32	9.62	-	5.97
Leucine	Leu (L)	-CH ₂ -CH(CH ₃) ₂	97	2.36	9.60	-	5.98
Isoleucine	Ile (I)	-CH(CH ₃)-CH ₂ -CH ₃	99	2.36	9.68	-	6.02
Phenylalanine	Phe (F)		100	1.83	9.13	-	5.48
Tryptophan	Trp (W)		97	2.38	9.39	-	5.89
Methionine	Met (M)	-(CH ₂) ₂ -S-CH ₃	74	2.28	9.21	-	5.74
Cysteine	Cys (C)	-CH ₂ -SH	49	1.96	10.28	8.18	5.07
Proline	Pro (P)		-28	1.99	10.96	-	6.48

As depicted in Figure 2.2 the peptide bonds or amide links connecting amino acids arise from the condensation of the carboxyl function of one amino acid and the amino function of another. The sequence so obtained is called **primary structure** [7]. Except in the case of proline, for which the C_α-N bond is included into the pyrrolidine cycle, peptide bonds are planar and in the *trans* configuration in proteins. This configuration is energetically

favourable as steric interactions between groups attached to α -carbon are low. Rotations are possible around the C_{α} -N and C_{α} -C bonds, enabling the peptide backbone to adopt different spatial orientations. In order to adapt to their environment proteins self-fold to acquire particular conformations that are closely linked to their function. Several structure levels can be distinguished within proteins [7].

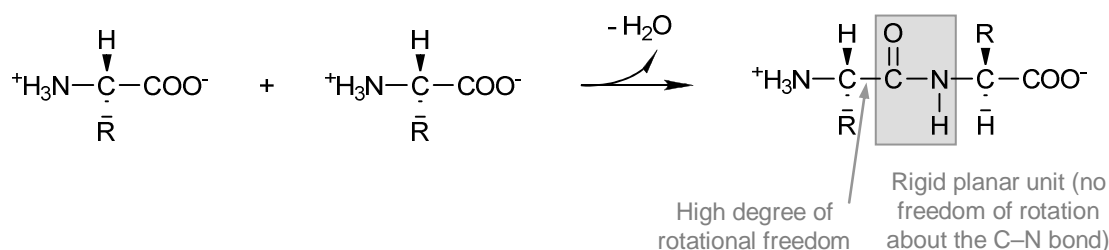


Figure 2.2. Amid bond formation between two amino acids at physiological pH (adapted from [6]).

Secondary structure designate the regular conformation stabilised by non-covalent hydrogen bonds found in some local parts of the peptide backbone. This feature leads to the formation of particular structural elements, the most common of which are α -helices and β -sheets. α -helices are characterised by a repeat unit (or turn) of 5.2 Å composed of 3.6 amino acids (Figure 2.3). Although left and right-handed helices exist, L-amino acids tend to favour right-handed helices. Parallel and antiparallel β -sheets are constituted of peptide strands pointing in the same or in opposite directions respectively. These structures generally result from the folding of the molecules to shelter hydrophobic residues from the aqueous environment. α -helices and β -sheets are commonly connected together with links such as β -turns.

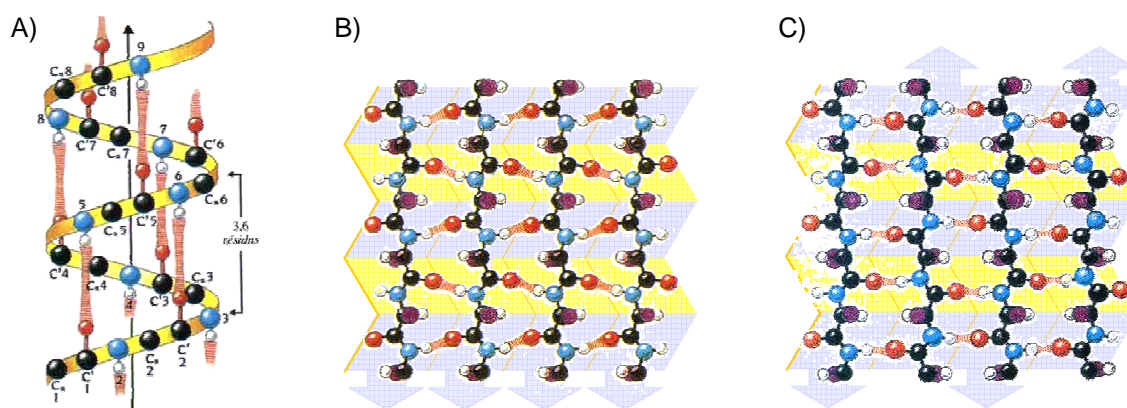


Figure 2.3. Schematic representations of **A)** a α -helix, **B)** a parallel β -sheet and **C)** an antiparallel β -sheet. Oxygen atoms are represented in red, nitrogens in blue, hydrogens of the NH groups in white and C_{α} in black. Hydrogen bonds between oxygens and nitrogens are in red and streaked. Amino acid lateral chains are symbolised by purple spheres (adapted from [6]).

Tertiary structure refers to the three-dimensional arrangement of the whole protein; it is stabilised through ionic bonds and hydrophobic interactions. **Quaternary structure** corresponds to the assembly of several protein sub-units into oligomers.

Amino acids do not have the same propensity to form α -helices, β -sheets, β -turns or loops. Alanine, leucine, methionine and glutamic acid for instance are often found in α -helices whereas valine, isoleucine, tyrosine, lysine, tryptophan and phenylalanine are more often found in β -sheets. Due to the structural particularity of proline mentioned above, rotation is not possible around the C_{α} -N bond. Thus, proline favours β -turn formation. Owing to the small size of its lateral chain, which induces conformational flexibility, glycine is also commonly present in β -turns [7]. It can however be difficult to foresee the type of secondary structure a peptides and proteins can adopt only from their primary structure.

As they comprise a weak amino group and a weak carboxylic acid group, amino acids are not totally ionised when dissolved into water. Depending on the pH of the environment these two functions can either be protonated or deprotonated. Amino acids are therefore distinguished by a particular pH condition, the isoelectric point (pI), at which their net electric charge (i.e. the sum of all the individual charges) is zero. As illustrated in Figure 2.4, both the amino and carboxyl functions are characterised by a pH, noted pK_a , at which each group is half protonated.

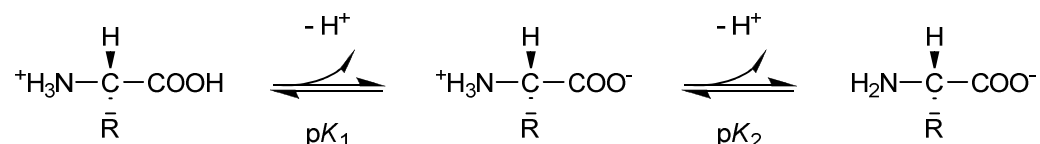


Figure 2.4. Ionic equilibrium reactions of an amino acid in aqueous solution depending on the pH (adapted from [7]).

The pK_a is defined as a function of the dissociation constant K_a :

$$pK_a = -\log_{10} K_a \quad \text{Equation 2.1}$$

Due to the range of amino acids available and the distinct physical properties associated with them, a variety of self-assembling peptides with specific characteristics can be created. Different types of forces can be exploited in the process: non-covalent interactions as described in Section 2.2.1 as well as covalent bonds in the form of disulphide bridge between cystein residues for example. By mimicking biological systems, specially designed peptides can be used as molecular building blocks in order to fabricate nanoscale supramolecular structures with well defined properties.

Relatively short peptides that spontaneously self-assemble into supramolecular structures, in particular fibrillar architectures, through intermolecular interactions have been investigated by many researchers. The advantage of these systems is that they are generally quick and relatively cheap to synthesise chemically. Peptide-based biomaterials are sensitive to their environment thus different parameters can be exploited to trigger gelation such as varying concentration and temperature, changing pH, applying UV radiation or using enzyme-responsive materials.

2.3.3.2. Cyclic Peptide Based Systems

Ghadiri and co-workers pioneered the engineering of peptide system designed to create nanotube structures [41]. By exploiting the chirality of amino acids and alternating L- and D-enantiomers, cyclic peptides with varied diameters were generated (Figure 2.5 A) [42].

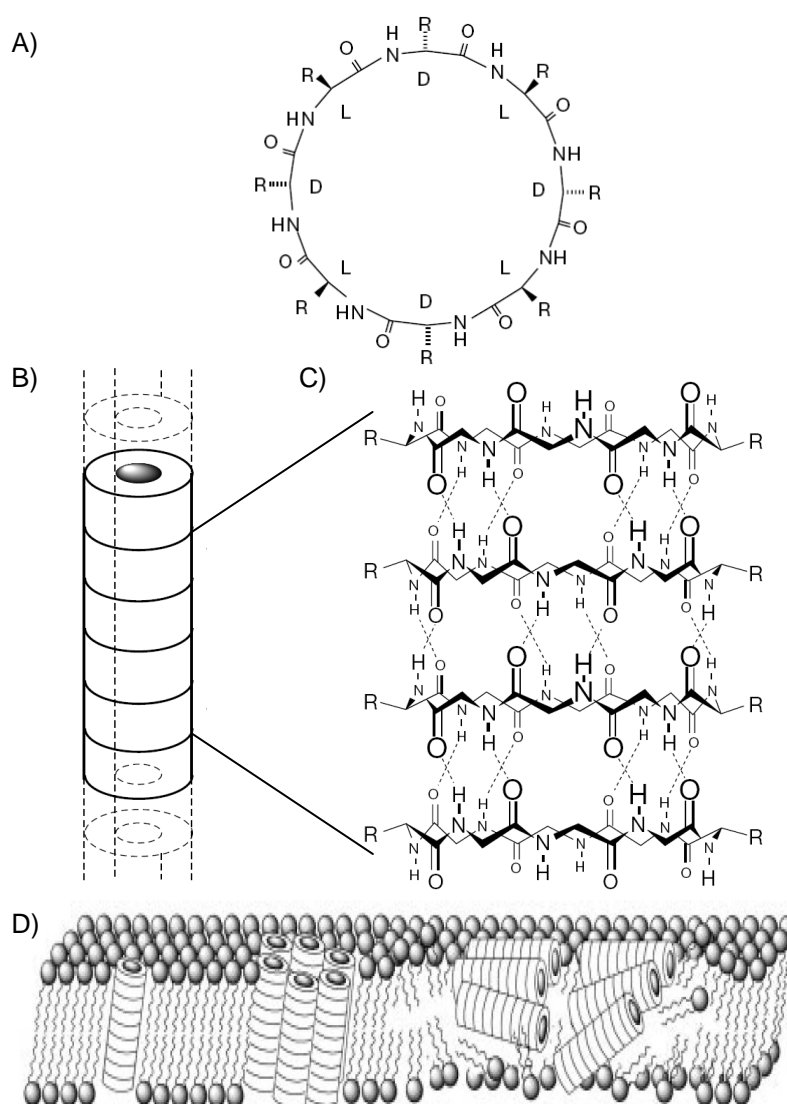


Figure 2.5. A) General structure of a cyclic *D,L*- α -octapeptide. B) Diagrammatic representation of the cyclic peptide self-assembly into a tubular structure. C) Antiparallel β -sheet-like arrangement of the peptide with hydrogen bonding in dotted lines. D) Schematic representation of the antimicrobial activity of the peptides within a lipid bilayer (adapted from [43]).

The circular molecules were first dissolved in alkaline conditions. Self-assembly was triggered by controlled acidification of the solutions to remove the electrostatic repulsion created between the carboxylate groups of the glutamic acid side chains. Hydrogen bond formation occurred between the monomers in a β -sheet like manner, leading to their stacking into nanotubes (Figure 2.5 B & C). The particular design of these peptides resulted in the amino acid side chains pointing outwards from the tubes, perpendicular to their long axis. Surface properties of the structures can therefore be simply modulated using different amino acids. A versatile range of cyclic peptide sequences with antibacterial properties has been reported in the literature (Figure 2.5 D) [43].

2.3.3.3. α -Helices and Coiled-Coils Based Systems

A coiled-coil is a quaternary structure made of two or more α -helices that twist around each other. The interhelical interactions involve a heptad motif (*abcdefg*) consisting of seven hydrophobic and polar amino acids, which is periodically repeated along each peptide. These residues are located at key positions so that they can laterally associate to form a pair (Figure 2.6). Because the amino acids involved in the inter-helix hydrophobic interactions are usually leucine repeats, these sequences are also called leucine zipper.

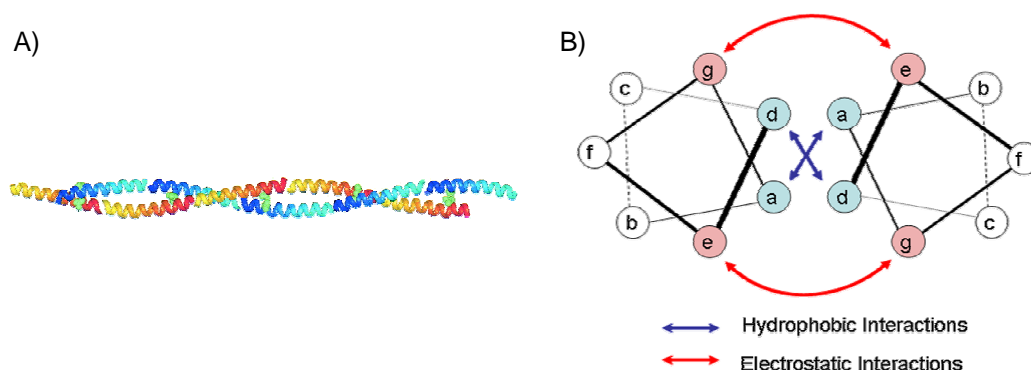


Figure 2.6. Schematic representation of **A)** a coiled-coil fibre and **(B)** a helical wheel of coiled-coil with heptad repeats showing interhelical interactions (adapted from [44]).

Woolfson and co-workers tailored a system constituted of a pair of 28 amino acid linear peptides in which two hydrophobic amino acids (isoleucine and leucine) positioned in *a* and *d* of each heptad interacted with each other to form a hydrophobic core whereas two complementary polar residues (glutamic acid and lysine) positioned in *e* and *g* of the repeated motif electrostatically interact to stabilise the core. The peptide sequences were designed to generate staggered pairs resulting in complementary overhanging ends, which further self-assembled to promote the longitudinal extension of the structure. Nanosized fibres were formed in pH 7 buffer, but were found to be sensitive to the ionic strength of the media. Presence of salts screened the charges of the polar residues involved in the ionic

interactions stabilising the assembly, which led to the unfolding of the fibres [44]. Since negatively charged aspartic acids were present at *b* sites of the heptamer, arginine residues were incorporated at specific *c* positions of the peptide in order to satisfy intermolecular salt bridges between opposite charges located on adjacent coiled-coil fibrils. As a result, the fibrillar structure was stabilised and fibre thickening promoted [45]. Although the fibrous network was found to be more robust at near-ambient and body temperatures as well as tolerant to salt, use of these materials for biomedical applications was limited by the non-gelling behaviour of the system, the fibres settling out of solution instead of trapping it. Positions *b*, *c* and *f* were subsequently replaced by a combination of alanine and tryptophan in order to promote hydrophobic interactions between fibrils. Stable hydrogels were consequently formed and were shown to support cell growth and differentiation [46].

Tirrell *et al.* also developed a system based on coiled coils. The molecules studied were small proteins made of two terminal leucine zipper domains flanking a polar segment with no defined supramolecular structure. The role of this linker, mainly composed of glutamic acid, was to provide high water solubility to the molecules. The material was characterised by gel dissolution in alkaline pH conditions and high temperature. Varying pH or temperature could hence trigger reversible gelation. Interestingly, the gels were found to be stable at around neutral pH and body temperature, ascribing the system potential utility for bioengineering purposes [47].

2.3.3.4. β -Sheets and β -Hairpins Based Systems

β -sheet structures are known to be involved in the fibrillisation and subsequent aggregation of amyloid proteins implicated in neurodegenerative diseases such as Alzheimer's and Parkinson's [48]. A common feature of β -strands is their composition of alternating hydrophilic and hydrophobic amino acids. Their self-assembly into sheets hence results in the formation of hydrophilic and hydrophobic surfaces in aqueous solutions. Further self-assembly can ensue depending on the affinity of the surfaces formed.

The first *de novo* peptide capable of self-assembly into nanofibrous scaffolds for tissue engineering purposes was designed by Zhang and co-workers [49]. This 16 amino acid peptide (Table 2.3, entry 1) was inspired from a sequence found in a yeast protein. Comprised of a repeated motif (EAK) made of an alternation of cationic, hydrophobic and anionic amino acid residues, it was shown to form stable β -sheets in physiological conditions. Once folded, these structures displayed hydrophobic surfaces of alanine

residues and polar surfaces with charged ionic side chains (from glutamic acid and lysine amino acids). Along with the usual hydrogen bonding, self-assembly of the peptides into β -sheets was facilitated by the complementarity of the β -strand polar surfaces [50]. Based on the same design, an analogous peptide has been developed. Negatively charged glutamic acids and positively charged lysines were replaced by arginines and aspartic acids respectively, resulting in a RAD repeated motif, in which the charge orientation was reversed (Table 2.3, entry 2) [51]. Both EAK16-II and RAD16-II formed particularly stable fibrous matrices consisting of interwoven filaments in salt solutions that were shown to support mammalian cell attachment [51]. Additionally, use of RAD16-II scaffolds, whose repeated motif presents similarity with the RGD recognition tripeptide, was reported to promote neurite outgrowth [52]. Systematic variations such as the nature of the side-chains, peptide length and charge distribution were also carried out on the repetitive segments. Increasing the relative hydrophobicity of the sequence using different residues such as in KFE12, KIE12 and KVE12 (Table 2.3, entries 3–5) was found to lower the critical concentration of salt needed for the systems to self-assemble, showing that intermolecular hydrophobic interaction was the driving force of the process. Elongating the peptides favoured the hydrophobic attraction between molecules too, however it also contributed to modify the entropy of the system, resulting in competitive effects for larger molecules as these would be subjected to more disorder, unfavourable to molecular self-assembly [53].

Table 2.3. Peptide names and sequences used by Zhang *et al.* The abbreviation used here for acetyl is Ac.

Entry	Peptide name	Peptide sequence	Ref.
1	EAK16-II	Ac-AEAEAKAKAEAEAKAK-NH ₂	[49,50]
2	RAD16-II	Ac-RARADADARARADADA-NH ₂	[51,52]
3	KFE12	Ac-FKFEFKFEFKFE-NH ₂	[53]
4	KIE12	Ac- IKIEIKIEIKIE -NH ₂	[53]
5	KVE12	Ac-VKVEVKVEVKVE-NH ₂	[53]

The effect of peptide concentration on self-assembly has also been investigated. Boden and co-workers have designed a series of undecapeptides capable of self-assembling into β -sheet tapes. The intrinsic chirality of the constitutive amino acids was exploited to generate twisted supramolecular structures. The molecules were shown to self-assemble hierarchically as a function of the peptide concentration, progressively revealing structures with distinct morphologies. Chiral rod-like units first associated into helical tapes through recognition of complementary groups located on each face of the molecules. Twisted

ribbons, fibrils and finally fibres were then formed by stacking of each intermediate type of supramolecular structure (Figure 2.7) [54].

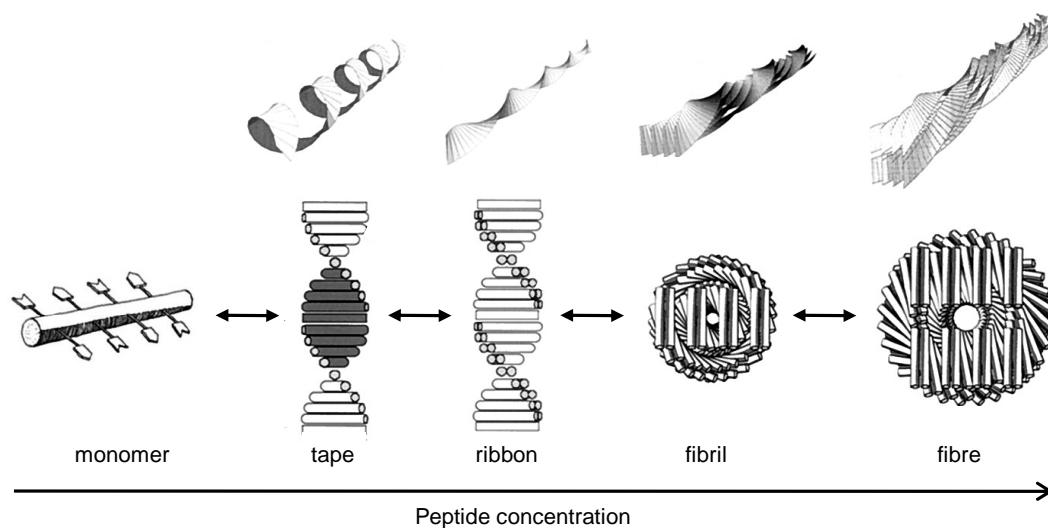


Figure 2.7. Formation of higher order intermolecular β -sheet structures from the self-assembly of chiral rod-like molecules. Each unit possesses distinct faces, which are represented in black and white (adapted from [54]).

Self-assembly of the systems was triggered by varying the pH, resulting in the formation of viscoelastic solutions of flexible tapes and ribbons at low concentrations or gelation of semi-rigid fibrils and fibres at higher concentrations. This series of peptides was mainly based on the use of glutamine amino acids, the side chains of which favoured intermolecular hydrophobic interactions in water and promoted hydrogen bonding between the antiparallel β -strands, as shown by FT-IR. A few hydrophobic residues (tryptophan and phenylalanine) were also incorporated at key positions in order to enhance molecular attraction [55]. In addition to this basic composition, P₁₁₋₂ (Table 2.4, entry 1) contained a cationic arginine residue and an anionic glutamic acid residue. For pH values between the apparent pK_a of the arginine and glutamic acid side chains (i.e. at $5 < \text{pH} < 10$, where both residues were charged, resulting in an electrically neutral peptide) the fibrils were found to flocculate, which rendered the hydrogel unstable. Below the apparent pK_a of the glutamic acid side chain (low pH) gels were formed, suggesting that one net positive charge per peptide (due to the arginine residue) was essential to disperse the fibrils and hence stabilise the network. Additional glutamic acid residues were introduced in P₁₁₋₄ (Table 2.4, entry 2) [56]. Following the previous reasoning, hydrogels were formed at low pH. At higher pH, negative charges appeared due to the deprotonation of the glutamic acids. Dissociation of the self-assembly was therefore caused by electrostatic repulsions occurring between neighbouring peptides. Hydrogels could reform by simple addition of hydrochloric acid and redissolved with sodium chloride. This process was reversible up to

a certain ionic strength, above which the samples did not respond to any further addition of acid or base and started to precipitate. The converse behaviour was observed with P₁₁₋₅ (Table 2.4, entry 3), a peptide rich in ornithine residues, which are cationic nonstandard amino acids [56]. Using the same method P₁₁₋₅ was designed to form solutions at low pH and hydrogels under basic conditions. Interestingly, equimolar mixture of P₁₁₋₄ and P₁₁₋₅ resulted in hydrogel formation under both acidic and alkaline conditions [57]. Subsequent modifications on the peptide sequence led to the formation of material which have found applications as injectable lubricants for osteoarthritis [58].

Table 2.4. Peptide names and sequences used by Boden et al. The abbreviation used here for ornithine is Or.

Entry	Peptide name	Peptide sequence	Ref.
1	P ₁₁₋₂	CH ₃ CO-QQRFQWQFEQQ-NH ₂	[55,56]
2	P ₁₁₋₄	CH ₃ CO-QQRFWEFEQQ-NH ₂	[56,57]
3	P ₁₁₋₅	CH ₃ CO-QQOrForWOrFQQQ-NH ₂	[56,57]

Pochan and Schneider also developed a series of pH sensitive 20-residue peptides, designed to self-assemble into β -hairpin based scaffolds in appropriate conditions. This variant of the β -sheet structure consists of two short β -strands linked together by a few turn inducing residues (V^DPPT). As mentioned in Section 2.3.3.1, proline is often involved in such turns due to its particular chemical structure, as it can induce a kink in the backbone of the peptide. As well as exploiting the properties of proline, the authors have introduced a D-enantiomer of the amino acid in the turn sequence, giving a more marked kink. Like in the β -sheet based systems described above, the rest of the peptides were mainly composed of alternating hydrophobic and hydrophilic residues (respectively valine and lysine). Under neutral and acidic conditions the lysine side chains were positively charged, hence electrostatic repulsion occurred between the residues, preventing MAX1 (Table 2.5, entry 1) from folding into β -hairpins, therefore suppressing hydrogel formation [59]. In contrast, gelation was triggered upon alkalisation of the solution to pH 9 or following ionic strength increase with sodium chloride or cell culture media (containing mono- and divalent inorganic salts) at physiological pH. Both methods resulted in the screening of the positive charges on the lysine residues so that MAX1 could fold into β -hairpins [60]. Intermolecular hydrogen bonds and hydrophobic interactions were subsequently formed between neighbouring β -hairpins, generating an organised nanostructure (Figure 2.8) characterised by hydrogel formation on the macroscale, as confirmed by oscillatory rheology. Interestingly, altering the net charge of the molecules by substituting hydrophilic residues enabled the authors to tune the pH responsiveness of the self-assembly process at

a given temperature. Each lysine of the peptide sequence was sequentially replaced by a glutamic acid residue, resulting in the reduction of the molecule's electropositive charge. Consequently, gelation could be triggered at lower pH, the values of which were found to be dependent on the position of the amino acid substituted in the sequence [61]. At physiological pH, incorporation of cells within the peptide scaffold was found to be successful in the presence of cell culture media, showing the potential of such a material as a cell delivery device for *in vivo* applications. However to avoid being spread into surrounding tissues, liquid systems should thicken quickly after their introduction in the target tissue. Gelation kinetics is therefore a crucial parameter that had to be controlled. By replacing a lysine by a glutamic acid residue the gelation was found to be accelerated. The resulting MAX8 (Table 2.5, entry 2) was shown to form mechanically rigid gels, capable of recovering their initial stiffness following a shear stress (performed in an injection syringe) within a few minutes [62]. Another approach consisted of increasing the peptide concentration as the rate of self-assembly was found to be concentration-dependent [59].

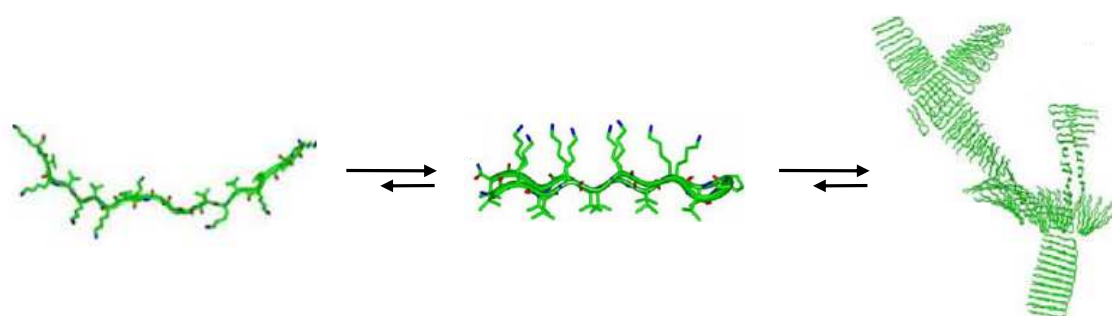


Figure 2.8. Schematic representation of peptides folding into β -hairpins in response to an external stimulus and subsequent self-assembly of the structures into fibrillar hydrogels (adapted from [60]).

MAX3 (Table 2.5, entry 3), another derivative of this series of peptides was developed as a thermally responsive material. Since more hydrophobic molecules tend to self-assemble at lower temperature, two valine amino acids of the MAX1 peptide sequence were replaced by threonine residues, the structure of which is similar to that of valine however it is less hydrophobic. The peptide was designed to be soluble at low temperature; upon heating the hydrophobic moieties dehydrated, triggering self-assembly and gel formation via hydrophobic collapse. As a result, MAX3 hydrogels were obtained at higher temperature than MAX1 hydrogels [63].

Light has also been used as a self-assembly trigger. MAX7CNB (Table 2.5, entry 4) resulted from the modification of the basic linear peptide sequence described above with a photo-cleavable group, which introduced electrostatic repulsion between the molecules [64]. Once exposed to UV radiation, this moiety was cleaved, enabling the

peptide to fold into a β -hairpin structure. As for the other peptides, intermolecular hydrogen bonding and hydrophobic interactions then led to the self-assembly of the molecules into hydrogel networks.

Table 2.5. Peptide names and sequences used by Pochan et al. X corresponds to a cystein residue capped with an α -carboxy-2-nitrobenzyl.

Entry	Peptide name	Peptide sequence	Ref.
1	MAX1	VKVKVKVKV ^D PPTKVKVKVKV-NH ₂	[59-61]
2	MAX8	VKVKVKVKV ^D PPTKVEVKVKV-NH ₂	[62]
3	MAX3	VKVKVTKV ^D PPTKVKTKVKV-NH ₂	[63]
4	MAX7CNB	VKVKVTKV ^D PPTKVKXKVKV-NH ₂	[64]

2.3.3.5. Amphiphile Based Systems

Peptide amphiphiles are typically constituted of a polar peptide head and an apolar tail linked together by electrostatic interactions [65] or by an amide bond [66]. Such molecules have the tendency to aggregate in aqueous solutions in order to minimise unfavourable interactions with their environment. The hydrophilic components are exposed while the apolar tails shield within the structure through hydrophobic interactions, which is exploited as the driving force of the self-assembly process. Amphiphilic peptide molecules can generally self-assemble into extremely diverse morphologies (micelles, sheets, rods, etc.) depending on the charge distribution, the shape of the monomers and on physico-chemical parameters, including concentration and ionic strength.

Stupp and co-workers developed a particular class of compounds in which long alkyl chains (10 to 22 carbons) were used as hydrophobic tails and peptides containing 6 to 12 amino acids as the hydrophilic heads. The molecules were found to self-assemble in water into fibrous networks, giving rise to self-supporting gels. The alkyl chains were buried in the centre of the rod-like structures, forming a hydrophobic core whereas the peptides arranged in β -sheets were located outwards, exposing peptide recognition motifs such as RGD or IKVAV (known to promote neurite growth) on the surface [67,68] (Figure 2.9 A). β -sheet formation, more precisely hydrogen bonding between the amino acids close to the core, was found to be essential in directing the self-assembly toward the formation of nanofibres rather than spherical micelles, vesicles or helices [69,70]. The authors demonstrated the structural versatility of this class of peptide amphiphiles by creating a variety of nanofibre networks displaying distinct morphologies and properties. As reported for other systems self-assembly could be reversibly induced by changing the pH of the

solution due to the ionic nature of the peptide head. Incorporation of photo-cleavable moieties in some of the studied systems also enabled the triggering of gel formation upon irradiation [70]. Stability and robustness of the material could be enhanced by simply incorporating cysteine residues and subsequent cross-linking of the self-assembled networks with formation of intermolecular disulphide bonds upon oxidation [67]. Self-assembly into nanofibres has also been performed in physiological conditions, in the presence of polyvalent metal ions or cell culture media, enabling cell entrapment within the hydrogel formed. Since metal ions are naturally present in body fluids, this result showed the potential of these biomaterials for cell transplantation or other *in vivo* tissue engineering applications [68,69].

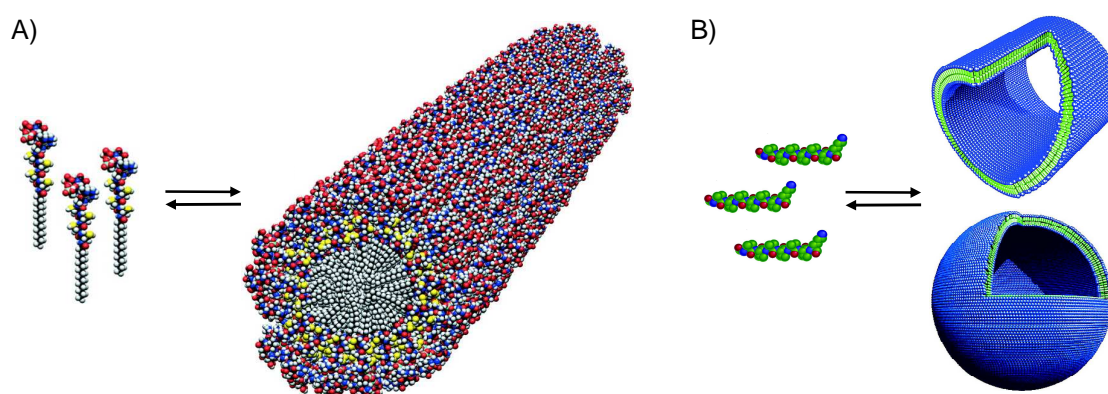


Figure 2.9. Schematic representation of peptide amphiphiles self-assembling into **A)** a cylindrical micelle and **B)** a nanotube (top) or a nanovesicle (bottom) (adapted from [67,71]).

Alternatively, peptide amphiphiles exclusively constituted of amino acids have also been designed. A few consecutive hydrophobic residues served as the hydrophobic tail while the polar head was constituted of a cationic (Table 2.6, entry 1) [71] or anionic amino acid (Table 2.6, entry 2) [72]. Due to their lipid-like feature these compounds were capable of self-assembling into nanotubes and nanovesicles in water (Figure 2.9 B) and were also reported to cause membrane protein solubilisation and stabilisation [71,72].

Table 2.6. Peptide amphiphile names and sequences used by Zhang *et al.*

Entry	Peptide name	Peptide sequence	Ref.
1	KV ₆	KVVVVVV	[71]
2	V ₆ D	Ac-VVVVVVD	[72]

2.3.3.6. Aromatic Interactions Based Systems

The use of short aromatic peptide derivatives has also been investigated to generate well-ordered structures by self-assembly. Aromatic moieties can be incorporated in peptide

systems either through the amino acid side chains or by addition to the peptide sequences. These particular groups interact through π - π stacking, directing the peptides to approach closer to each other and stabilising intermolecular hydrogen bonding and ionic interactions. Such attractive forces associated with the restricted geometry introduced by the aromatic moieties provide order and directionality, which is thought to drive the self-assembly process [73].

Aromatic amino acids

Short peptides composed of aromatic amino acids were found to self-assemble into tubular nanostructures. For example, diphenylalanine (FF), a possible constituting structural motif of β -amyloid fibrils, was found to self-assemble into nanotubes that were subsequently employed as templates for the formation of metal nanowires with potential application in nanoelectronics [73]. Gazit and co-workers showed that the dipeptides adopted a β -sheet arrangement within the self-assembled structure [73], which is controversial due to the short length of the peptides [74]. The group of Ventura showed that IF, an analogous dipeptide in which one of the phenylalanine residues was substituted by a non-aromatic amino acid with a comparable relative hydrophobicity, was also enabled to self-assemble into gelling high-order structures [75]. Such observation suggested that hydrophobic interactions may also play an important role in the self-assembly of short peptides.

Influence of the aromatic ligand

To exclude any potential electrostatic contribution between terminal amine and carboxylic functions and focus on the role of aromatic interaction, FF has been modified by a number of researchers with aromatic ligands such as benzyloxycarbonyl (Cbz), naphthalene (Nap) and 9-fluorenylmethoxycarbonyl (Fmoc). Cbz-FF, Nap-FF and Fmoc-FF were found to form fibrous networks [76,77]. Circular dichroism (CD) and FT-IR spectroscopy data showed that all systems were similar at the molecular scale, all displaying a β -sheet conformation. However nanofibres with different morphology and dimensions were observed at the supramolecular level, depending on the N-termini aromatic ligand.

Solubilisation of the peptide derivatives

A change in environmental conditions has been exploited in order to induce spontaneous self-assembly of short aromatic peptide derivatives into nanostructured hydrogels. Solubilisation of the molecules in aqueous solution constituted a key step in the procedure and was found to be challenging due to the amphiphilic character of the peptide derivatives. Various methods have been reported in the literature. A first one consisted in bringing the medium to its boiling point. These extreme conditions allowed the peptide

derivatives to dissolve at neutral pH and hydrogel formation was observed upon cooling of the solutions [78]. Use of organic solvents, including dimethyl sulfoxide (DMSO) and fluorinated solvents such as hexafluoroisopropanol (HFIP) has also been widely employed to solubilise such molecules. Self-assembly was triggered by modifying the solvent polarity upon dilution into aqueous solutions [73,75,76,79-81]. Another method involving pH-triggered self-assembly has been commonly used. The pH of aqueous peptide suspensions was first raised by addition of sodium hydroxide to ionise and therefore solubilise the molecules. It was subsequently adjusted until gelation by addition of hydrochloric acid [82,83] or sugar precursors which generated acid through *in situ* hydrolysis [84,85]. Use of borate buffer has also been reported to solubilise peptide derivatives, however in this case the pH was not reduced and gels were obtained at alkaline pH [86].

Enzymatic reactions

Alternatively, enzymatic reactions have been reported to induce self-assembly and associated hydrogel formation of short aromatic peptide derivatives. For example, Ulijn and co-workers showed that simple methyl ester removal from Fmoc-peptide methyl ester restored the amphiphilic character of the molecules, allowing them to spontaneously self-assemble [87,88]. This subtilisin-catalysed hydrolysis resulted in the formation of nanotubes with varying diameters depending on the amino acid building blocks. Similarly, the group of Xu demonstrated that Fmoc-Y-P(O)(OH)₂ [89] and Nap-FFGEY-P(O)(OH)₂ [90], two phosphorylated tyrosine-based compounds, presented a sol-gel transition upon addition of alkaline phosphatase under basic conditions (Figure 2.10 A). In solution, the tyrosine side chain of the precursor was ionised, preventing the self-assembly of the molecules due to electrostatic repulsion. Removal of the phosphate group (i.e. dephosphorylation) yielded Fmoc-Y and Nap-FFGEY, neutral compounds capable of self-assembly into fibrous hydrogels. The apparent molecular order of the structures was shown to be dependent on the enzyme concentration [91]. Oscillatory rheology confirmed the viscoelastic nature of the material. Slow diffusion of aqueous calcium chloride and phosphate buffer was exploited to form a calcium phosphate coating on the surface of the fibres, resulting from the coprecipitation of the salts. Such biomineralisation was found to improve the mechanical properties of the initial material [92]. Fluorescence spectroscopy data suggested that π -stacking of fluorenyl pairs was at the origin of the self-assembly of the Fmoc derivatives. On the other hand, strong interactions of the naphthyl groups with the phenylalanine side chains rather than π -stacking of the naphthyl moieties only were

found to be the driving force of the self-assembly of Nap-pentapeptide systems. Interestingly, dephosphorylation and the subsequent phase transition were found to be reversible upon addition of tyrosine kinase to Nap-FFGEY hydrogels in the presence of adenosine triphosphate (ATP) [90].

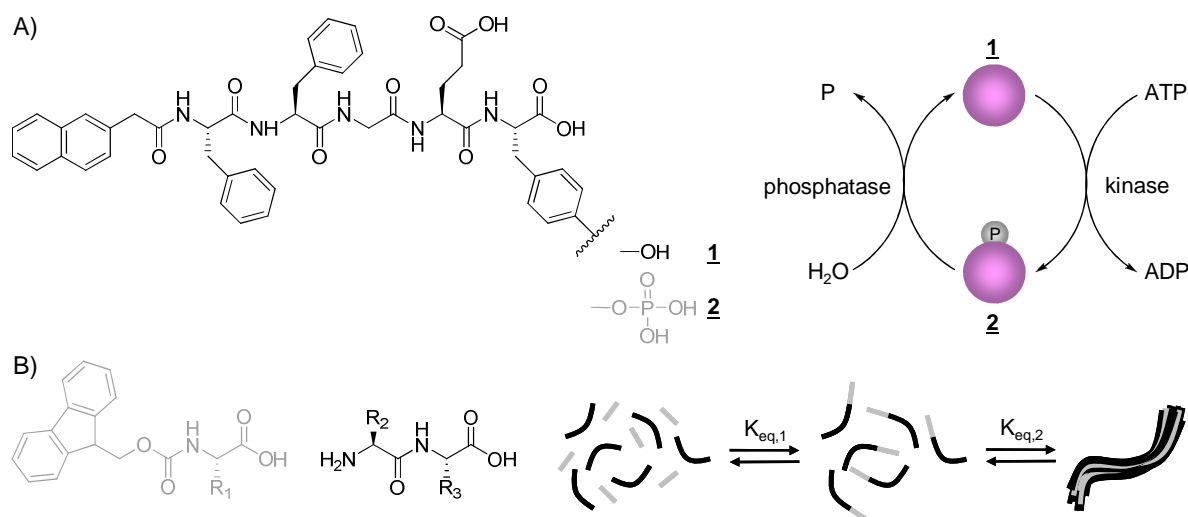


Figure 2.10. (A) Molecular structure and schematic representation of a Nap-peptide involved in an enzymatic dephosphorylation and phosphorylation. The dephosphorylated species is noted 1 and phosphorylated 2. ATP, ADP and P stand for adenosine triphosphate, adenosine diphosphate and phosphate respectively (adapted from [90]). (B) Molecular structure and schematic representation of Fmoc-amino acids and dipeptides forming tripeptides, which self-assemble into hydrogels (adapted from [93]).

Enzyme-catalysed reactions can be used to perform reverse hydrolysis (i.e. condensation reaction), which has also been reported to drive self-assembly. Addition of thermolysin to non-assembling, non-gelling Fmoc-amino acid and unmodified dipeptides led to the formation of Fmoc-tripeptides and their subsequent hydrogelation (Figure 2.10 B). The self-assembly process (Figure 2.10 B, equilibrium 2) was thought to be the driving force for the reaction, which favoured peptide bond creation (Figure 2.10 B, equilibrium 1) [93]. This condensation reaction was found to be completely reversible and to favour the formation of the most thermodynamically stable components [94].

General characteristics

Fmoc-oligopeptides are common intermediates in peptide synthesis and have been reported to have anti-inflammatory properties [95]. Based on the non-enzymatic and enzymatic methods described above, a series of Fmoc-dipeptides and -tripeptides covering a large range of hydrophobicities has been extensively investigated. Under specific conditions and depending on the peptide sequence, spontaneous self-assembly can be achieved, resulting in the formation of materials with different morphological, physical and mechanical properties. However not all the molecules tested lead to hydrogel formation. For instance, despite the same amino acid composition, Fmoc-FG (Table 2.7, entry 4) formed hydrogels

whereas Fmoc-GF did not [83]. No evidence allowed determination of whether non-gelling self-assembled structures of Fmoc-GF were formed. On the other hand, gel formation was observed from both Fmoc-VLK(Boc) and Fmoc-K(Boc)LV – in which the lysine side chain was protected by *tert*-butyloxycarbonyl (Boc), a non-aromatic protecting group to prevent any interferences arising from charges and additional aromatic moieties. However, both systems exhibited distinct self-assembling behaviours and conformational differences [86]. Modifying the order of the amino acid sequence therefore altered the structural properties of the systems, which had a substantial impact on self-assembly.

Table 2.7. Peptide sequences used by the groups of Xu and Ulijn and their pH conditions. The fibre diameters were measured for different peptide concentrations.

Entry	Peptide sequence	pH	Fibre diameter / nm	Ref.
1	Fmoc-GG	< 4	33 ± 8	[82,83]
2	Fmoc-AA	< 4	68 ± 18	[82,83]
3	Fmoc-FF	< 8	56 ± 13	[83]
4	Fmoc-FG	< 4	25 ± 6	[83]
5	Fmoc-LG	< 4	22 ± 5	[83]

Although, for some systems, hydrogels with similar properties could be generated using different methods, the preparation route followed was also found to be determinant in some other cases. For instance, Fmoc-LL nanotubes were obtained upon hydrolysis of the corresponding pre-synthesised ester whereas sheet-like structures were observed from precursors formed via reverse hydrolysis [87]. The mechanical properties of the hydrogels formed were also found to be dependent on the route and conditions of sample preparation, as shown by the difference of one order of magnitude in elastic modulus reported for Fmoc-FG [81,85]. Another example is that of Fmoc-AA, which formed hydrogels in acidic conditions upon pH change (Table 2.7, entry 2) [82,83,85] whereas turbid solutions rather than gels were obtained by enzyme-triggered reaction [87], suggesting the pH conditions related to the enzyme activity were not appropriate for gelation. Table 2.7 provides a list of Fmoc-dipeptides constituted of different hydrophobic residues that have been studied using pH methods and were found to form fibrillar supramolecular structures.

Interestingly, Fmoc-FF (Table 2.7, entry 3) was the only system for which gelation was observed at pH near physiological. Fluorescence data showed evidence of the pairing of fluorenyl groups in an antiparallel manner, emphasising the role of π -stacking in the self-assembly process. The Fmoc group has been reported to have the propensity to induce β -sheet conformations [96], as confirmed for Fmoc-FF by CD [83]. In addition to displaying fibre diameters in line with those found in the ECM, Fmoc-FF hydrogels were found to be

strong and rigid (G' of 10000 Pa and ten times higher than G'') under small oscillatory deformation, showing the potential of such hydrogels for tissue engineering applications [80]. Besides, the mechanical properties were strengthened in the presence of cell culture media [97]. 2D and/or 3D culture of cells such as bovine chondrocytes [83] or Chinese hamster ovary [80] were performed successfully on Fmoc-FF hydrogels, showing the biocompatibility of the scaffold [83]. Chemical functionalisation of these matrices has recently been reported by mixing Fmoc-FF with Fmoc protected single amino acids with various side chains. Depending on the functional groups incorporated in the fibrous networks, hydrogels with distinct mechanical properties were formed and were found to suit specifically different cell types [97]. Bioactive hydrogels have also been developed by self-assembly of Fmoc-FF with Fmoc-RGD molecules. Used for 3D cell culture, the produced substrate was shown to promote adhesion of human dermal fibroblasts, the spreading of which was found to be dependent on the tuneable density of RGD sequences decorating the scaffold [98].

2.4. SUMMARY AND OBJECTIVES

To date various peptide systems capable of self-assembly and hydrogel formation have been developed. Under specific conditions these structures have shown the ability to mimic the ECM and to support tissue culture, demonstrating their potential for tissue engineering applications. Such biomaterials have been obtained by exploiting the spontaneous or induced molecular self-assembly of peptides and their derivatives. This process can be achieved through a combination of hydrogen bonding between peptide backbones, hydrophilic and hydrophobic cooperative effects of amphiphile molecules or π -stacking of aromatic moieties. As expected, since amino acids are characterised by particular pK_a values, self-assembly occurred under specific pH conditions depending on the peptide sequence, showing the importance of this environmental parameter.

The previously investigated systems, most of which formed β -sheet rich structures, were typically constituted of over 10 amino acids. In order to simplify the systems and make them more easily tuned, a few groups including ours have adopted a strategy that centred on the exploitation of π -interactions, enabling the use of shorter peptides. One of the main challenges of molecular self-assembly remains to control the self-assembly process in order to ensure the formation of uniform, reproducible structures, hence most of the studies published so far mainly focus on the self-assembly properties of the systems. However, the literature suffers from a lack of documentation on the gelation properties and structural characterisation of the gels formed, which will be investigated in this thesis. Overall, this

work aims to provide further understanding of the self-assembly mechanism of aromatic short peptide derivatives in order to rationally design biomaterials with tuneable properties to match the requirements of specific cell types or allow stem cell differentiation.

The main focus of this project is to characterise the behaviour in solution, as well as the self-assembly and gelation properties of Fmoc-dipeptides containing either aromatic or non-aromatic hydrophobic residues using a pH change approach. Due to its proven ability to form hydrogels at neutral pH, Fmoc-FF will receive particular attention. In order to evaluate how the aromatic side chains of the amino acids affect the self-assembly behaviour of the molecules, glycine will be introduced in the peptide sequence, giving rise to Fmoc-FG, Fmoc-GF and Fmoc-GG. As suggested in the literature, substitution of aromatic amino acids by non-aromatic amino acids possessing alkyl side chains that exhibit a similar hydrophobicity may not alter the self-assembly and gelation properties of the systems. Phenylalanine will therefore be replaced by leucine to allow the study of Fmoc-LL, Fmoc-LG and Fmoc-GL. Further understanding of the self-assembly mechanism of this set of Fmoc-dipeptides will be provided based on potentiometry, FT-IR, fluorescence spectroscopy, wide angle X-ray scattering (WAXS), transmission electron microscopy (TEM) and shear rheometry.

2.5. REFERENCES

1. Langer, R. and Vacanti, J.P., *Tissue engineering*. Science, **1993**, 260 (5110), 920-926.
2. Peppas, N.A., Hilt, J.Z., Khademhosseini, A., *et al.*, *Hydrogels in biology and medicine: From molecular principles to bionanotechnology*. Advanced Materials, **2006**, 18 (11), 1345-1360.
3. Lee, K.Y. and Mooney, D.J., *Hydrogels for tissue engineering*. Chemical Reviews, **2001**, 101 (7), 1869-1880.
4. Griffith, L.G., *Polymeric biomaterials*. Acta Materialia, **2000**, 48 (1), 263-277.
5. Ma, P.X., *Scaffolds for tissue fabrication*. Materials Today, **2004**, 7 (5), 30-40.
6. Alberts, B., Bray, D., Lewis, J., *et al.*, *Molecular biology of the cell* 3rd ed. **1994**, New York: Garland Publishing, Inc.
7. Nelson, D.L. and Cox, M.M., *Lehninger principles of biochemistry* 3rd ed. **2000**, New York: Worth.
8. Elsdale, T. and Bard, J., *Collagen substrata for studies on cell behavior*. The Journal of Cell Biology, **1972**, 54 (3), 626-637.
9. Ruoslahti, E. and Pierschbacher, M.D., *New perspectives in cell adhesion: RGD and integrins*. Science, **1987**, 238 (4826), 491-497.
10. Abbott, A., *Cell culture: Biology's new dimension*. Nature, **2003**, 424 (6951), 870-872.
11. Zhang, S., Gelain, F., and Zhao, X., *Designer self-assembling peptide nanofiber scaffolds for 3D tissue cell cultures* Seminars in Cancer Biology, **2005**, 15 (5), 413-420.
12. Stevens, M.M. and George, J.H., *Exploring and engineering the cell surface interface*. Science, **2005**, 310 (5751), 1135-1138.
13. Hoffman, A.S., *Hydrogels for biomedical applications*. Annals of the New York Academy of Sciences, **2001**, 944 (1), 62-73.
14. Leong, K.F., Cheah, C.M., and Chua, C.K., *Solid freeform fabrication of three-dimensional scaffolds for engineering replacement tissues and organs*. Biomaterials, **2003**, 24 (13), 2363-2378.
15. Engler, A.J., Sen, S., Sweeney, H.L., *et al.*, *Matrix elasticity directs stem cell lineage specification*. Cell, **2006**, 126 (4), 677-689.
16. Smith, L.A. and Ma, P.X., *Nano-fibrous scaffolds for tissue engineering*. Colloids and Surfaces B: Biointerfaces, **2004**, 39 (3), 125-131.
17. Barnes, C.P., Sell, S.A., Boland, E.D., *et al.*, *Nanofiber technology: Designing the next generation of tissue engineering scaffolds*. Advanced Drug Delivery Reviews, **2007**, 59 (14), 1413-1433.
18. Yang, F., Murugan, R., Ramakrishna, S., *et al.*, *Fabrication of nano-structured porous PLLA scaffold intended for nerve tissue engineering*. Biomaterials, **2004**, 25 (10), 1891-1900.
19. Zhang, R. and Ma, P.X., *Synthetic nano-fibrillar extracellular matrices with predesigned macroporous architectures*. Journal of Biomedical Materials Research Part A, **2000**, 52 (2), 430-438.
20. Matthews, J.A., Wnek, G.E., Simpson, D.G., *et al.*, *Electrospinning of collagen nanofibers*. Biomacromolecules, **2002**, 3 (2), 232-238.
21. Yoshimoto, H., Shin, Y.M., Terai, H., *et al.*, *A biodegradable nanofiber scaffold by electrospinning and its potential for bone tissue engineering*. Biomaterials, **2003**, 24 (12), 2077-2082.
22. Hamley, I.W., *Peptide fibrillization*. Angewandte Chemie International Edition, **2007**, 46 (43), 8128-8147.

23. Whitesides, G.M. and Grzybowski, B., *Self-assembly at all scales*. Science, **2002**, 295 (5564), 2418-2421.
24. Philp, D. and Stoddart, J.F., *Self-assembly in natural and unnatural systems*. Angewandte Chemie International Edition in English, **1996**, 35 (11), 1154-1196.
25. Lindoy, L.F. and Atkinson, I.M., *Self-assembly in supramolecular systems*. **2000**, Cambridge: Royal Society of Chemistry.
26. Steed, J.W. and Atwood, J., L., *Supramolecular Chemistry*. 2nd ed. **2009**, Chichester: Wiley.
27. Lee, K.Y., Rowley, J.A., Eiselt, P., *et al.*, *Controlling mechanical and swelling properties of alginate hydrogels independently by cross-linker type and cross-linking density*. Macromolecules, **2000**, 33 (11), 4291-4294.
28. Shin, H., Jo, S., and Mikos, A.G., *Biomimetic materials for tissue engineering*. Biomaterials, **2003**, 24 (24), 4353-4364.
29. Parkhurst, M.R. and Saltzman, W.M., *Quantification of human neutrophil motility in three-dimensional collagen gels. Effect of collagen concentration*. Biophysical Journal, **1992**, 61 (2), 306-315.
30. Choi, Y.S., Hong, S.R., Lee, Y.M., *et al.*, *Studies on gelatin-containing artificial skin: II. Preparation and characterization of cross-linked gelatin-hyaluronate sponge*. Journal of Biomedical Materials Research, **1999**, 48 (5), 631-639.
31. Lee, C.R., Grodzinsky, A.J., and Spector, M., *The effects of cross-linking of collagen-glycosaminoglycan scaffolds on compressive stiffness, chondrocyte-mediated contraction, proliferation and biosynthesis*. Biomaterials, **2001**, 22 (23), 3145-3154.
32. Hubbell, J.A., *Biomaterials in tissue engineering*. Nature Biotechnology, **1995**, 13 (6), 565-576.
33. Nguyen, K.T. and West, J.L., *Photopolymerizable hydrogels for tissue engineering applications*. Biomaterials, **2002**, 23 (22), 4307-4314.
34. Hern, D.L. and Hubbell, J.A., *Incorporation of adhesion peptides into nonadhesive hydrogels useful for tissue resurfacing*. Journal of Biomedical Materials Research, **1998**, 39 (2), 266-276.
35. West, J.L. and Hubbell, J.A., *Polymeric biomaterials with degradation sites for proteases involved in cell migration*. Macromolecules, **1998**, 32 (1), 241-244.
36. Bryant, S.J. and Anseth, K.S., *Controlling the spatial distribution of ECM components in degradable PEG hydrogels for tissue engineering cartilage*. Journal of Biomedical Materials Research, **2003**, 64A (1), 70-79.
37. Pelton, R., *Temperature-sensitive aqueous microgels*. Advances in Colloid and Interface Science, **2000**, 85 (1), 1-33.
38. Yu, T.T. and Shoichet, M.S., *Guided cell adhesion and outgrowth in peptide-modified channels for neural tissue engineering*. Biomaterials, **2005**, 26 (13), 1507-1514.
39. Stile, R.A., Burghardt, W.R., and Healy, K.E., *Synthesis and characterization of injectable poly(N-isopropylacrylamide)-based hydrogels that support tissue formation in vitro*. Macromolecules, **1999**, 32 (22), 7370-7379.
40. Monera, O.D., Sereda, T.J., Zhou, N.E., *et al.*, *Relationship of sidechain hydrophobicity and α -helical propensity on the stability of the single-stranded amphipathic α -helix*. Journal of Peptide Science, **1995**, 1 (5), 319-329.
41. Ghadiri, M.R., Granja, J.R., Milligan, R.A., *et al.*, *Self-assembling organic nanotubes based on a cyclic peptide architecture*. Nature, **1993**, 366 (6453), 324-327.
42. Khazanovich, N., Granja, J.R., McRee, D.E., *et al.*, *Nanoscale tubular ensembles with specified internal diameters. Design of a self-assembled nanotube with a 13-Å pore*. Journal of the American Chemical Society, **1994**, 116 (13), 6011-6012.

43. Fernandez-Lopez, S., Kim, H.-S., Choi, E.C., *et al.*, *Antibacterial agents based on the cyclic d,l- α -peptide architecture*. *Nature*, **2001**, 412 (6845), 452-455.
44. Pandya, M.J., Spooner, G.M., Sunde, M., *et al.*, *Sticky-end assembly of a designed peptide fiber provides insight into protein fibrillogenesis*. *Biochemistry*, **2000**, 39 (30), 8728-8734.
45. Smith, A.M., Banwell, E.F., Edwards, W.R., *et al.*, *Engineering increased stability into self-assembled protein fibers*. *Advanced Functional Materials*, **2006**, 16 (8), 1022-1030.
46. Banwell, E.F., Abelardo, E.S., Adams, D.J., *et al.*, *Rational design and application of responsive α -helical peptide hydrogels*. *Nature Materials*, **2009**, 8 (7), 596-600.
47. Petka, W.A., Harden, J.L., McGrath, K.P., *et al.*, *Reversible hydrogels from self-assembling artificial proteins* *Science*, **1998**, 281 (5375), 389-392.
48. Koo, E.H., Lansbury, P.T., Jr., and Kelly, J.W., *Amyloid diseases: Abnormal protein aggregation in neurodegeneration*. *Proceedings of the National Academy of Sciences of the United States of America*, **1999**, 96 (18), 9989-9990.
49. Zhang, S., Holmes, T., Lockshin, C., *et al.*, *Spontaneous assembly of a self-complementary oligopeptide to form a stable macroscopic membrane*. *Proceedings of the National Academy of Sciences of the United States of America*, **1993**, 90 (8), 3334-3338.
50. Chen, P., *Self-assembly of ionic-complementary peptides: a physicochemical viewpoint*. *Colloids and Surfaces A: Physicochemical and Engineering Aspects*, **2005**, 261 (1-3), 3-24.
51. Zhang, S., Holmes, T.C., Michael DiPersio, C., *et al.*, *Self-complementary oligopeptide matrices support mammalian cell attachment*. *Biomaterials*, **1995**, 16 (18), 1385-1393.
52. Holmes, T.C., de Lacalle, S., Su, X., *et al.*, *Extensive neurite outgrowth and active synapse formation on self-assembling peptide scaffolds*. *Proceedings of the National Academy of Sciences of the United States of America*, **2000**, 97 (12), 6728-6733.
53. Caplan, M.R., Schwartzfarb, E.M., Zhang, S., *et al.*, *Control of self-assembling oligopeptide matrix formation through systematic variation of amino acid sequence*. *Biomaterials*, **2002**, 23 (1), 219-227.
54. Aggeli, A., Nyrkova, I.A., Bell, M., *et al.*, *Hierarchical self-assembly of chiral rod-like molecules as a model for peptide -sheet tapes, ribbons, fibrils, and fibers*. *Proceedings of the National Academy of Sciences of the United States of America*, **2001**, 98 (21), 11857-11862.
55. Fishwick, C.W.G., Beevers, A.J., Carrick, L.M., *et al.*, *Structures of helical β -tapes and twisted ribbons: the role of side-chain interactions on twist and bend behavior*. *Nano Letters*, **2003**, 3 (11), 1475-1479.
56. Aggeli, A., Bell, M., Carrick, L.M., *et al.*, *pH as a trigger of peptide β -sheet self-assembly and reversible switching between nematic and isotropic phases*. *Journal of the American Chemical Society*, **2003**, 125 (32), 9619-9628.
57. Aggeli, A., Bell, M., Boden, N., *et al.*, *Self-Assembling Peptide Polyelectrolyte beta-Sheet Complexes Form Nematic Hydrogels*¹³. *Angewandte Chemie International Edition in English*, **2003**, 42 (45), 5603-5606.
58. Bell, C., J., Carrick, L., M., Katta, J., *et al.*, *Self-assembling peptides as injectable lubricants for osteoarthritis*. *Journal of Biomedical Materials Research Part A*, **2006**, 78A (2), 236-246.
59. Schneider, J.P., Pochan, D.J., Ozbas, B., *et al.*, *Responsive hydrogels from the intramolecular folding and self-assembly of a designed peptide* *Journal of the American Chemical Society*, **2002**, 124 (50), 15030-15037.

60. Ozbas, B., Kretsinger, J., Rajagopal, K., *et al.*, *Salt-triggered peptide folding and consequent self-assembly into hydrogels with tunable modulus*. *Macromolecules*, **2004**, *37* (19), 7331-7337.
61. Rajagopal, K., Lamm, M.S., Haines-Butterick, L.A., *et al.*, *Tuning the pH responsiveness of β -hairpin peptide folding, self-assembly, and hydrogel material formation*. *Biomacromolecules*, **2009**, *10* (9), 2619-2625.
62. Haines-Butterick, L., Rajagopal, K., Branco, M., *et al.*, *Controlling hydrogelation kinetics by peptide design for three-dimensional encapsulation and injectable delivery of cells*. *Proceedings of the National Academy of Sciences of the United States of America*, **2007**, *104* (19), 7791-7796.
63. Pochan, D.J., Schneider, J.P., Kretsinger, J., *et al.*, *Thermally reversible hydrogels via intramolecular folding and consequent self-assembly of a de novo designed peptide*. *Journal of the American Chemical Society*, **2003**, *125* (39), 11802-11803.
64. Haines, L.A., Rajagopal, K., Ozbas, B., *et al.*, *Light-activated hydrogel formation via the triggered folding and self-assembly of a designed peptide*. *Journal of the American Chemical Society*, **2005**, *127* (48), 17025-17029.
65. Brizard, A., Dolain, C., Huc, I., *et al.*, *Asp-gly based peptides confined at the surface of cationic gemini surfactant aggregates*. *Langmuir*, **2006**, *22* (8), 3591-3600.
66. Löwik, D.W.P.M. and van Hest, J.C.M., *Peptide based amphiphiles*. *Chemical Society Reviews*, **2004**, *33*, 234-245.
67. Hartgerink, J.D., Beniash, E., and Stupp, S.I., *Self-assembly and mineralization of peptide-amphiphile nanofibers*. *Science*, **2001**, *294* (5547), 1684-1688.
68. Silva, G.A., Czeisler, C., Niece, K.L., *et al.*, *Selective Differentiation of Neural Progenitor Cells by High-Epitope Density Nanofibers*. *Science*, **2004**, *303* (5662), 1352-1355.
69. Beniash, E., Hartgerink, J.D., Storie, H., *et al.*, *Self-assembling peptide amphiphile nanofiber matrices for cell entrapment* *Acta Biomaterialia*, **2005**, *1* (4), 387-397.
70. Muraoka, T., Cui, H., and Stupp, S.I., *Quadruple helix formation of a photoresponsive peptide amphiphile and its light-triggered dissociation into single fibers*. *Journal of the American Chemical Society*, **2008**, *130* (10), 2946-2947.
71. von Maltzahn, G., Vauthey, S., Santoso, S., *et al.*, *Positively charged surfactant-like peptides self-assemble into nanostructures*. *Langmuir*, **2003**, *19* (10), 4332-4337.
72. Vauthey, S., Santoso, S., Gong, H., *et al.*, *Molecular self-assembly of surfactant-like peptides to form nanotubes and nanovesicles*. *Proceedings of the National Academy of Sciences of the United States of America*, **2002**, *99* (8), 5355-5360.
73. Reches, M. and Gazit, E., *Casting metal nanowires within discrete self-assembled peptide nanotubes*. *Science*, **2003**, *300* (5618), 625-627.
74. Görbitz, C.H., *The structure of nanotubes formed by diphenylalanine, the core recognition motif of Alzheimer's β -amyloid polypeptide*. *Chemical Communications*, **2006**, 2332-2334.
75. de Groot, N.S., Parella, T., Aviles, F.X., *et al.*, *Ile-Phe dipeptide self-assembly: clues to amyloid formation*. *Biophysical Journal*, **2007**, *92* (5), 1732-1741.
76. Reches, M. and Gazit, E., *Self-assembly of peptide nanotubes and amyloid-like structures by charged-termini-capped diphenylalanine peptide analogues*. *Israel Journal of Chemistry*, **2005**, *45* (3), 363-371.
77. Jayawarna, V., Smith, A., Gough, J.E., *et al.*, *Three-dimensional cell culture of chondrocytes on modified di-phenylalanine scaffolds*. *Biochemical Society Transactions*, **2007**, *035* (3), 535-537.

78. Vegners, R., Shestakova, I., Kalvinsh, I., *et al.*, *Use of a gel-forming dipeptide derivative as a carrier for antigen presentation*. *Journal of Peptide Science*, **1995**, *1* (6), 371-378.
79. Liebmann, T., Rydholm, S., Akpe, V., *et al.*, *Self-assembling Fmoc dipeptide hydrogel for in situ 3D cell culturing*. *BMC Biotechnology*, **2007**, *7* (1), 88-98.
80. Mahler, A., Reches, M., Rechter, M., *et al.*, *Rigid, self-assembled hydrogel composed of a modified aromatic dipeptide*. *Advanced Materials*, **2006**, *18* (11), 1365-1370.
81. Orbach, R., Adler-Abramovich, L., Zigerson, S., *et al.*, *Self-assembled Fmoc-peptides as a platform for the formation of nanostructures and hydrogels*. *Biomacromolecules*, **2009**, *10* (9), 2646-2651.
82. Zhang, Y., Gu, H., Yang, Z., *et al.*, *Supramolecular hydrogels respond to ligand-receptor interaction* *Journal of the American Chemical Society*, **2003**, *125* (45), 13680-13681.
83. Jayawarna, V., Ali, M., Jowitt, T.A., *et al.*, *Nanostructured hydrogels for three-dimensional cell culture through self-assembly of fluorenylmethoxycarbonyl-dipeptides*. *Advanced Materials*, **2006**, *18* (5), 611-614.
84. Adams, D.J., Butler, M.F., Frith, W.J., *et al.*, *A new method for maintaining homogeneity during liquid-hydrogel transitions using low molecular weight hydrogelators*. *Soft Matter*, **2009**, *5* (9), 1856-1862.
85. Adams, D.J., Mullen, L.M., Berta, M., *et al.*, *Relationship between molecular structure, gelation behaviour and gel properties of Fmoc-dipeptides*. *Soft Matter*, **2010**, *6*, 1971-1980.
86. Cheng, G., Castelletto, V., Moulton, C.M., *et al.*, *Hydrogelation and self-assembly of Fmoc-tripeptides: Unexpected influence of sequence on self-assembled fibril structure, and hydrogel modulus and anisotropy*. *Langmuir*, **2010**, *26* (7), 4990-4998.
87. Das, A.K., Collins, R.F., and Ulijn, R.V., *Exploiting enzymatic (reversed) hydrolysis in directed self-assembly of peptide nanostructures*. *Small*, **2008**, *4* (2), 279-287.
88. Xu, H., Das, A.K., Horie, M., *et al.*, *An investigation of the conductivity of peptide nanotube networks prepared by enzyme-triggered self-assembly*. *Nanoscale*, **2010** (in press).
89. Yang, Z., Gu, H., Fu, D., *et al.*, *Enzymatic formation of supramolecular hydrogels*. *Advanced Materials*, **2004**, *16* (16), 1440-1444.
90. Yang, Z., Liang, G., Wang, L., *et al.*, *Using a kinase/phosphatase switch to regulate a supramolecular hydrogel and forming the supramolecular hydrogel in vivo*. *Journal of the American Chemical Society*, **2006**, *128* (9), 3038-3043.
91. Thornton, K., Smith, A.M., Merry, C.L.R., *et al.*, *Controlling stiffness in nanostructured hydrogels produced by enzymatic dephosphorylation*. *Biochemical Society Transactions*, **2009**, *37* (4), 660-664.
92. Schnepf, Z.A.C., Gonzalez-McQuire, R., and Mann, S., *Hybrid biocomposites based on calcium phosphate mineralization of self-assembled supramolecular hydrogels*. *Advanced Materials*, **2006**, *18* (14), 1869-1872.
93. Toledano, S., Williams, R.J., Jayawarna, V., *et al.*, *Enzyme-triggered self-assembly of peptide hydrogels via reversed hydrolysis*. *Journal of the American Chemical Society*, **2006**, *128* (4), 1070-1071.
94. Williams, R.J., Smith, A.M., Collins, R., *et al.*, *Enzyme-assisted self-assembly under thermodynamic control*. *Nature Nanotechnology*, **2009**, *4* (1), 19-24.
95. Burch, R.M., Weitzberg, M., Blok, N., *et al.*, *N-(fluorenyl-9-methoxycarbonyl) amino acids, a class of antiinflammatory agents with a different mechanism of*

- action*. Proceedings of the National Academy of Sciences of the United States of America, **1991**, 88 (2), 355-359.
96. Larsen, B.D., Christensen, D.H., Holm, A., *et al.*, *The Merrifield peptide synthesis studied by near-infrared Fourier-transform Raman spectroscopy*. Journal of the American Chemical Society, **1993**, 115 (14), 6247-6253.
97. Jayawarna, V., Richardson, S.M., Hirst, A.R., *et al.*, *Introducing chemical functionality in Fmoc-peptide gels for cell culture*. Acta Biomaterialia, **2009**, 5 (3), 934-943.
98. Zhou, M., Smith, A.M., Das, A.K., *et al.*, *Self-assembled peptide-based hydrogels as scaffolds for anchorage-dependent cells*. Biomaterials, **2009**, 30 (13), 2523-2530.

— Chapter 3 —

Materials and Methods

3.1. MATERIALS

3.1.1. Raw Materials

All Fmoc-dipeptides were purchased from Bachem (Bubendorf, Switzerland) or C S Bio Co. (Menlo Park, USA) and used without any further purification. The purity of the compounds was checked by HPLC (>98 %) and mass spectrometry. HPLC grade water was purchased from Merck, and deuterated water (99.9 atom % D) from Sigma-Aldrich.

3.1.2. Sample Preparation

Depending on the desired concentration, the required amount of commercial Fmoc-dipeptide powder was suspended into 2 mL of HPLC grade water. Sodium hydroxide (0.5 M) was added to the aqueous suspensions of peptide derivatives until pH 10.5 was reached (~ 55 μL for 10 mmol L^{-1} sample). The samples were vortexed and sonicated (VWR ultrasonicator bath, 30 W) for 1 minute to fully dissolve the modified peptide. Depending on the concentration and on the target pH, a required volume of dilute hydrochloric acid (0.085 M) was then added drop-wise while the solution was vortexed and sonicated until the target pH was obtained. Next, the samples were heated to 75–80 °C for different time periods depending on the system (Table 3.1) and homogenised.

Table 3.1. Molecular weight, mass and weight percentage corresponding to Fmoc-dipeptide 2 mL samples at 10 mmol L^{-1} , and typical heating times.

	MW / g mol^{-1}	m / mg	Wt %	t_{heating} / min
Fmoc-FF	534.61	10.7	0.53	1.0
Fmoc-FG	444.49	8.9	0.44	2.5
Fmoc-GG	354.36	7.1	0.35	1.0
Fmoc-GF	444.49	8.9	0.44	2.0
Fmoc-LL	466.58	9.3	0.47	1.0
Fmoc-LG	410.47	8.2	0.41	2.5
Fmoc-GL	410.47	8.2	0.41	1.5

The samples were subsequently cooled and maintained at 4 °C for ~ 12 hours (overnight) to promote gelation. To allow comparison between the studied samples, all were

investigated after this same aging time (the point at which they were considered to be in a temporal equilibrium). Reported pH values were those measured after storage. They were found to be identical to the pH values measured before heating within ± 0.3 units.

3.2. METHODS

In this section we will take an interest in the theoretical and technical aspects of the methods employed to characterise the studied systems. For each technique a brief overview of the background focused towards our uses as well as the experimental procedure will be described.

3.2.1. Reverse Phase High Performance Liquid Chromatography

3.2.1.1. Theory

High performance liquid chromatography is an analytical method enabling the separation of polar molecules depending on their affinity with a mobile and a stationary phase.

The stationary phase is typically composed of silica gel beads, with a particle size of 2–5 μm and a pore diameter of 10 nm [1]. The silica particles can be covalently modified with non-polar hydrocarbon chains, with the alkyl chain length determining the affinity to hydrophobic solutes. Long chains (e.g., containing 18 carbons, ‘C-18’) tend to retain more hydrophobic molecules, while short chains (e.g., containing 8 carbons, ‘C-8’) preferably retain less hydrophobic compounds.

The mobile phase is a solvent or a mixture of solvents of different polarity (commonly methanol or acetonitrile with water). In the case of reverse phase HPLC, the polarity of the mobile phase is higher than the polarity of the stationary phase (as opposed to normal HPLC where the stationary phase is more polar than the mobile phase) leading to the retention of hydrophobic molecules and the elution of the hydrophilic compounds first. While the flow of the mobile phase is maintained with high pressure, its composition can be varied in order to modify its polarity with time as an elution gradient. The polarity of the solvent mixture is decreased as the separation proceeds to elute more hydrophobic molecules.

Different types of detectors can be used to quantify the amount of eluted compounds. The most widely used for HPLC exploit the molecules’ optical properties such as refractive index, fluorescence or absorption [1]. In the later case the analyte absorption can be measured at one (monochromatic detection) or several (polychromatic detection) wavelengths in the UV-visible spectrum.

HPLC chromatograms are commonly presented as the absorbance detected as a function of time. Each separated component, i , appears in the form of a peak, the area, A_i , of which is proportional to the molar amount of the compound in the sample [1]. After attribution of the elution peaks the proportion of each component, x_i , can be calculated using the following equation:

$$x_i = \frac{A_i}{\sum_1^n A_i} \times 100 \quad \text{Equation 3.1}$$

where n is the total number of components contained in the sample.

3.2.1.2. Experimental Procedure

HPLC analyses were carried out using diluted samples prepared in a water/acetonitrile (50:50) mixture. Chromatograms were recorded using Chromeleon software on a Dionex HPLC system consisting of a P680 pump connected to an ASI-100 automated sample injector and equipped with a UVD170U detector. Aliquots of 100 μL were injected with a flow rate of 1 mL min^{-1} into a Macherey-Nagel C-18 column (length: 250 mm, diameter: 4.6 mm) containing silica particles (diameter: 5 μm , pores diameter: 10 nm). The gradient used was a linear exchange between water/acetonitrile (80:20, 0.1% TFA) at 4 minutes to water/acetonitrile (20:80, 0.1% TFA) at 35 minutes. The commercial compounds and the cleaved product were quantified by monitoring the absorbance of the peptide bonds and aromatic groups at a wavelength of 265 nm.

3.2.2. Potentiometry

3.2.2.1. Theory

Potentiometry allows measurement of the potential difference between two electrodes, an external reference and an internal reference, immersed in a solution. These two electrodes are usually of the same type e.g. silver/silver chloride. For more convenience they are often grouped as a 'combination electrode' in a glass shaft (Figure 3.1).

The internal electrode can be ion selective: pH electrodes for example are specific to protons (H^+ ions). This type of electrode consists of a silver wire coated with silver chloride (Ag/AgCl) immersed in a solution of HCl (0.1 M) saturated with potassium chloride (KCl). Its extremity is a pH sensitive glass membrane which contains positively charged ions (typically Na^+) [1].

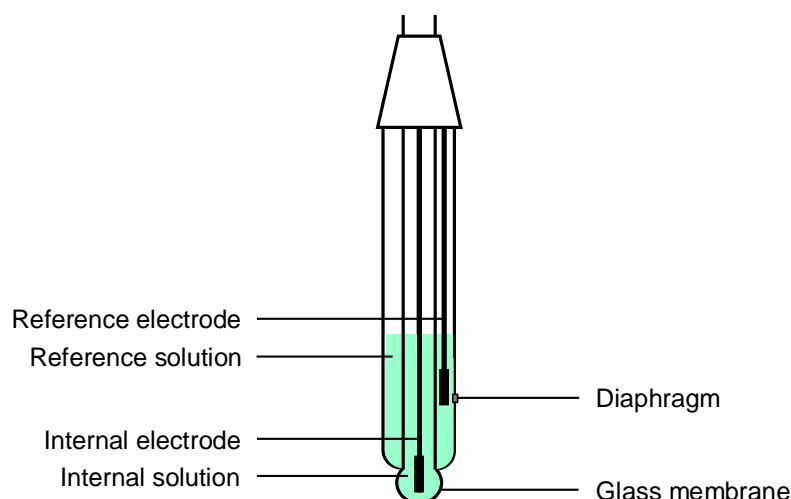


Figure 3.1. Schematic representation of a combination pH electrode (adapted from [2]).

When the combined electrode is immersed in the studied solution, equilibrium is created between the cations contained in the glass membrane and the H^+ ions contained in the sample. This equilibrium is at the origin of the potential measured. The potential provided by the internal reference electrode is proportional to the proton activity, a_{H^+} , whereas the potential provided by the external reference electrode is proportional to a standard potential. The pH displayed on the pH meter results from the difference between these two potentials.

Clotting of the membrane can occur when analysing gels or viscous solutions. Lack of flow over the electrode's membrane in such type of sample may affect measurements and result in improper pH values. To prevent aggregate formation and ensure the samples remain in a liquid state during the experiment constant stirring is commonly applied using magnetic stirrers for example.

pH is a measure of the acidity of a solution. It is defined as a function of the hydronium ion activity, $a_{H_3O^+}$. For more convenience pH is commonly expressed as a function of the hydrogen ion, a_{H^+} although it is in its solvated form $a_{H_3O^+}$:

$$pH = -\log_{10} a_{H_3O^+} \quad \text{or} \quad pH = -\log_{10} a_{H^+} \quad \text{Equation 3.2}$$

and

$$10^{-pH} = a_{H_3O^+} \quad \text{or} \quad 10^{-pH} = a_{H^+} \quad \text{Equation 3.3}$$

In very dilute solutions Equation 3.2 can take the form of:

$$pH = -\log_{10} [H^+] \quad \text{Equation 3.4}$$

where $[H^+]$ is the concentration of protons [2].

In deuterated solvents the pH analogue for deuterium ion activity is denoted pD . This variable can be measured using a standard glass electrode by simply applying a constant correction to the pH meter reading, pH_0 , as described in the following equation [2]:

$$pD = pH_0 + 0.40 \quad \text{Equation 3.5}$$

3.2.1.2. Experimental Procedure

pH measurements were performed using a Hanna Instruments pH210 pH-meter equipped with a Hamilton Spinrode pH-probe (reference system: Ag/AgCl, electrolyte: 3 M KCl, diaphragm: ceramic, sensitivity: 58 mV / pH unit at 25 °C). The pH-meter was calibrated before each experiment to check the response of the electrode with two buffer solutions purchased from Fisher Scientific: phthalate pH 4.01 and phosphate pH 7.01 solutions.

3.2.1.3. 'Titration' Experiments

For 5, 10 and 20 mmol L⁻¹ samples, the required amount of Fmoc-dipeptide was directly suspended into 2 mL of HPLC grade water. Sodium hydroxide (0.5 M, volumes are indicated in Table 3.2) was added to the aqueous suspensions of Fmoc-dipeptide until pH 10.5 was reached. The samples were vortexed and sonicated for 1 minute to fully dissolve the modified peptide. For less concentrated samples, 5 mmol L⁻¹ samples at pH 10.5 were used as stock solutions and diluted to the desired concentration in a final volume of 2 mL. The pH of the final solutions was then adjusted to pH 10.5. The 'titration' experiments were performed by step-wise addition of small volumes of diluted HCl (0.085 M), up to a total added volume of 750 µL. The volumes added at each step were adjusted appropriately during the titrations; for example 2 µL per step at high pH whilst volumes of up to 60 µL per step at lower pH, towards the end of the experiments. After each addition the samples were heated to 75–80 °C for one minute, vortexed, sonicated, and subsequently cooled back to room temperature using a water bath. pH values were recorded before and after heating of the samples. The samples were deemed fully mixed when no significant difference (± 0.3 pH unit) was observed between the two pH measurements. As a control, water was also titrated using the same methodology described above; that is, NaOH was added to the water in order to bring the pH of the solution to 10.5 and then HCl was added step-wise.

Table 3.2. Typical volume of NaOH needed to bring the pH of the solution to 10.5 depending on the concentration of Fmoc-dipeptide.

Sample concentration / mmol L ⁻¹	0 (H ₂ O)	0.01	0.1	1	5	10	20
V _{NaOH} / μL	2	3	4	7	28	55	103

3.2.3. Transmission Electron Microscopy

3.2.3.1. Theory

Transmission electron microscopy employs smaller wavelengths than visible wavelengths, which enables observation of structures at high resolution ($\sim 1 \text{ \AA}$). The relative wavelength of an electron beam depends on the accelerating voltage applied (typically high tension of 100 kV corresponds to a wavelength of 0.037 \AA) [3]. This technique is based on the transmission of an electron beam when it travels through a specimen.

As shown in Figure 3.2, a filament (usually of tungsten) attached to a high voltage supply is electrically heated and produces electrons that are subsequently accelerated between their source and the anode. Emerging from the electron gun, the electron beam is focused by electromagnetic fields onto the sample through condenser lenses, providing sufficient illumination for its visualisation. After passing through the specimen, the transmitted beam is focused by the objective lens, which supplies an initial enlarged image. This intermediate image of the sample is then magnified further through the projector lenses, where the electron beam is refocused. The final magnified image, which consists of variations of electron density, can be transmitted to a detector such as a charge-coupled device (CCD), to a photographic emulsion or projected onto a fluorescent sulphide-based (typically a mixture of zinc and cadmium sulphides) viewing screen [4].

The carbon coated grids on which the samples are loaded and organic specimen themselves have similar electron density. To improve contrast, samples often require metal shadowing or staining. Solutions of heavy metal salt such as phosphotungstic acid or uranyl acetate are commonly used to stain thin specimens [4]. While positive staining requires substantial sample preparation – fixation, dehydration and embedding – (that might considerably alter the microstructures) and involves chemical interaction between the specimen and the stain, negative staining is relatively quick and simple and is not specific to the sample. Negative staining is therefore widely used. This method provides good enhancement of the sample density, however it can be the origin of artefacts, since the stain can deposit on the surroundings of the structures, increasing their apparent size. As TEM experiments have to

be carried out under high vacuum, sample desolvation is necessary prior to observation. This step in the sample preparation can also cause the structures in solution to collapse or to shrink upon drying.

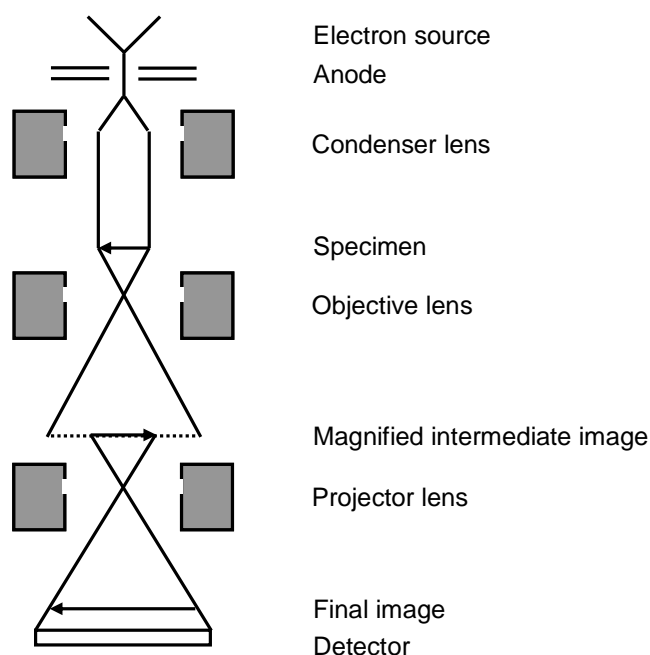


Figure 3.2. Schematic representation of an electron microscope (adapted from [5]).

3.2.3.2. Experimental procedure

Transmission electron microscopy was performed using a JEOL 1220 transmission electron microscope connected to a high resolution (up to 3 \AA pixel^{-1} resolution) Gatan Orius CCD camera. A carbon coated copper grid (400 mesh, Agar Scientific) was glow discharged for 30 seconds then placed on $10 \mu\text{L}$ of sample for 15 seconds. After blotting on Whatman 50 filter paper, the loaded grid was washed in double distilled water for 30 seconds and blotted. The sample was then stained with $10 \mu\text{L}$ of 2 % (w/v) uranyl acetate (centrifugated for 5 minutes beforehand) for 1 minute and blotted for 10 seconds. The grid was inserted in the microscope through a sample holder and subjected to high vacuum. Images were subsequently taken at an accelerating voltage of 100 kV.

3.2.4. X-Ray Scattering

3.2.4.1. Theory

X-rays are electromagnetic radiation with wavelengths, λ , in the order of angstroms (typically $0.5\text{--}2.5 \text{ \AA}$ for X-ray crystallography) [6]. Since periodic distances within matter are also typically of this order of magnitude, the resolution provided by X-rays is therefore

adequate for investigating the structure of materials and self-assembled morphologies [7]. X-ray diffraction techniques are mainly used to study crystalline compounds that are characterised by the regular repeat of three-dimensional arrays of atoms.

For laboratory-scale experiments X-rays are generated by an X-ray tube, in which electrons impact upon a target metal such as copper (for more details about electron production, see section 3.2.3.1). The resultant radiation has a wavelength, λ , of 1.5418 Å.

A beam of X-rays can be regarded as a stream of photons, the energy, E , of each X-ray photon being defined as:

$$E = \frac{hc}{\lambda} \quad \text{Equation 3.6}$$

where h is Planck's constant and c is the speed of light. During sample irradiation, a monochromatic beam of X-rays, the direction of which is defined by the incident unit vector, S_i , penetrates the matter and interacts with electrons surrounding the atoms. Although part of the incident radiation is absorbed by the material or directly transmitted, a fraction of the beam is scattered by the molecules and reemitted in another direction following the scattered unit vector, S_s . This reemission can either be done in an elastic (without energy loss) or inelastic (with energy loss) manner. Here, we will focus on the elastic phenomenon which implies $|S_i| = |S_s|$.

The scattering geometry is characterised by the scattering vector, s , the magnitude of which is given by:

$$|s| = s = \frac{2 \sin \theta}{\lambda} \quad \text{Equation 3.7}$$

As illustrated in Figure 3.3, scattering of X-rays by a crystalline sample – which is regarded as a stack of parallel crystallographic planes separated by a distance, d – occurs according to Bragg's law:

$$\lambda = 2d \sin \theta \quad \text{Equation 3.8}$$

where θ represents the angle of incidence.

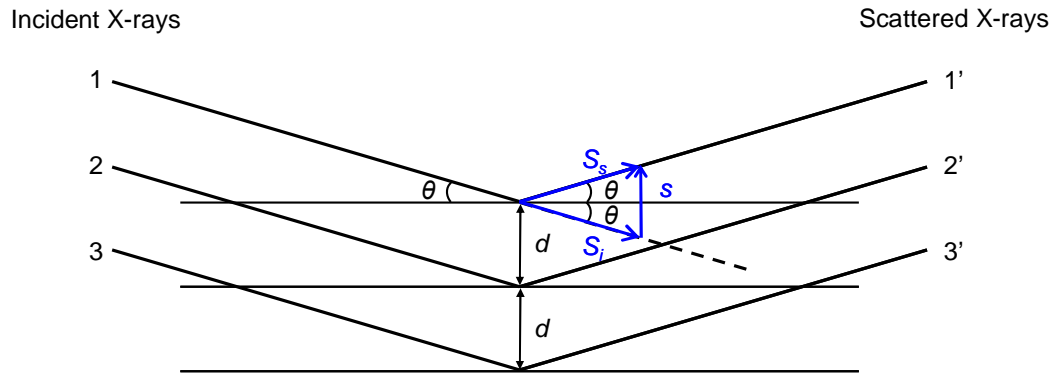


Figure 3.3. Schematic representation of X-rays scattering according to Bragg's law (adapted from [8]).

The scattered X-rays reach a (one- or two-dimensional) detector where their energy is converted into an electric current, which is subsequently transformed into voltage pulses. These pulses can be counted in order to measure the intensity of the X-rays scattered as a function of the scattering angle, θ [8]. Crystalline materials produce sharp patterns due to diffraction whereas amorphous samples usually lead to the detection of broad peaks. Data are commonly presented as a function of the radial scattering vector, q , the magnitude of which is defined as follows:

$$q = 2\pi s \quad \text{Equation 3.9}$$

and can also be written:

$$q = \frac{4\pi}{\lambda} \sin \theta \quad \text{Equation 3.10}$$

By combining Equations 3.8 and 3.10, the distance between the planes d can be determined through the following equation:

$$d = \frac{2\pi}{q} \quad \text{Equation 3.11}$$

X-ray scattering experiments can be undertaken in different configurations depending on the source-detector distance and therefore on the range of angles of incidence accessible. Depending on θ , X-ray scattering can enable access to structural information at short distances (typically 0.1–1 nm, i.e. for wide angles) or provide information about order at long distances (typically 1–1000 nm, i.e. for small angles) [9]. Small angle neutron scattering (SANS) is frequently used as a complementary method to small angle x-ray scattering (SAXS) for structural investigations of self-assembled morphologies. Indeed, neutrons provide the same resolution as X-rays, however the neutrons interact with the nuclei of the atoms whereas the electrons interact with the electron cloud surrounding the atoms [7].

3.2.4.2. Experimental Procedure

Solvent scattering can be an issue for water based materials such as hydrogels, since water, their main component, has the particularity to have a broad, diffuse scattering overwhelming the scattering pattern of the sample, especially for low concentration samples. To bypass this concern, samples can be desolvated by freeze drying or dried as thin layers. This procedure is based on the assumption that the specimen are in a pseudo-crystalline state and that the molecular organisation is the same in the hydrated and dehydrated states. The powder diffraction spectra obtained this way enables the structural identification of the compounds depending on their scattering pattern [8].

WAXS experiments were conducted using 10 mmol L⁻¹ samples. Wet samples were spread onto glass slides as thin films and allowed to air-dry for 48 hours prior to data collection. Experiments were performed on a Philips X'Pert diffractometer equipped with a copper source, applying scans from Bragg angles of 1° to 33°.

3.2.5. Fourier Transform Infrared Spectroscopy

3.2.5.1. Theory

The infrared spectral range is composed of three groups: near IR ($\lambda = 1\text{--}2.5\ \mu\text{m}$), mid IR ($\lambda = 2.5\text{--}25\ \mu\text{m}$) and far IR ($\lambda > 25\ \mu\text{m}$). Infrared spectroscopy measurements are usually undertaken in the mid IR frequency range i.e. between 4000 and 400 cm⁻¹.

Fourier transform infrared (FT-IR) is a vibrational spectroscopy technique that gives access to the conformational and structural organisation of the studied systems. Since vibrational interactions occur with a characteristic frequency that depends on the type of chemical bonds, the atoms' mass and the molecular environment FT-IR can provide information about the type of bonds existing within molecules or interactions between molecules.

A molecule composed of N atoms has $3N$ degrees of freedom that can be described in the three Cartesian coordinates. For a non-linear molecule, three degrees of freedom are associated to the translational motion of the molecule and three others to its rotational motion. The number of vibrational degrees of liberty hence is equal to $(3N - 6)$. Among these possibilities the most widely known molecular movements are stretching (symmetrical and asymmetrical) and bending (in and out of plane) vibrations. When a compound is subjected to infrared radiation, an interaction between the electromagnetic wave and chemical bonds of the molecules occurs, which can result in a transfer of energy.

The material can only absorb the radiation energy and therefore be infrared (IR)-active at two conditions: the radiation and the chemical bonds of the molecules must oscillate at similar frequencies and the radiation must cause a change in the dipole moments (i.e. in the charge distribution) of the bonds. In the reverse case, the vibrational modes would be IR-inactive [10].

Characteristic functional groups give rise to vibrational bands in distinctive frequency ranges on IR spectra regardless of the molecule in which they belong. However these bands can be shifted depending on the environment of the molecules, which is whether the chemical bonds are involved in intra or intermolecular interactions for instance. Hydrogen bonding, which plays an important role in self-assembly processes, typically leads to a shift to lower frequencies of stretching vibrations and to an increase in the band width. Thus, FT-IR is particularly adapted to the study of peptide structures as peptide amide bonds absorb infrared radiation at characteristic frequencies (amide bands). Different amide bands exist but in practice the amide I band is primarily used to identify protein and peptide structures as its frequency values are associated with different widely known secondary structures (Table 3.3) [11,12]. This band, which appears at $\sim 1650\text{ cm}^{-1}$, is intense and is related to the stretching of the C=O bond.

Table 3.3. Amide I frequency values (in cm^{-1}) generally associated with some secondary structures in water and deuterated water (adapted from [11,12]).

Type of conformation	H ₂ O	D ₂ O
α -helix	1648–1657	1642–1660
β -sheet	1612–1641	1615–1638
Antiparallel β -sheet	1670–1695 (weak)	1672–1694 (weak)
β -turn	1662–1686	1653–1691
Random coil	1640–1657	1639–1654

The main disadvantage of IR spectroscopy is the large absorption peak of water which appears in the middle of the amide I band at 1650 cm^{-1} . To avoid this issue, samples are usually prepared in deuterated water (D₂O). As illustrated in Table 3.3, this method causes the infrared signal to shift towards lower frequencies.

Fourier transform spectrometers are commonly used as they are based on the use of a Michelson interferometer, which enables the full spectral range to be recorded in one measurement [1].

Sample analysis can be conducted in various ways using infrared spectroscopy: on hydrated samples or dry powder, in transmission or reflection.

For reflection experiments (e.g. by attenuated total reflection (ATR)) measurements are based on the difference in refractive index, n , of the two media: the crystal and the sample. The crystal such as diamond or zinc selenide (ZnSe) is characterised by a high refractive index ($n = 2.4$ for diamond and ZnSe) whereas the sample has a lower refractive index. As illustrated in Figure 3.4, when an incident beam reaches the interface between the two media with a particular angle, it is totally reflected. However, an evanescent wave extends in the less dense medium and is attenuated due to absorption by the sample before being completely reflected. The light beam can be reflected once using a ‘single bounce’ accessory or several times using a ‘multiple bounce’ device in order to increase the signal-to-noise ratio by accumulating a succession of total reflections.

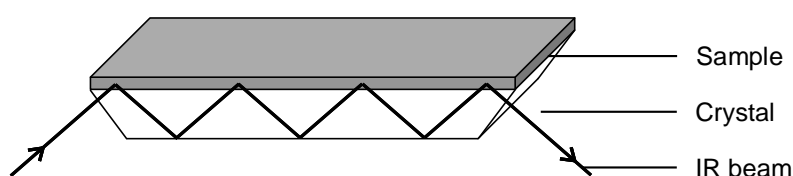


Figure 3.4. Schematic representation of a multiple bounce ATR-FTIR crystal-sample setup.

For transmission experiments the sample is deposited between windows of IR non-absorbent materials such as potassium bromide (KBr) or sodium chloride (NaCl). A spacer of known thickness can be inserted between the windows allowing quantitative measurements to be made.

3.2.5.2. Experimental Procedure

Multiple bounce ATR-FTIR experiments were undertaken using samples prepared in deuterated water. Spectra were recorded on a Thermo Nicolet 5700 spectrometer equipped with a trough plate comprising of a ZnSe crystal, which permitted 12 reflections with a 45° angle of incidence. The samples were spread directly on the surface of the trough plate. Spectra were acquired in the $4000\text{--}400\text{ cm}^{-1}$ range with a resolution of 4 cm^{-1} over 128 scans. The deuterated water spectrum was used as background and subtracted from all spectra (software used: Omnic version 7.2, Thermo Electron Corporation).

Single bounce ATR-FTIR experiments were performed on the commercial Fmoc-peptide powders and on thin films. Spectra were recorded on the same spectrometer as above equipped with a platter comprising of a diamond plate, which led to a 42° angle of incidence. The samples were pressed in intimate physical contact with the plate. Spectra were acquired using the same parameters as above. The ambient air spectrum was used as background and subtracted from all spectra.

3.2.6. Fluorescence Spectroscopy

3.2.6.1. Theory

Fluorescence spectroscopy is an optical method allowing the environment of aromatic molecules to be probed, providing insight about their structure, dynamics and the manner in which they interact with each other. When excited by visible or near ultraviolet (UV) radiation range, some compounds re-emit all or part of the energy absorbed in the form of light. This luminescent phenomenon is at the origin of fluorescence.

The Jablonski diagram shown in Figure 3.5 describes the different deactivation processes that can occur after absorption of a photon. First, absorption of a photon arises when molecules are excited: initially in the ground electronic state S_0 , molecules reach the excited electronic state S_2 . Then molecules relax by vibrational deactivation (internal conversion) to the lowest vibrational energy level S_1 without photon emission (non-radiative transitions). At this stage, energy is released in the form of heat. After this step molecules can return to S_0 vibrational levels at longer wavelength, by releasing energy in a radiative way (i.e. with emission of photon) either directly by fluorescence or via intersystem crossing to an excited triplet state T_1 by phosphorescence. Both phenomena are characterised by different time scale that is the average time between excitation and return to the ground state. Fluorescence has a typical lifetime of a few nanoseconds whereas phosphorescence is characterised by a lifetime of the order of the milliseconds to seconds [13].

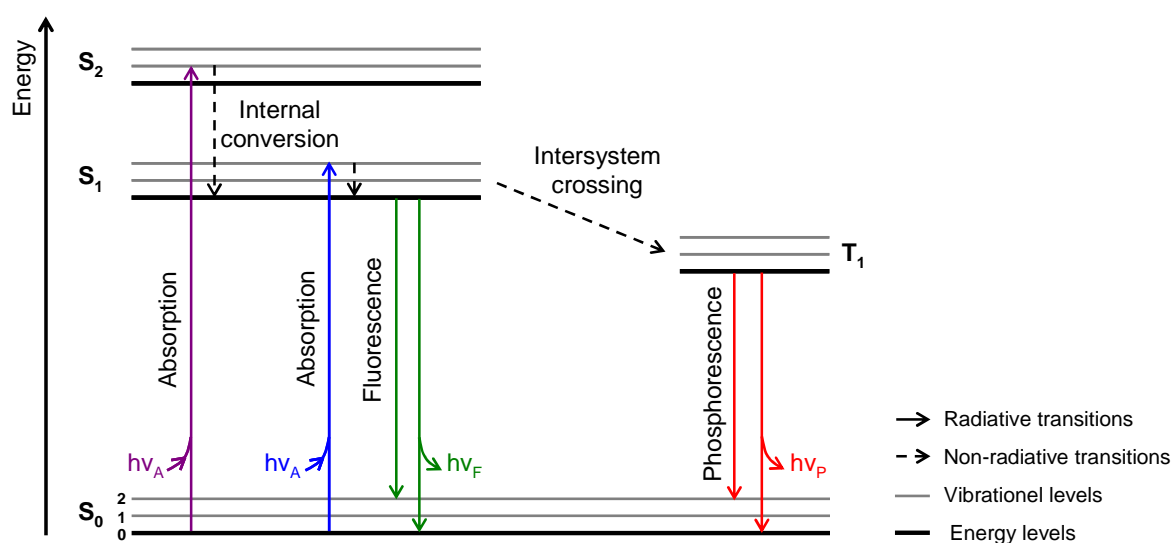


Figure 3.5. Simplified version of the Jablonski diagram (adapted from [13]).

In a spectrofluorometer (Figure 3.6), the light source (typically a xenon lamp) produces polychromatic light which passes through an excitation monochromator, allowing a certain

range of wavelengths to strike the sample and induce its fluorescence. As fluorescent samples behave like light sources which emit in all directions, the emitted radiation has to be separated from the incident radiation. Hence, the emitted light is measured at a right angle to the incident beam through an emission monochromator, enabling a narrow band of wavelengths to be detected for measurements [1].

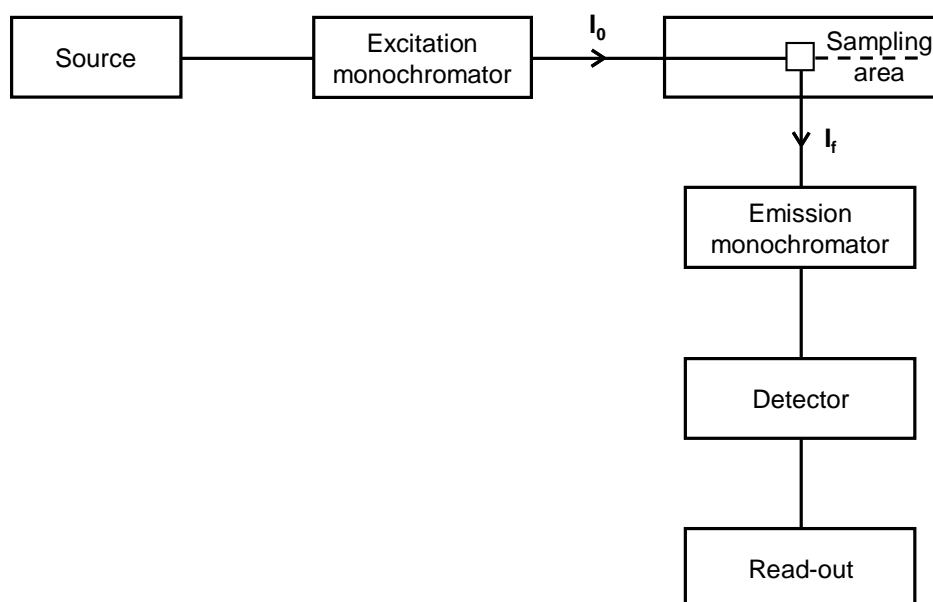


Figure 3.6. Layout of the different components of a typical fluorescence spectrometer, with I_0 the intensity of the incident beam and I_f the intensity of fluorescence (adapted from [14]).

Fluorescence phenomenon usually occurs from molecules containing multiple conjugated double bonds or aromatic compounds. The latter are generally defined as cyclic systems containing $(4n + 2)$ π -electrons according to the Hückel rule. Fluorescence can be enhanced in the presence of electron donor groups such as hydroxyl ($-\text{OH}$) and amine ($-\text{NH}_2$) functions. The intensity of the fluorescent signal also depends on the temperature, concentration, pH conditions and solvent nature [1].

Peptides can contain intrinsic chromophores since certain amino acids such as phenylalanine, tryptophan and tyrosine side chains contain aromatic groups. Extrinsic chromophores can also be introduced to peptides by chemically modifying them with fluorescent moieties.

3.2.6.2. Experimental Procedure

Fluorimetry experiments were undertaken using a Perkin-Elmer LS55 luminescence spectrometer equipped with a Julabo F25 temperature control device. After their preparation, the samples were transferred into PMMA disposable cuvettes of 1 cm in width

(Fisher Scientific) and left at 4 °C overnight. Emission spectra (excitation at 265 nm) were acquired at 25 °C in the 300–600 nm range with a scan speed of 300 nm min⁻¹ using FL WinLab software.

3.2.7. Rheology

3.2.7.1. Theory

Rheology is defined as the study of the deformation (e.g. elasticity, viscosity, plasticity, etc.) and flow of matter, whether it is in a solid, liquid or gas form [15].

Stress, σ , is defined as a force per unit area (Pa). The application of a stress to a material results in a relative deformation called strain, γ . When a stress is imparted within the linear regime (i.e. where stress is proportional to strain) the subsequent deformation of the material does not affect its structural properties. This behaviour is usually observed at low deformation [16]. As illustrated in Figure 3.7 one way to apply stress to matter is to shear it by applying a stress parallel to the plane on which the material lies on.

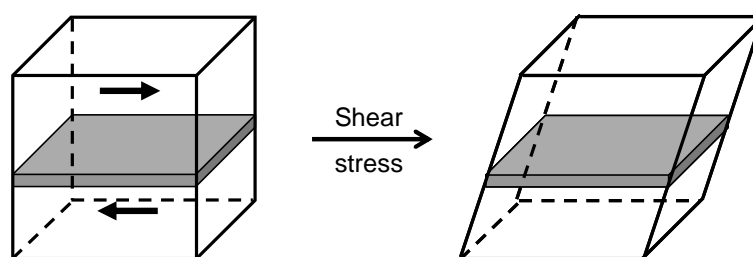


Figure 3.7. Schematic representation of shear stress applied on a material.

Elasticity is characteristic of solid materials. A perfect solid deforms instantaneously under external forces and returns to its original shape when the stress is removed. In the linear regime, such solid response to an applied stress is described by Hooke's law:

$$\sigma = G\gamma \quad \text{Equation 3.12}$$

where G is the rigidity modulus or shear modulus (constant) and γ is the shear strain.

On the contrary, viscosity is a characteristic of liquid materials. Under the smallest stress a pure liquid flows slowly and does not revert to its initial dimensions after release of the applied force following Newton's law:

$$\sigma = \eta\dot{\gamma} \quad \text{Equation 3.13}$$

where η is the viscosity (constant) and $\dot{\gamma}$ is the shear strain rate or shear rate.

However these particular examples represent the two extremes of behaviour from a rheological point of view [17]. Many real materials, including gels, are characterised by the

coexistence of both elastic and viscous properties and are therefore defined as viscoelastic. There are two approaches to the investigation of the rheological properties of such materials. Small deformation measurements are usually employed to determine the viscoelastic properties of the material upon shear stress or strain whereas large deformation measurements are typically used to assess the mechanical behaviour of the gel up to failure upon extensional stress or strain [18].

Oscillatory rheology is typically used to make dynamic measurements which involve the harmonic variation of stress and strain with time. If the stress applied at a particular frequency oscillates with time then the resulting strain will also do so with a delay in phase called phase angle, δ . However for perfect elastic solids the stress is in phase with the strain (i.e. $\delta = 0 \text{ rad s}^{-1}$) whereas it is $\pi/2 \text{ rad s}^{-1}$ ahead of the strain for purely viscous liquids. Figure 3.8 represents the two wave-forms varying in a sinusoidal manner with an angular frequency, ω (rad s^{-1}), defined as:

$$\omega = 2\pi f \quad \text{Equation 3.14}$$

where f is the frequency of oscillation (Hz).

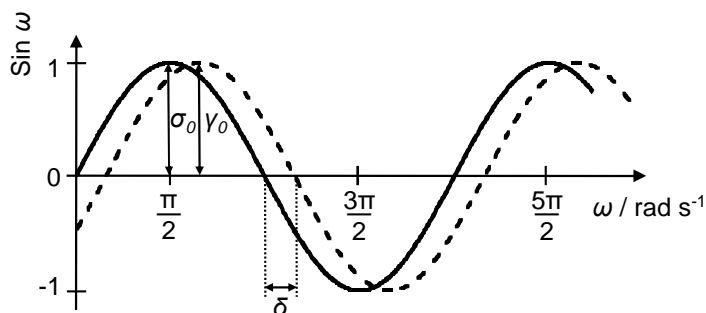


Figure 3.8. Wave-forms for oscillatory stress input and strain output: shear stress (solid line) in advance by angle δ compared to the shear strain response (dashed line) for a viscoelastic material (adapted from [15]).

The determination of the complex shear modulus, G^* (Pa), defined as follows, allows the full characterisation of the studied material:

$$G^* = \frac{\sigma_0}{\gamma_0} \quad \text{Equation 3.15}$$

where σ_0 and γ_0 are the stress amplitude and the strain amplitude respectively.

This value can also be decomposed as:

$$G^* = G' + iG'' \quad \text{Equation 3.16}$$

where G' refers to the elastic modulus and G'' corresponds to the viscous modulus [15].

The elastic modulus or storage modulus (Equation 3.17) reflects the amount of energy stored during (and released after) deformation and characterise the solid-like contribution.

The viscous modulus or loss modulus (Equation 3.18) measures the energy dissipated during the experiment and characterise the fluid-like contribution. Both dynamic moduli can be expressed as a function of the complex shear modulus and the phase angle as follows:

$$G' = G^* \cos \delta \quad \text{Equation 3.17}$$

$$G'' = G^* \sin \delta \quad \text{Equation 3.18}$$

The damping factor, $\tan \delta$, enables the viscoelasticity of a material to be quantified since it is defined as the ratio of the energy dissipated to the energy stored in the material during one cycle of oscillation:

$$\tan \delta = \frac{G''}{G'} \quad \text{Equation 3.19}$$

The main advantage of using rheometers with forced oscillations is that they cover a wide frequency range, typically from 10^{-3} to 10^3 s^{-1} [15]. The material is contained by capillary forces between a parallel-plate or a concentric cylinder and a flat stationary plate. In the second case, a small angle is formed between the cone and the fixed plate. During the measurements, the mobile geometry oscillates in a sinusoidal manner with time and the motion is transmitted to the fixed plate through the material [15].

3.2.7.2. Experimental Procedure

Mechanical properties were assessed using a stress-controlled rheometer (Bohlin C-VOR) equipped with a Peltier device (Bohlin Instruments) to control temperature. Cone-plate (40 mm diameter, 4°) and parallel-plate (40 mm diameter) geometries were used for stiff and weak gels respectively. To ensure the measurements were made in the linear regime, amplitude sweeps were performed and showed no variation in G' and G'' up to a strain of 1% (Appendix B). The dynamic moduli of the hydrogel were measured as a function of frequency in the range $0.01\text{--}100 \text{ rad s}^{-1}$ with a strain of 1%. The samples were allowed to rest for a few minutes after loading and the measurements were undertaken without any pre-shear conditioning. To keep the sample hydrated, a solvent trap was used and the atmosphere within the sample chamber was saturated with water. Unless otherwise stated the experiments were performed at 25°C and repeated at least three times (each time on new samples) to ensure reproducibility. The standard deviation of multiple experiments is represented by error bars in the dynamic frequency sweeps.

3.3. REFERENCES

1. Rouessac, F. and Rouessac, A., *Chemical analysis: Modern instrumental methods and techniques*. **2000**, Chichester: Wiley.
2. Westcott, C.C., *pH measurements*. **1978**, New York: Academic Press.
3. Thomas, G. and Goringe, M.J., *Transmission electron microscopy of materials*. **1979**, New York: Wiley.
4. Wischnitzer, S., *Introduction to electron microscopy*. 2nd ed. **1970**, New York: Pergamon Press.
5. Watt, I.M., *The principles and practice of electron microscopy*. **1985**, Cambridge: Cambridge University Press.
6. Guinier, A., *X-ray diffraction in crystals, imperfect crystals, and amorphous bodies*. **1963**, San Francisco: W.H. Freeman.
7. Roe, R.J., *Methods of X-ray and neutron scattering in polymer science*. **2000**, New York: Oxford University Press.
8. Jenkins, R. and Snyder, R.L., *Introduction to X-ray powder diffractometry*. **1996**, New York: Wiley.
9. Narayanan, T., *Synchrotron small-angle X-ray scattering*. *Soft Matter Characterization*, **2008**, 899-952.
10. Günzler, H. and Gremlich, H.-U., *IR spectroscopy: An introduction*. **2002**, Weinheim: Wiley-VCH.
11. Pelton, J.T. and McLean, L.R., *Spectroscopic methods for analysis of protein secondary structure*. *Analytical Biochemistry*, **2000**, 277 (2), 167-176.
12. Barth, A. and Zscherp, C., *What vibrations tell about proteins*. *Quarterly Reviews of Biophysics*, **2002**, 35 (4), 369-430.
13. Lakowicz, J.R., *Principles of fluorescence spectroscopy*. 3rd ed. **2006**, Boston: Springer.
14. Rendell, D. and Mowthorpe, D.J., *Fluorescence and phosphorescence spectroscopy*. **1987**, Chichester: Wiley.
15. Barnes, H.A. and Howard, A., *An introduction to rheology*. **1989**, Amsterdam: Elsevier.
16. Goodwin, J.W. and Hughes, R.W., *Rheology for chemists: An introduction*. **2000**, Cambridge: Royal Society of Chemistry.
17. Houwink, R. and De Decker, H.K., *Elasticity, plasticity and structure of matter*. 3rd ed. **1971**, London: Cambridge University Press.
18. Clark, A.H. and Ross-Murphy, S.B., *Structural and mechanical properties of biopolymer gels*. *Advances in Polymer Science*, **1987**, 83, 57-192.

Solution Behaviour Investigation for the Development of a Controlled Sample Preparation Method*

4.1. ABSTRACT

Fmoc-dipeptide hydrogels initially prepared by sequential pH change were found to be relatively stiff. However the rigidity of the scaffolds appeared to be related to the presence of aggregates within the samples. In order to gain a better understanding of the onset of the molecular self-assembly, the ionisation behaviour of the molecules was investigated and ‘titrations’ were carried out on the systems. The sample preparation method was accordingly modified, leading to the formation of reproducible and more homogeneous hydrogels.

4.2. INTRODUCTION AND OBJECTIVES

The main focus of our work was to characterise the self-assembling behaviour of the four peptide derivatives presented in Figure 4.1. These molecules are based on the pairing of two amino acids, phenylalanine and glycine, modified with an Fmoc group.

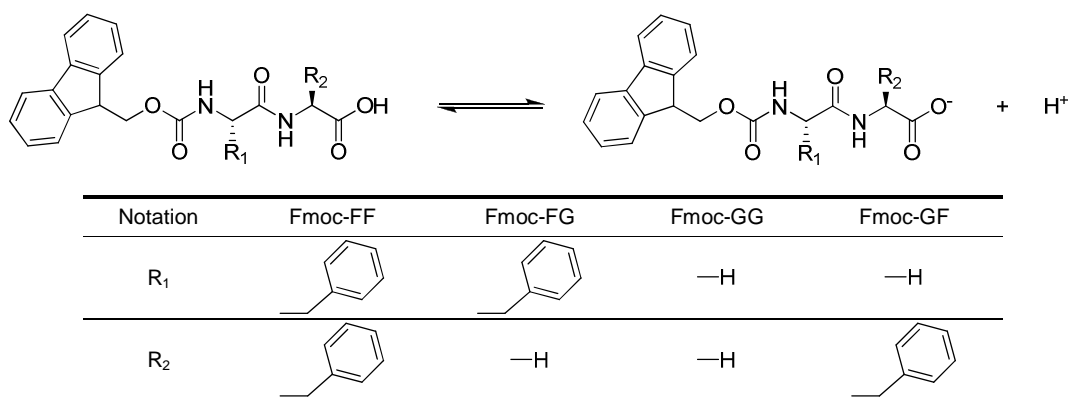


Figure 4.1. Equilibrium between Fmoc-dipeptide neutral (acid) and ionised (conjugated base) forms and notation.

* Part of this chapter has been published as: Smith, A.M., Williams, R.J., Tang, C., Coppo, P., Collins, R.F., Turner, M.L., Saiani, A., and Ulijn, R.V. *Fmoc-diphenylalanine self-assembles to a hydrogel via a novel architecture based on π - π interlocked β -sheets*. *Advanced Materials*, **2008**. 20(1): p. 37-41 and Tang, C., Smith, A.M., Collins, R.F., Ulijn, R.V., and Saiani, A. *Fmoc-diphenylalanine self-assembly mechanism induces apparent pK_a shifts*. *Langmuir*, **2009**. 25(16): p. 9447-9453.

Samples were initially prepared as described previously by Jayawarna *et al.*, using a sequential pH change method [1]. The pH of aqueous peptide suspensions was raised by addition of sodium hydroxide to ionise and therefore solubilise the molecules. Hydrogel formation was pH-triggered by subsequent adjustment of the pH with hydrochloric acid. However the hydrogels generated displayed heterogeneity. In order to rationalise and ameliorate the formation of the self-assembled scaffolds, ‘titrations’ were undertaken, providing a better understanding of the molecules behaviour in solution.

The objectives of this section are to investigate the different aspects of the current sample preparation method that can be perfected and improve them. Ultimately materials resulting from a modified method should be reproducible and reliable enough to perform full accurate characterisation.

4.3. RESULTS AND DISCUSSION

4.3.1. Preliminary Study: Sequential pH Change Method

As previously described [1], samples were prepared using a sequential pH change method to induce gelation from solutions of Fmoc-dipeptides. Aqueous suspensions of peptide derivatives were first turned into clear solutions by supplementing the samples with NaOH. The pH of the solutions was then adjusted by addition of HCl, drops of which were constantly dispersed within the samples by vortexing until gels were obtained. Amounts of NaOH and HCl to add were simply assessed in a visual manner. No pH control was undertaken at this stage. As soon as hydrogels started to form, the samples were placed at 4 °C for ~ 12 hours before characterisation.

Fmoc-FF, Fmoc-FG and Fmoc-GG all formed turbid hydrogels at different pH values (about pH 7.5, pH 5 and pH 4 respectively) whereas precipitates rather than self-supported hydrogels were obtained under all pH conditions for Fmoc-GF (Figure 4.2).

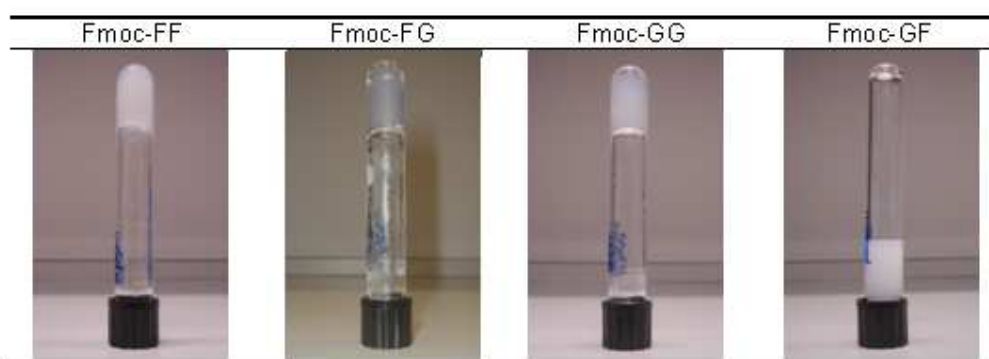


Figure 4.2. Macroscopic appearance of Fmoc-dipeptide hydrogels and precipitate formed by sequential pH change: Fmoc-FF (pH ~ 7.5), Fmoc-FG (pH ~ 5), Fmoc-GG (pH ~ 4) and Fmoc-GF (pH ~ 5) samples at 10 mmol L⁻¹.

The viscoelastic properties of the hydrogels formed after ~ 12 hours storage at 4°C were assessed using oscillatory rheology. Figure 4.3 A shows the mechanical properties obtained at room temperature for Fmoc-FF ($\text{pH} \sim 7.5$), Fmoc-FG ($\text{pH} \sim 5$) and Fmoc-GG ($\text{pH} \sim 4$) at 10 mmol L^{-1} .

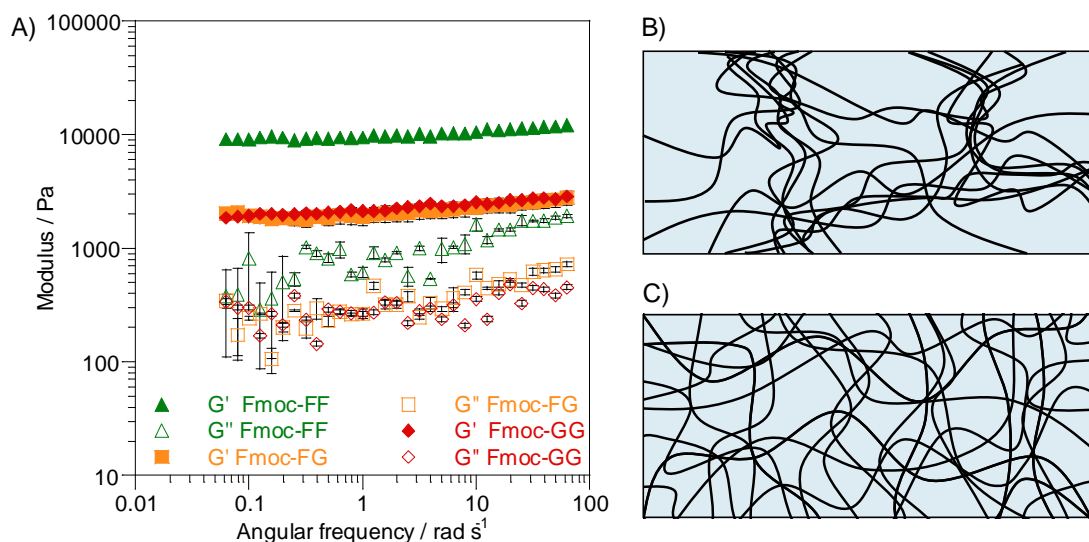


Figure 4.3. A) Dynamic frequency sweep of Fmoc-dipeptides hydrogels formed by sequential pH change: Fmoc-FF ($\text{pH} \sim 7.5$), Fmoc-FG ($\text{pH} \sim 5$) and Fmoc-GG ($\text{pH} \sim 4$) samples at 10 mmol L^{-1} . Schematic representation of B) a heterogeneous fibrillar network containing kinetically trapped aggregates and C) a homogeneous fibrillar network.

For all three samples G' was approximately one order of magnitude higher than G'' with both moduli nearly independent of frequency between 0.01 and 100 rad s^{-1} . Such behaviour indicated the materials were all elastic rather than viscous, confirming their gel-like nature. Cryo-scanning electron microscopy (cryoSEM) of the gels revealed they were constituted of rigid, physically cross-linked fibrillar networks [1]. Fmoc-FF hydrogels displayed particularly high storage modulus values ($G' \sim 10000 \pm 900 \text{ Pa}$) [2] compared to Fmoc-FG and Fmoc-GG gels ($G' \sim 1800\text{--}2900 \text{ Pa}$). This significant difference between the systems could be related to morphologically and structurally distinct fibrillar networks, suggesting that simple variations in the peptide sequence of the molecules could enable to tune the stiffness of the self-assembled structures.

The three systems were characterised by large storage moduli given the low concentration of peptide. G' values of different orders of magnitude have been reported for peptide based hydrogels depending on the kinetics of the self-assembly process [3,4]. By increasing the ionic strength of solutions used, Pochan *et al.* [3] were able to accelerate the self-assembly kinetics of their peptides. The addition of salts resulted in the formation of networks with higher cross-link density leading to stiffer hydrogels (Figure 4.3 B). G' values were found to increase from $\sim 100 \text{ Pa}$ to $\sim 3000 \text{ Pa}$ when 20 mM and 400 mM of salt solutions, were

employed respectively. Investigating enzyme-triggered β -peptide hydrogels, Xu *et al.* [4] have also shown that the morphology of the network generated depends strongly on the kinetics of hydrogelation. Using low concentrations of enzyme, thin, uniform fibrils were formed slowly resulting in relatively weak hydrogels with G' of ~ 300 Pa (Figure 4.3 C). On the other hand, when higher concentrations of enzyme were used, the formation of nanofibrils was found to be almost instantaneous, leading to the formation of heterogeneous bundles of fibres resulting in hydrogels with G' of ~ 4000 Pa (Figure 4.3 B). From these observations we hypothesised that the high modulus values obtained for Fmoc-FF, Fmoc-FG and Fmoc-GG resulted from the presence of kinetically trapped aggregates formed during the sample preparation (see section 4.3.2), which reinforced the mechanical properties of the materials (Figure 4.3 B). The existence of such heterogeneities in the micrometre size was confirmed by the turbid aspect of the samples.

Gels formed from the studied Fmoc-dipeptides were also found not to be particularly stable with time. Within a couple of hours at room temperature, the hydrogels would typically begin to flow. The kinetics of gel alteration were slower at 4°C : after a few days, expulsion of water from the samples accompanied by an increase of their turbidity was typically observed for Fmoc-FF and Fmoc-FG whereas precipitation started to occur in Fmoc-GG hydrogels. These macroscopic aspect alterations were accompanied by a change in pH. We believe such changes in aspect and pH were related to the presence of heterogeneities, probably arising from the addition of HCl during sample preparation. Indeed, addition of acid to the alkaline solutions led to the instantaneous formation of gel around the drops, where acid was locally relatively concentrated. As a consequence, the pH might not have been homogeneous through the specimen at this stage. It is likely that local acidity diffused slowly through the samples as the pH of the hydrogels was found to vary (± 0.6 pH units) during overnight storage at low temperature. Although the evolution of the pH with time has not been rigorously monitored, it was found to still shift after a few days. This observation suggested the systems were progressing towards an equilibrium state over a long period of time.

Scaffolds presenting interesting and promising mechanical properties were obtained from Fmoc-dipeptides. However these properties were found to be related to the presence of acid pockets that were causing heterogeneities within the hydrogels. Additionally, stability issues were encountered with samples prepared using the sequential pH change method. In order to perform full characterisation of the systems, reliable measurements on reproducible specimen were needed. To improve stability and homogeneity of the samples,

addition of NaOH and HCl had to be rigorously controlled. The solution behaviour of the systems was therefore investigated.

4.3.2. Towards a Controlled Sample Preparation Method

4.3.2.1. Sodium Hydroxide and Fmoc Loss

Addition of NaOH during the sequential pH change was uncontrolled. As a result the pH of the dissolved Fmoc-dipeptide solutions could reach high pH values (up to pH 11–11.5). Fmoc groups are known to be particularly instable under alkaline conditions [5], hence NaOH had to be added in a controlled manner. The minimum volumes of NaOH needed to dissolve the peptide derivatives were therefore assessed for the four Fmoc-dipeptides. Optimisation of the method revealed that all were fully dissolved from pH 10.5. At 10 mmol L^{-1} , all systems turned out to require an optimised volume of $\sim 55 \mu\text{L}$ of NaOH (0.5 M) to reach the solubility pH limit. To ensure that these conditions did not lead to significant hydrolysis of the carbamate and loss of the fluorenyl moiety (Figure 4.4), HPLC was used to estimate the cleavage percentage. Figure 4.6 shows the chromatograms obtained for a solution of Fmoc-FF in the presence of NaOH only (pH 10.5) 1 hour, 2 hours and 6 days after addition of the alkaline solution.

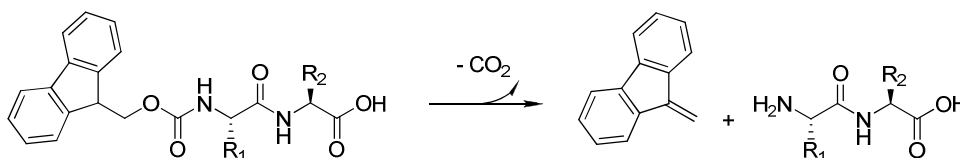


Figure 4.4. Cleavage of the Fmoc group from an Fmoc-dipeptide giving rise to a carbamate and a dipeptide.

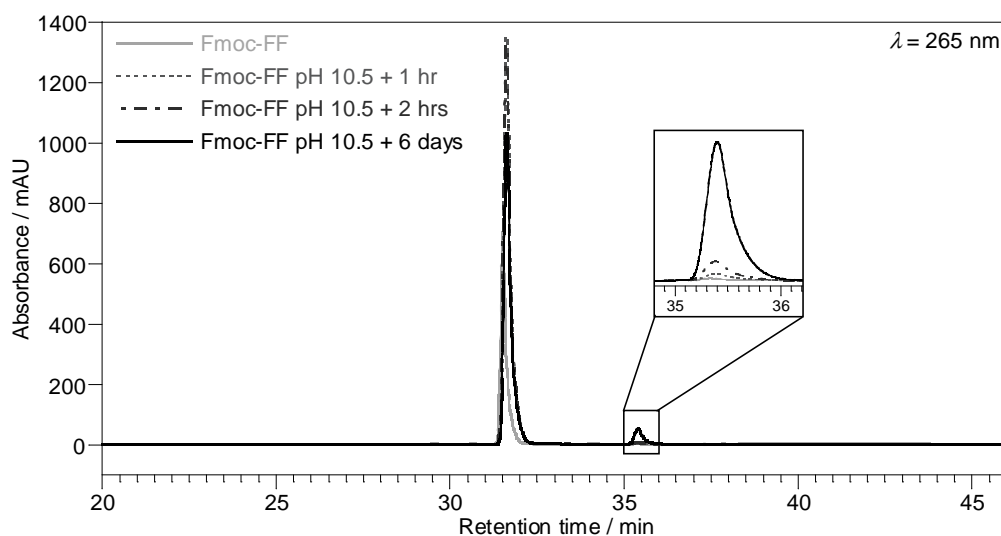


Figure 4.5. HPLC chromatogram of a diluted solution of Fmoc-FF at pH 10.5 as a function of time.

Comparing these chromatograms with the one corresponding to the solution of Fmoc-FF without NaOH shows that the elution peak at 31.5 minutes corresponds to Fmoc-FF molecules. In alkaline conditions Fmoc-dipeptides are expected to be cleaved and produce two additional components: the dipeptides and the carbamate groups. Being less hydrophobic the dipeptides were assumed to come off the column rapidly that is in the injection peak. The component eluted after 36.5 minutes was therefore ascribed to carbamate groups which are more hydrophobic. The molar percentage of Fmoc cleaved was estimated from HPLC analyses. After 1 hour, 2 hours and 6 days (144 hours) less than 1%, ~ 4% and ~ 30% of Fmoc groups were removed from Fmoc-FF respectively. It was assumed that comparable Fmoc cleavage occurred for the other Fmoc-dipeptides of interest. Since the specimens were not left in the presence of NaOH (pH 10.5) for more than 10 minutes during sample preparation, the proportion of molecules cleaved was negligible.

4.3.2.2. *Solution Behaviour*

Addition of HCl to alkaline solutions led to the formation of acid pockets that were related to the fibrillar network being mainly constrained in some domains of the samples. These strong junction points were difficult to completely disperse by simply vortexing the gels, hence the samples were heated following the addition of acid to dissolve the kinetically trapped aggregates. In order to obtain clear and homogeneous solutions, it was found that the optimum heating temperature was 75–80°C. As reported in Table 3.1, the heating time were adjusted depending on the systems.

To regulate the addition of HCl and control the pH during sample preparation, ‘titration’ experiments highlighting the ionisation behaviour of the molecules were performed on the Fmoc-dipeptides below and above their critical gelation concentration, at 1, 5, 10, and 20 mmol L⁻¹ with additional experiments at 0.01 and 0.1 for Fmoc-FF only (Figure 4.6). All experiments started at pH 10.5 (conditions at which the Fmoc-dipeptides were fully dissolved at all concentrations) following addition of NaOH. The samples’ pH variations were then recorded as a function of added HCl. Here the samples were heated after each addition of acid. Due to the strong and constant agitation applied, samples were liquid at all times during the ‘titration’ experiments. Water was also titrated in the same way as a control.

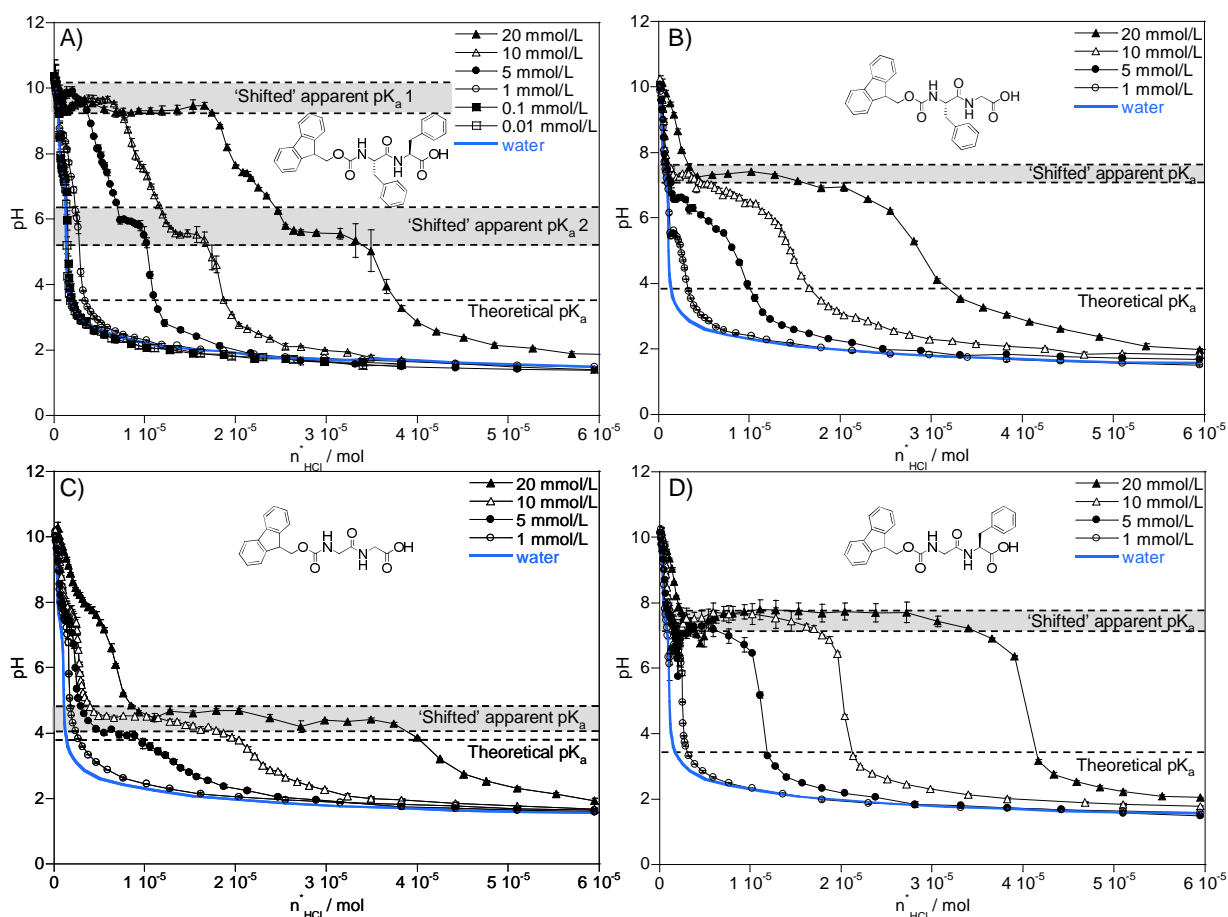


Figure 4.6. ‘Titration’ curves (pH vs. moles of added HCl) of water and **A)** Fmoc-FF at 0.01, 0.1, 1, 5, 10 and 20 mmol L⁻¹, **B)** Fmoc-FG, **C)** Fmoc-GG and **D)** Fmoc-GF samples at 1, 5, 10 and 20 mmol L⁻¹. The theoretical pK_a values of the Fmoc-dipeptides were assessed using SPARC web calculator (<http://ibmlc2.chem.uga.edu/sparc>).

At 0.01 mmol L⁻¹ Fmoc-FF was found to be soluble at all pH values. The ‘titration’ curve obtained at this concentration was similar to that of water. At 0.1 mmol L⁻¹ Fmoc-FF was found to be soluble at pH values above 7, while at lower pH values the peptide was found to precipitate. The overall pH variation as a function of added HCl was in this case also similar to that of water. For samples prepared at 1 mmol L⁻¹ and above, Fmoc-FF was found to be fully soluble at high pH (≥ 10.5) only. At this pH most of the Fmoc-FF molecules are expected to be ionised. When HCl was added to the solutions, the pH gradually dropped for all the samples (Figure 4.6 A). Once a pH of ~ 9.2 was reached, the pH of the 5, 10 and 20 mmol L⁻¹ samples was found to increase slightly to 9.5–10.2 and in the case of the 10 and 20 mmol L⁻¹ samples became constant. For the 1 mmol L⁻¹ sample, no increase in pH was observed and a transition was observed at a slightly lower pH of ~ 8.6. As the samples went through this first transition, they became slightly cloudy. Once the first transition was complete, the pH of all samples was found to decrease again with addition of HCl. The samples became more turbid as the pH decreased. At a pH of 6.2–5.2,

a second transition was observed and the pH of the 5, 10 and 20 mmol L⁻¹ samples was found to become constant. As the samples went through this second transition, a white precipitate appeared. For samples with pH values below 5, phase separation occurred with the emergence of a clear liquid phase at the top and a white precipitate at the bottom of the test tube when left at room temperature. As the pH was decreased further, the precipitation and phase separation were found to become more pronounced and rapid. At low pH (< 3), all the ‘titration’ curves were found to merge with the water ‘titration’ curve. The two transitions observed on the ‘titration’ curves of the 1, 5, 10 and 20 mmol L⁻¹ samples were more marked as the peptide concentration was increased. They are reminiscent of p*K*_a-type transitions. As we will see in Chapter 5, these two ‘shifted’ apparent p*K*_a transitions (p*K*_a 1 and p*K*_a 2, Figure 4.6 A) are related to two marked structural transitions resulting from the peptide self-assembly. As Fmoc-FF is a weak acid, at high pH we can assume in a first approximation that addition of one mol of HCl results in the neutralisation of one mol of Fmoc-FF⁻, its conjugated weak base (Figure 4.1). Assuming that at pH 10.5 (before addition of HCl) all molecules are ionised (Fmoc-dipeptide-COO⁻), the peptide degree of ionisation, α , can simply be written as:

$$\alpha = 1 - \frac{n_{HCl}}{n_{Fmoc-dipeptide-COOH}} \quad \text{Equation 4.1}$$

where n_{HCl} is the number of moles of HCl added corrected for the number of moles of HCl needed to titrate the water and $n_{Fmoc-dipeptide-COOH}$ is the number of moles of peptide present in the sample. In Figure 4.7, n_{HCl} is plotted as a function of $n_{Fmoc-FF}$ for the 1, 5 and 10 mmol L⁻¹ samples at three pH values: 8.9, just below the apparent p*K*_a 1 transition, 7 and 4.3, just above and below the apparent p*K*_a 2 transition, respectively. The degrees of ionisation derived from the slope of the fitted linear curve are given in the inset of Figure 4.7. As can be seen for the three samples, α is the same at a fixed pH, suggesting that the same processes are occurring in the concentration range investigated.

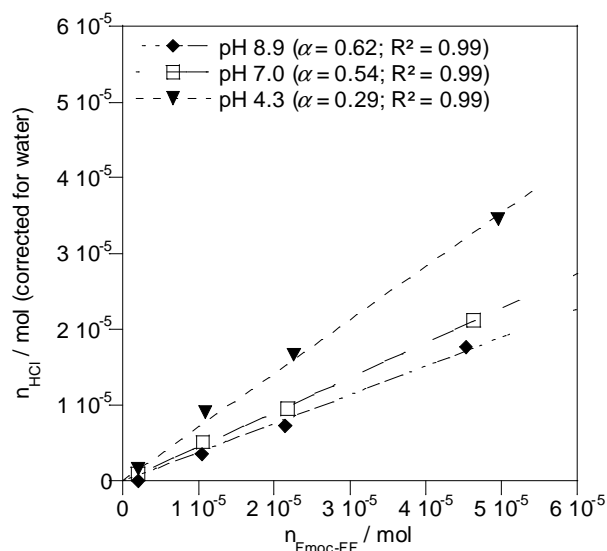


Figure 4.7. n_{HCl} (moles of HCl added corrected for moles of HCl needed to titrate water) vs. $n_{\text{Fmoc-FF}}$ (moles of peptide present in the sample) for the 1, 5, 10 and 20 mmol L^{-1} samples at pH values of 8.9, 7.0 and 4.3. Inset: Degree of ionisation, α , derived from the slope of the fitted linear curves.

At pH 10.5 most of the Fmoc-FG molecules were expected to be ionised. However at 10 and 20 mmol L^{-1} samples were slightly cloudy in these pH conditions and went through a clear phase only after they were heated (i.e. following the first addition of HCl). In all cases as HCl was added to the solutions, their pH gradually decreased while the samples became slightly cloudy (Figure 4.6 B). Once a pH of ~ 7.3 was reached the pH of the 10 and 20 mmol L^{-1} samples was found to become constant. This transition occurred at a pH of about 6.3 and 5.5 for 5 and 1 mmol L^{-1} samples respectively. Once the transition was completed, the pH dropped again and the samples turned into more turbid solutions with addition of HCl. From pH 3.8 a white precipitate started to appear at 1 mmol L^{-1} whereas the samples became more viscous and started to aggregate at 5 mmol L^{-1} and above. As the pH decreased, further precipitation of the samples occurred and all the ‘titration’ curves were found to merge with the control curve.

At all concentrations tested Fmoc-GG peptide derivatives were totally dissolved at pH 10.5. A shoulder was observed at a pH of ~ 8.0 and was found to be more marked as the concentration in Fmoc-GG was increased. This feature was believed to be due to the neutralisation of excess of NaOH in solution by HCl as it was also detected in the water ‘titration’ curve. This shoulder was also present in the other Fmoc-dipeptides ‘titration’ curves but was more apparent here because unlike for the other systems the apparent $\text{p}K_{\text{a}}$ did not occur at similar pH values. At 1 mmol L^{-1} the sample remained clear over the range of pH studied and no transition was observed. At 5 mmol L^{-1} and above, the samples were all clear at high pH and became slightly cloudy upon addition of HCl as the solutions’ pH was gradually lowered. The pH was found to be stable at values of about 4.9, 4.5 and 4.0

for 20, 10 and 5 mmol L⁻¹ samples respectively (Figure 4.6 C). Towards the end of the transition, samples became more viscous and turbid. At low pH (< 3) precipitate appeared and the ‘titration’ curves started to merge with the water curve [6].

At all concentrations tested, Fmoc-GF peptides were also fully dissolved at pH 10.5. The samples’ pH decreased upon addition of HCl. Once a pH of ~ 6.2 was reached, samples started to become cloudy. Then the pH of the samples was found to rise and became constant at about pH 7.6, 7.2, 7.0 and 6.7 for 20, 10, 5 and 1 mmol L⁻¹ samples respectively (Figure 4.6 D). As the samples went through this transition they became more turbid. After the transition, the samples’ pH decreased again and at all concentrations studied, precipitation occurred at pH of ~ 3.5. As the pH decreased further all the ‘titration’ curves merged with the control curve.

Only one transition was observed for Fmoc-FG, Fmoc-GG and Fmoc-GF. However, like Fmoc-FF these Fmoc-dipeptides are weak acids and can all be assumed to be fully ionised at high pH (10.5). In such conditions their conjugated weak bases, Fmoc-dipeptide-COO⁻, can be neutralised by addition of HCl in a molar ratio of 1:1. The molecules degree of ionisation can be estimated for all systems using Equation 4.1. To determine the degree of ionisation at each stage, n_{HCl} was plotted against $n_{\text{Fmoc-dipeptide-COOH}}$ above and below the apparent pK_a that is at pH 6.5 and 3.8 for Fmoc-GG and pH 8.5 and 5.0 for Fmoc-FG and Fmoc-GF. As shown in Figure 4.8, α was extracted from the slope of the fitted linear curves and indicated that in the three cases almost all of the molecules remained ionised before the transition at pH 8.5: 96%, 88% and 97% of Fmoc-FG, Fmoc-GG and Fmoc-GF respectively. As opposed to Fmoc-FF, which gradual self-assembly mechanism was associated with a two-transition feature, these three systems were characterised by a one-transition feature, suggesting different self-assembling processes were involved.

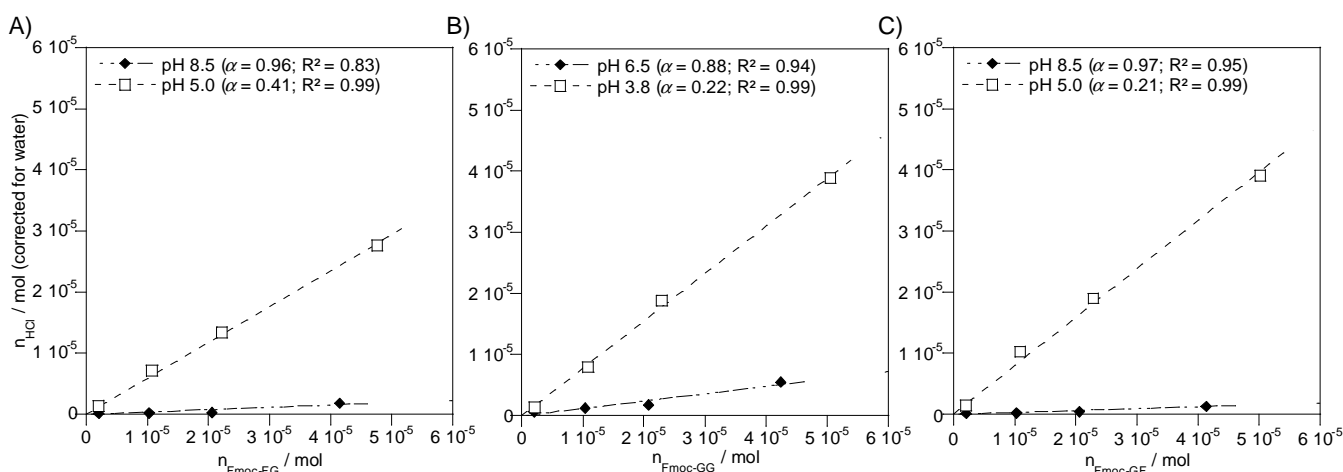


Figure 4.8. n_{HCl} (moles of HCl added corrected for moles of HCl needed to titrate water) vs. $n_{Fmoc-dipeptide-COOH}$ (moles of Fmoc derivative present in the sample) for the 1, 5, 10 and 20 mmol L^{-1} samples of **A)** Fmoc-FG at pH values of 8.5 and 5.0, **B)** Fmoc-GG at pH values of 6.5 and 3.8 and **C)** Fmoc-GF at pH values of 8.5 and 5.0. Inset: Degree of ionisation α derived from the slope of the fitted linear curves.

For all the studied Fmoc-peptide derivatives the transitions were found to be more marked upon increasing the concentration of the peptide derivatives. Figure 4.9 A shows that the pK_a shifts increased with the Fmoc-dipeptides concentration up to 5 mmol L^{-1} for Fmoc-FF and 10 mmol L^{-1} for the three other systems. Beyond this threshold, the transition pHs were found to be independent of the peptide derivatives concentration.

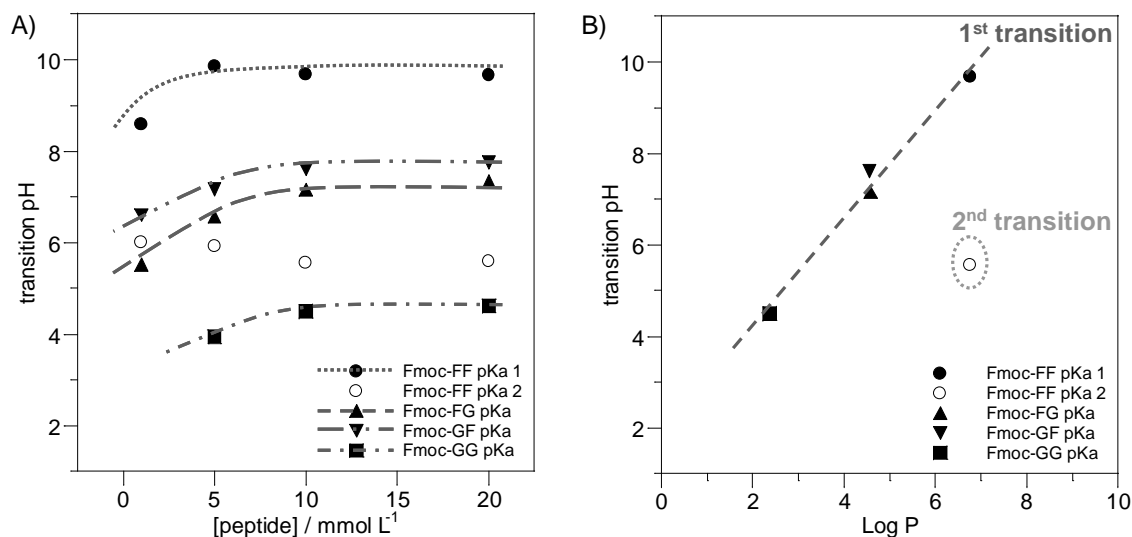


Figure 4.9. **A)** Transition pH values versus concentration of the Fmoc-dipeptides studied (1, 5, 10 and 20 mmol L^{-1}). **B)** Transition pH values versus Log P values of the Fmoc-dipeptides at 10 mmol L^{-1} .

All apparent pK_a transitions occurred at pHs higher than the theoretical pK_a^{th} , of the Fmoc-dipeptides, which confirms the results recently reported by Adams *et al.* [7]. Shifts of about 6.3 (and 2.1) 3.0, 0.6 and 3.7 pH units on average were observed for Fmoc-FF ($pK_a^{\text{th}} = 3.58$), Fmoc-FG ($pK_a^{\text{th}} = 3.76$), Fmoc-GG ($pK_a^{\text{th}} = 3.82$) and Fmoc-GF ($pK_a^{\text{th}} = 3.64$) respectively at 10 mmol L^{-1} (concentration at which full characterisation of the systems will be carried out in Chapter 5). The pK_a shifts were found to be related to the

chemical structure of the molecules and more precisely to their Log P value (octanol-water partition coefficient), which again is in agreement with observations described elsewhere [7]. These values correspond to a measure of the molecules hydrophobicity and were determined using ACD/Labs v. 12.01/ChemSketch. As shown in Figure 4.9 B the transition pH for Fmoc-GG, the less hydrophobic molecule of this set of peptide derivatives, occurred at relatively low pH, close to its theoretical pK_a value. On the other hand, the apparent pK_a 1 for Fmoc-FF occurred at much higher pH resulting in a more pronounced pK_a shift.

4.3.2.3. Optimised Sequential pH Change Method for Gel Formation

Based on the observations reported above the gel preparation method was modified in order to improve the control of the samples' pH and their homogeneity. NaOH was added to the suspensions of peptide derivatives until their dissolution at pH 10.5. HCl was subsequently added drop-wise until a target pH was reached while the solutions were constantly vortexed and sonicated in order to avoid aggregate formation. Both the required volume of acid and the target pH varied in function of the studied Fmoc-dipeptides and were estimated from the 'titration' curves presented in Figure 4.6. Next, the samples were heated to dissolve remaining aggregates at a temperature of 75–80 °C. The heating times were optimised at this temperature for the different studied systems and are reported in Chapter 3. This step ensured all samples went through a liquid phase before they were cooled and maintained at 4 °C for ~ 12 hours to promote gelation. Under appropriate pH conditions, the sol-gel transition of Fmoc-FG was found to occur while the samples were being heated. These samples appeared to be particularly stable at low and room temperature only at the condition that the hydrogels were completely formed at high temperature. Removing the samples from the block heater while they were still in a liquid state led to their irreversible precipitation during storage at low temperature. The difference in pH before and after storage was reduced to ± 0.3 pH units using this method, however hydrogels were obtained at slightly different pH values than the non-heated samples (Figure 4.2). In particular Fmoc-FF gels were obtained at pH 9.0 whereas their non-heated homologues formed under near-physiological (pH ~ 7.5). As illustrated in Figure 4.10 clearer self-supporting hydrogels suggesting more homogeneous samples were formed although Fmoc-FF and Fmoc-GG gels looked weaker than the corresponding non-heated samples. Again, Fmoc-GF did not form hydrogels.

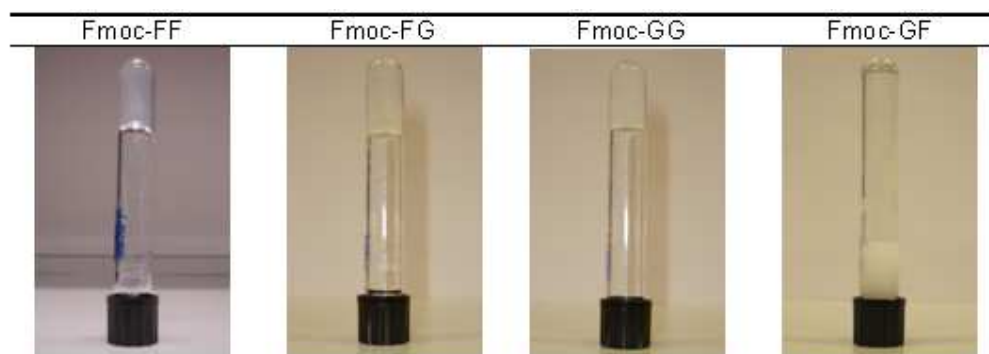


Figure 4.10. Macroscopic appearance of Fmoc-dipeptides hydrogels and precipitate formed by the optimised sequential pH change: Fmoc-FF (pH 9.0), Fmoc-FG (pH 5.1), Fmoc-GG (pH 4.4) and Fmoc-GF (pH 4.7) samples at 10 mmol L^{-1} .

The viscoelastic properties of the newly formed gels were determined by oscillatory rheology. The storage moduli, G' , of the studied hydrogels prepared using the optimised and the previously reported methods are compared in Figure 4.11 A. In all cases the rheological data confirmed the weakness of the more homogeneous samples. G' values obtained for the heated samples were lower than those measured for the non-heated samples with a difference of one order of magnitude for Fmoc-FG and Fmoc-GG ($G' \sim 100\text{--}400 \text{ Pa}$), and up to four orders of magnitude for Fmoc-FF ($G' \sim 0.5\text{--}5 \text{ Pa}$). Therefore the better homogeneity of the samples had an impact on their mechanical properties. However as shown in Figure 4.11 B, the optimised sample preparation method did not affect the structure of the self-assemblies as the same WAXS pattern was observed for Fmoc-FF hydrogels prepared using the two different methods. These Bragg peaks were related to different features of the molecular self-assembly and will be discussed in detail in Chapter 5.

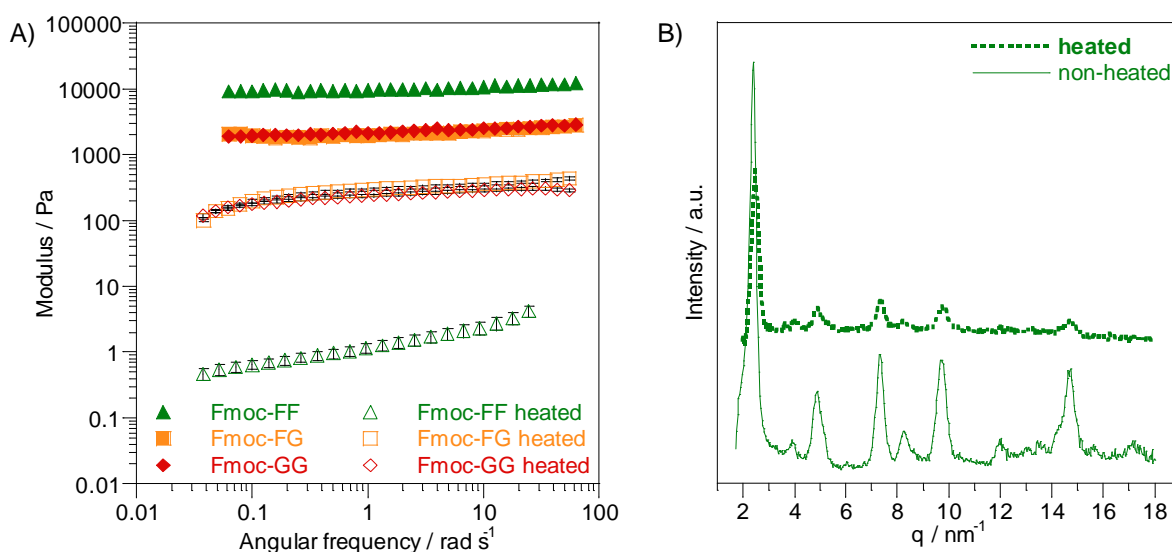


Figure 4.11. A) Storage modulus, G' , of Fmoc-FF, Fmoc-FG and Fmoc-GG hydrogels at 10 mmol L^{-1} formed using the optimised (open symbols) and the previously reported sample preparation method (plain symbols). B) WAXS spectrum of a dried layer of Fmoc-FF hydrogel prepared using the optimised and the previously reported method.

4.4. CONCLUSION

All four systems studied in this section displayed completely distinct behaviours mainly due to their difference in hydrophobicity. Depending on the amino acids side chain, hydrogels were obtained in different pH and heating conditions. Investigations on the solution behaviour of the systems enabled to modify the previously reported sample preparation method. Control of the sample pH was increased and formation of kinetically trapped aggregates was reduced, improving the homogeneity of the samples. Although in all cases the newly obtained hydrogels appeared to be less stiff, their molecular organisation did not seem to be modified. The impact of the better homogeneity on the sample properties will be discussed in more detail in Chapter 5.

4.5. REFERENCES

1. Jayawarna, V., Ali, M., Jowitt, T.A., *et al.*, *Nanostructured hydrogels for three-dimensional cell culture through self-assembly of fluorenylmethoxycarbonyl-dipeptides*. *Advanced Materials*, **2006**, 18 (5), 611-614.
2. Smith, A.M., Williams, R.J., Tang, C., *et al.*, *Fmoc-diphenylalanine self assembles to a hydrogel via a novel architecture based on π - π interlocked β -sheets*. *Advanced Materials*, **2008**, 20 (1), 37-41.
3. Ozbas, B., Kretsinger, J., Rajagopal, K., *et al.*, *Salt-triggered peptide folding and consequent self-assembly into hydrogels with tunable modulus*. *Macromolecules*, **2004**, 37 (19), 7331-7337.
4. Yang, Z., Liang, G., Ma, M., *et al.*, *In vitro and in vivo enzymatic formation of supramolecular hydrogels based on self-assembled nanofibers of a β -amino acid derivative*. *Small*, **2007**, 3 (4), 558-562.
5. Kocienski, P.J., *Protecting groups*. Foundations of organic chemistry series. **1994**, Stuttgart: Thieme.
6. Zhang, Y., Gu, H., Yang, Z., *et al.*, *Supramolecular hydrogels respond to ligand-receptor interaction* *Journal of the American Chemical Society*, **2003**, 125 (45), 13680-13681.
7. Adams, D.J., Mullen, L.M., Berta, M., *et al.*, *Relationship between molecular structure, gelation behaviour and gel properties of Fmoc-dipeptides*. *Soft Matter*, **2010**, 6, 1971-1980.

Effect of Hydrophobic Aromatic Moieties on the Self-Assembly of Fmoc-Dipeptides*

5.1. ABSTRACT

pH conditions were found to have an effect on the self-assembly process of Fmoc-dipeptides (Fmoc-FF, -FG, -GG and -GF), resulting in apparent pK_a shifts above their theoretical pK_a . Using Fourier transform infrared (FT-IR) and fluorescence spectroscopy, transmission electron microscopy (TEM), wide-angle X-ray scattering (WAXS), and oscillatory rheology, these transitions were shown to coincide with significant structural changes. Overall, this study provides further understanding of the self-assembly mechanism of aromatic short peptide derivatives.

5.2. INTRODUCTION AND OBJECTIVES

In the previous chapter, Fmoc-dipeptides based on the pairing of phenylalanine and glycine were found to form hydrogels in particular pH conditions. The α -carboxylic acid groups of amino acids are in their anionic form at neutral pH. N-protected nonpolar peptides have pK_a values of 3.7 on average [1].[†] In dilute solutions, one would therefore expect terminal carboxylic acid groups to be ionised at pH values higher than 3.7 and the molecules to be negatively charged. Self-assembly would presumably be unfavoured at pH higher than 3.7 due to electrostatic repulsion between the negatively charged molecules. Indeed, a number of Fmoc-peptides including Fmoc-FG and Fmoc-GG only showed self-assembly at low pH [2,3]. However, Fmoc-FF, a highly hydrophobic peptide derivative, was found to self-assemble at neutral pH [4]. It is known that pK_a can shift dramatically in protein and peptide self-assembly especially in hydrophobic environments [5]. For example, a shift of 6.1 pH units has been observed for aspartic acid side chain carboxylic acid in a family of protein based polymers composed of the repeat of polypentapeptides [6]. pK_a shifts have

* Part of this chapter has been published as: Smith, A.M., Williams, R.J., Tang, C., Coppo, P., Collins, R.F., Turner, M.L., Saiani, A., and Ulijn, R.V. *Fmoc-diphenylalanine self-assembles to a hydrogel via a novel architecture based on π - π interlocked β -sheets*. *Advanced Materials*, **2008**. 20(1): p. 37-41 and Tang, C., Smith, A.M., Collins, R.F., Ulijn, R.V., and Saiani, A. *Fmoc-diphenylalanine self-assembly mechanism induces apparent pK_a shifts*. *Langmuir*, **2009**. 25(16): p. 9447-9453.

[†] SPARC web calculator to be found at <http://ibmlc2.chem.uga.edu/sparc>.

also been encountered in fatty acids, for instance, palmitic acid (C₁₆) revealed a pK_a shift of up to 3.9 which is related to the formation of foam by these molecules [7].

Hydrogels of aromatic short peptide derivatives were previously formed by sequential pH change [2], dilution from fluorinated solvents [8], as well as enzymatic hydrolysis of corresponding esters [9]. Here we focus on the pH dependence of the Fmoc-FF, Fmoc-FG, Fmoc-GG and Fmoc-GF self-assembly process using the modified sample preparation method described in Chapter 4. We show that self-assembly of the studied Fmoc-dipeptides results in a suppressed ionisation leading to dramatic pK_a shifts related to significant structural transitions.

5.3. RESULTS AND DISCUSSION

5.3.1. Fmoc-FF

5.3.1.1. Proposed Molecular Model

From a biotechnological point of view Fmoc-FF appeared to be particularly interesting as it has recently been shown to form hydrogels at physiological pH on which cells could grow and proliferate [2,10,11]. Supported by spectroscopic data collected on specimens at neutral pH prepared by sequential pH change, a molecular model for the self-assembled structure formed by this system has subsequently been proposed by Smith *et al.* [4].

Based on circular dichroism and FT-IR analyses, Fmoc-FF peptides were shown to form antiparallel β -sheets. From fluorescence spectroscopy data, fluorenyl groups were found to self-assemble in antiparallel dimers through π - π stacking. Additionally, evidence for the presence of extensive aromatic aggregates was observed, suggesting the phenyl rings from the phenylalanine side chains interacted with the pairs of Fmoc groups. The combination of these three features was explored using molecular modelling (Hyperchem software), in which energy minimisation of the structures was performed using the Amber force field. Fmoc-FF molecules were arranged in antiparallel β -sheets through hydrogen bonding of the peptide components, leaving the fluorenyl moieties on the edges of the sheets (Figure 5.1 A). In this configuration, the phenyl rings of the C-terminal phenylalanine residues interacted with the fluorenyl moieties, forcing the molecules to bend, resulting in a kink in the peptide backbone. Such molecular organisation revealed the Fmoc groups located on the same edge would be too far apart to be able to π -stack. The sheets were therefore positioned side by side, to enable the overlapping of Fmoc groups from one sheet with the Fmoc groups of another one. This molecular arrangement resulted in the formation of π -stacked pairs of fluorenyl groups alternating with phenyl rings

(Figure 5.1 B). β -strands are intrinsically twisted due to the chiral nature of their constitutive amino acids. Hence, the lateral association of four β -sheets was found to result in the formation of a cylindrical fibril with an external diameter of $\sim 30 \text{ \AA}$ (Figure 5.1 C). As a consequence of the twisted nature of the sheets, the distance between the centres of the fluorene pairs would be $\sim 16 \text{ \AA}$ and $\sim 8 \text{ \AA}$ along the long and diagonal axes of the fibril respectively (Figure 5.1 D). These fibrils would then further self-assemble laterally, forming large flat ribbons that were observed by TEM. For a detailed discussion of the model built by A. M. Smith, we refer the reader to reference [4].

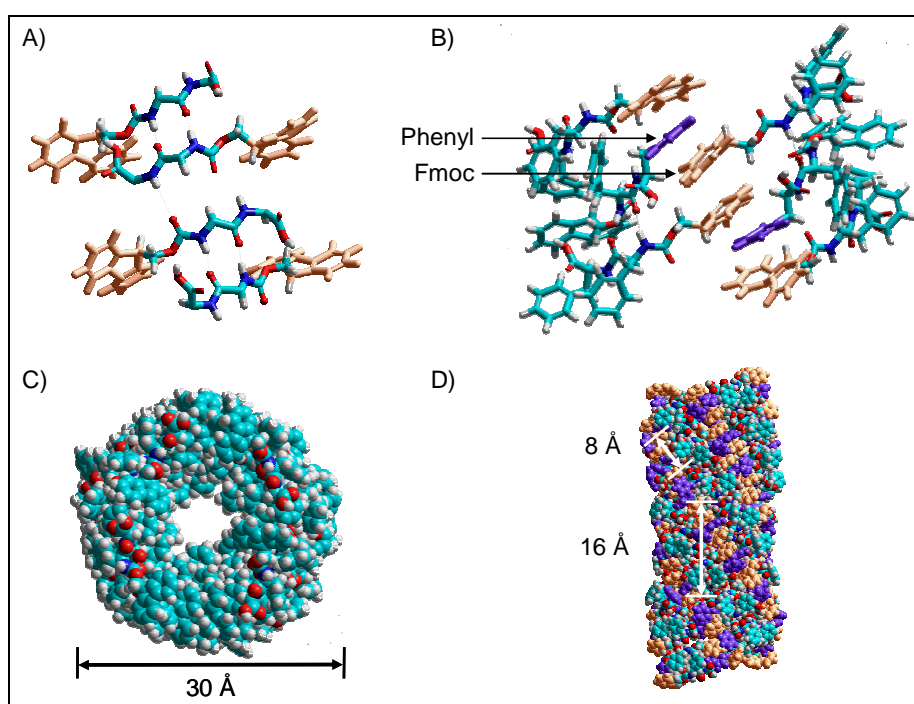


Figure 5.1. Proposed model structure of **A)** Fmoc-FF peptides arranged in an antiparallel β -sheet pattern. **B)** interlocking laterally through π -stacked pairs of Fmoc groups and phenyl rings to create a cylindrical structure. **(C)** Top view and **(D)** side view of the structure. The fluorenyl groups are coloured orange and the phenyl groups are coloured purple [4].

In order to confirm the proposed molecular model, further structural analyses were undertaken using wide angle X-ray scattering. Fmoc-FF hydrogels at $\text{pH} \sim 7.5$ were prepared using the method employed by Smith *et al.* (i.e. sequential pH change without heating of the samples). The gels were deposited onto glass slides and allowed to air-dry slowly ($\sim 48 \text{ hrs}$) until thin dried layers were obtained. A scattering pattern characteristic of a relatively well-ordered structure was obtained and showed a series of scattering peaks that we were able to relate to the different features of the proposed model (Figure 5.2).

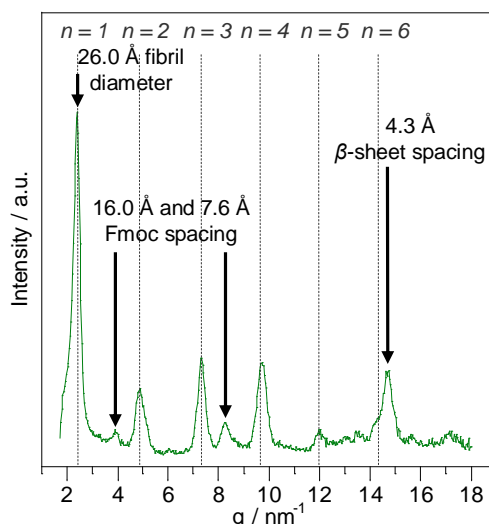


Figure 5.2. WAXS spectra of Fmoc-FF hydrogel at 10 mmol L^{-1} dried at $\text{pH} \sim 7.5$.

The strong reflection peak detected at $q = 2.4 \text{ nm}^{-1}$ corresponds to a repeat distance, $d = 26.0 \text{ \AA}$, which is consistent with the diameter of the individual fibrils predicted by the model (Figure 5.1 C). Up to six higher orders of this reflection were observed at spacings corresponding to d/n ($1 \leq n \leq 6$), which is characteristic of a lamellar organisation. The presence and number of these reflections is consistent with the relatively large flat ribbons observed by TEM [4]. In this publication, examination of torn ribbons revealed that these structures resulted from the lateral assembly of single fibrils of 26.0 \AA in diameter. The absence of any further series of Bragg peaks in addition to the series of six higher order reflections detected suggests that the ribbons were one-dimensional structures (Figure 5.3 A). Indeed, the two-dimensional packing of cylinders would generate non-flat ribbons and result in the detection of a hexagonal phase with reflections at spacings of d , $d/\sqrt{3}$, $d/\sqrt{4}$, $d/\sqrt{7}$, $d/\sqrt{9}$... (Figure 5.3 B).



Figure 5.3. Schematic representation of cylinders in **A)** a lamellar packing (1D growth) and **B)** a hexagonal packing (2D growth).

A peak at 4.3 \AA ($q = 14.6 \text{ nm}^{-1}$) was also observed and ascribed to the inter- β -strand distance. Although such a low spacing was reported for silk hydrogels [12], this periodicity is lower than the one usually observed for β -sheet arrangements (4.7 to 4.8 \AA [13]), suggesting that the β -sheet conformation in our system is probably not ‘ideal’. This unusual periodicity could be due to the kink in the peptide backbone resulting from the interaction of Fmoc pairs with phenyl rings of the C-terminal phenylalanine residues

discussed above. Two additional reflections were observed at 3.9 and 8.3 nm⁻¹, corresponding to repeat distances of 16.0 and 7.6 Å. These peaks were ascribed to the distance between the pairs of Fmoc groups along the cylindrical structure and its diagonal axis respectively (Figure 5.1 D). Although the molecular model was built from Fmoc-derivatives arranged in an antiparallel manner it is unlikely that such short peptide components formed sufficiently stable β -sheets capable of driving the self-assembly. As we will see later, the self-assembly of such systems is driven by π -stacking of the fluorenyl groups, and depending on the amino acid sequence β -sheets can be formed.

5.3.1.2. pH Study

As observed in Chapter 4 the ‘titration’ of Fmoc-FF is characterised by two transitions. In order to relate the ionisation behaviour of Fmoc-FF to its self-assembly properties, we have performed a structural investigation of the samples around four different pH values:

- 10.5, the starting point of the ‘titration’
- 9.0, below the apparent p*K*_a 1 transition
- 7.4, above the apparent p*K*_a 2 transition
- 4.7, below the apparent p*K*_a 2 transition.

The samples were prepared as described in Chapter 3. The main difference compared to the sample used for the ‘titration’ experiments is that, in this case after homogenisation, the samples were stored at 4 °C overnight to promote gelation.

First we discuss the 10 mmol L⁻¹ samples. At pH 10.5 (above the ‘shifted’ apparent p*K*_a 1), Fmoc-FF was solubilised by addition of NaOH. As can be seen from Figure 5.4, the FT-IR spectrum of the sample at pH 10.5 showed a barely detectable peak at 1625 cm⁻¹, which is usually characteristic of the presence of β -sheet structures [14]. The broad band centred around 1592 cm⁻¹ is associated with the asymmetrical stretching motions of the ionised carboxyl end group of the peptides [15].

At this same pH, TEM micrographs showed a small population of fibres (Figure 5.5 A) compared to what was observed at lower pH values as will be discussed later. At this high pH, most of the Fmoc-FF molecules are expected to be ionised, and therefore, due to the electrostatic repulsion between peptides, their self-assembly is thought not to be favoured.

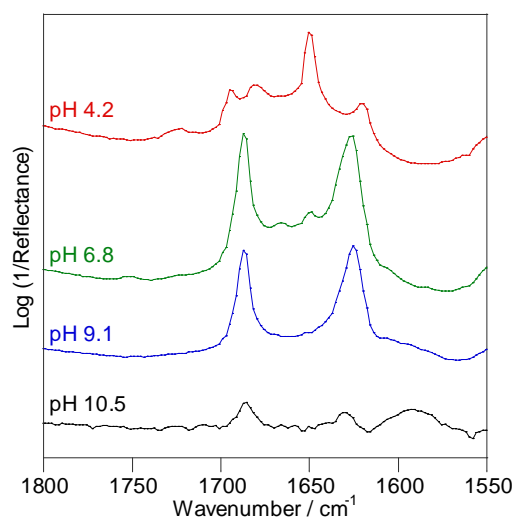


Figure 5.4. FT-IR spectra of Fmoc-FF samples at 10 mmol L^{-1} prepared in D_2O at pH 10.5 starting point of the 'titration' experiment, pH 9.1 (below apparent $\text{pK}_a 1$) and pH 6.8 and 4.2 (above and below apparent $\text{pK}_a 2$ respectively).

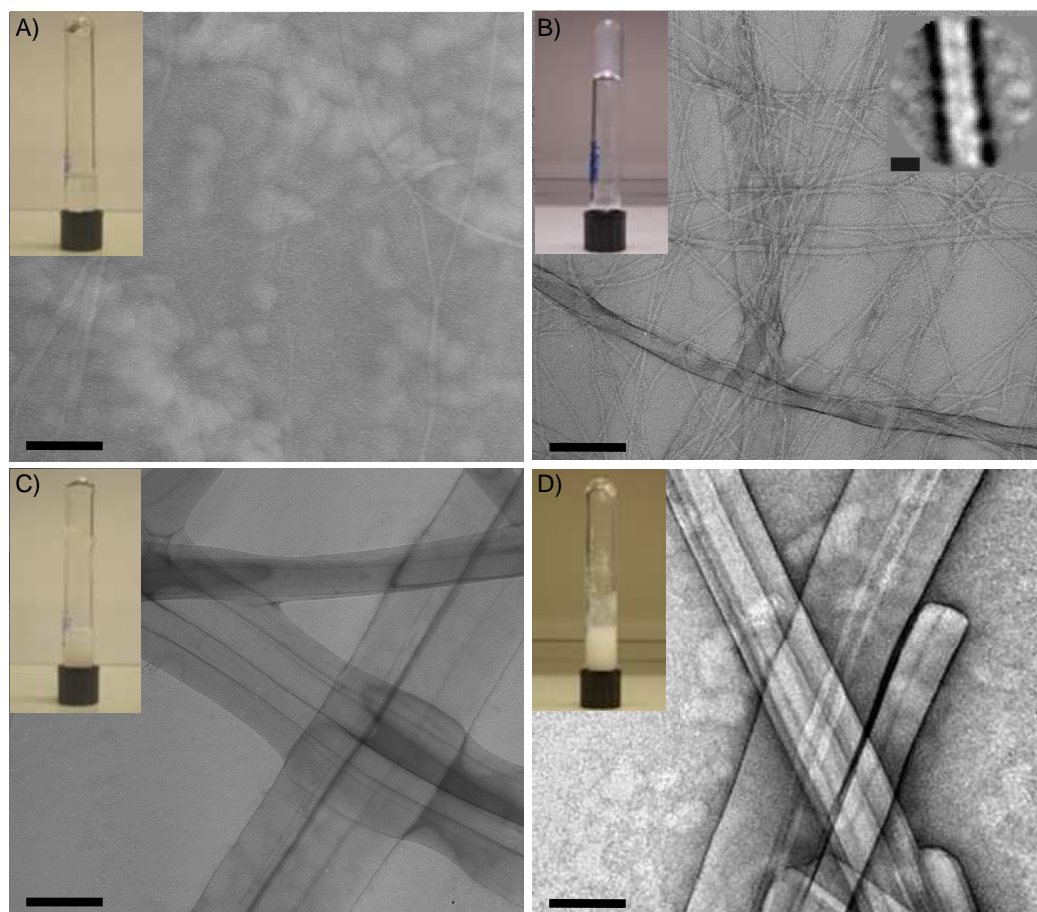


Figure 5.5. TEM micrographs of Fmoc-FF samples at 10 mmol L^{-1} **A)** at pH 10.5 starting point of the 'titration' experiment; **B)** at pH 9.0 (below apparent $\text{pK}_a 1$) – the right hand side inset illustrates a projection average of the fibres, scale bar represents 6 nm, **C)** at pH 7.4 (above apparent $\text{pK}_a 2$) and **D)** at pH 4.7 (below apparent $\text{pK}_a 2$). Scale bars represent 100 nm. Left hand side insets correspond to photographs of the samples showing their macroscopic appearance.

When the pH was reduced to ~ 9.0 (just below apparent $pK_a 1$ transition), a weak, translucent, self-supporting hydrogel was obtained. As shown on the infrared spectrum of the sample, the band at $\sim 1592\text{ cm}^{-1}$ related to COO^- was weaker at this pH, confirming the partial protonation of the peptide derivatives (Figure 5.4). A strong peak at 1625 cm^{-1} consistent with the presence of β -sheet structures and a second one at 1687 cm^{-1} characteristic of an antiparallel arrangement of the β -sheets were also displayed in the FT-IR spectrum [14]. It should be noted that although the positions of these two peaks are consistent with an antiparallel arrangement of the β -sheets, their relative intensity is not. For ‘ideal’ antiparallel β -sheet arrangements, usually encountered in longer peptide sequences and proteins, the band at 1687 cm^{-1} is expected to be much weaker [16,17]. The exact origin of this effect is not yet fully understood. It is thought that insertion of phenylalanine side chains between π -stacked pairs of Fmoc groups induces a kink in the peptide backbone, which would result in the antiparallel β -sheet arrangement not being ‘ideal’. This observation is in agreement with the unusual β -sheet spacing observed by WAXS. It should be noted that IR band intensities are sensitive to small changes in bond environment. Additionally, the infrared spectra obtained from a thin dried layer (prepared as described in Section 3.2.4.2 for the WAXS experiments) showed the presence of the characteristic antiparallel β -sheet peaks (Appendix C). This result indicates that the drying process did not affect the molecular arrangement. The presence of these two peaks in both the hydrated and dried states indicates clearly that at this pH self-assembly of the Fmoc-FF had occurred. This observation was confirmed by TEM (Figure 5.5 B). Analysis of the micrograph revealed the presence of an extended entangled network composed of mainly (80 %) thin flexible fibres with a width of $6.0 \pm 0.4\text{ nm}$. Image analysis of the averaged fibre projection map (inset Figure 5.5 B) revealed a thin high-contrast line running along the middle of the fibres parallel to the long axis. This feature suggests that the fibres either correspond to a hollow tube of 6 nm in diameter or are formed by the lateral association of two smaller fibrils, each of $\sim 3\text{ nm}$ in diameter. The latter interpretation is favoured; indeed, the accumulation of stain down the centre of a hollow fibre of this size would be difficult with the particular staining technique used here. From the TEM micrograph, the diameter of the central hole would be less than 5 \AA . Keeping in mind that the fibres are first deposited on the grid and then stained, the even staining of the central part of the tube over several micrometers, as observed here, would likely result in incomplete staining. The fact that the stain is even along the full length of the fibres is more consistent with a surface coating staining action caused by the accumulation of stain in the ‘cavity’ at the

interface between two fibrils. Each fibril would then correspond to the cylindrical structure described previously [4].

The exact reason and origin of the association of these fibrils in pairs has not yet been elucidated. It is also of interest to note that along the length of the paired fibrils a clear 3.0 nm periodic repeat can be observed (inset Figure 5.5 B). The cylindrical nature of the model proposed by Smith *et al.* [4] is due to four β -sheets forming a square cross section, with each face corresponding to one β -sheet, rotating around a central axis (Figure 5.6 A). Based on the model, the pitch of the helical structure would be 120 Å. As a consequence, an alternation of flat to ridged to flat surfaces from the square cross section (Figure 5.6 B) with a periodicity of 30 Å should be observed. As revealed in the TEM micrograph, the alternation of bright and dark ‘patches’ along the long axis of the fibres was indeed observed and would result from the difference in stain densities between the flat and ridged surfaces, with the ridged surfaces appearing darker as they collect more stain.

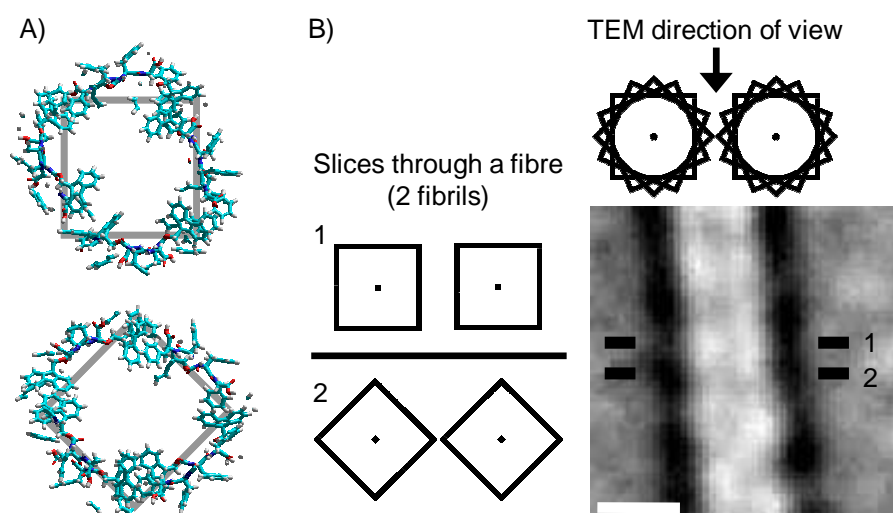


Figure 5.6. **A)** Cross sections of the fibril previously described in reference [4] corresponding to 4 β -sheets forming a square tube that rotates around a central axis. As a consequence, viewed down the long section, it appears to give a cylinder. Slices 15 Å apart are rotated 45° to each other. **B)** Schematic representation of a view down the length of a fibre (top) with 1 and 2 (left) representing two slices 15 Å apart rotated by 45° through the depicted structure showing flat and ridged surfaces, and fibre projection map (right) obtained from the TEM micrographs showing the parallel arrangement of two fibrils. The light and darker regions correspond to the alternation of flat (light) and ridged (dark) surfaces. Scale bar represents 6 nm. (For more details, see the text)

As can be seen in Figure 5.7, the intensity of the scattering pattern was lower for the gels formed at pH ~ 9.0 using the modified sample preparation method than for the gels prepared at pH ~ 7.5 using the previously reported sequential pH change (Figure 5.2). Although hydrogels were formed in both cases, the pH conditions at which they were obtained were different due to the improved homogeneity of the samples resulting from the

modified method. However, the reflection at $2.3\text{--}2.5\text{ nm}^{-1}$, corresponding to a repeat distance of $25.6\text{--}27.7\text{ \AA}$ was still observed. This periodicity is in agreement with both the fibril size estimated by TEM and the repeat unit observed along the long axis of the fibril. TEM and WAXS experiments were undertaken using dried samples, which could introduce artefacts on the morphologies observed and the scattering pattern detected. However, FT-IR spectra of dried and hydrated samples showed no structural difference, suggesting that drying did not affect the architecture of the fibres.

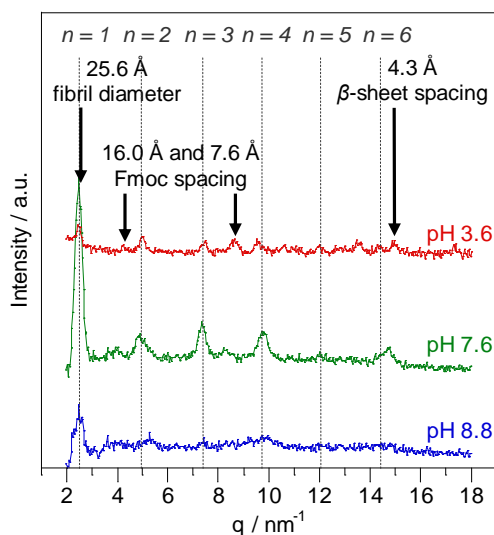


Figure 5.7. WAXS spectra of Fmoc-FF samples at 10 mmol L^{-1} dried at pH 8.8 (below apparent $pK_a 1$) and pH 7.6 and 3.6 (above and below apparent $pK_a 2$, respectively).

The gel-like nature of the sample at this pH was confirmed by dynamic rheology. As can be seen from Figure 5.8, at pH 9.0, the elastic modulus (G') was higher than the viscous modulus (G''), indicating the material was elastic rather than viscous. Both G' and G'' were weakly dependent on frequency between 0.01 and 100 rad s^{-1} . This behaviour is characteristic of entangled polymer networks and is in good agreement with the type of network topology revealed by TEM. G' values were in the range of $0.5\text{--}5\text{ Pa}$ which confirms the hydrogels were weak compared to the Fmoc-FF hydrogels prepared using the previous pH change method [4] or upon dilution from organic solvents [8] (10^4 Pa). As discussed in Chapter 4 we believe that heating the samples at $75\text{--}80\text{ }^\circ\text{C}$ increased their homogeneity and storing them at $4\text{ }^\circ\text{C}$ resulted in a slow hydrogelation dynamic producing more homogeneous hydrogels with lower moduli.

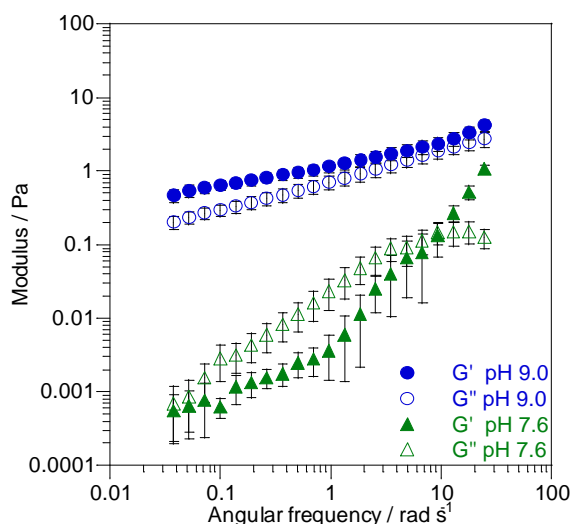


Figure 5.8. Dynamic frequency sweep of Fmoc-FF samples at 10 mmol L^{-1} at pH 9.0 (below apparent $pK_a 1$) and pH 7.6 (above apparent $pK_a 2$).

As clearly shown, self-assembly of the peptide derivatives occurs during the apparent $pK_a 1$ transition. Neutralisation of Fmoc-FF⁻ by addition of HCl is thought to favour self-assembly as the electrostatic repulsion between the peptide derivatives is decreased. As the Fmoc-FF⁻ molecules are neutralised, they self-assemble to form the cylindrical structures described above (Figure 5.9). At the end of apparent $pK_a 1$ transition, only 34 % (i.e. $\alpha = 0.66$) of the Fmoc-FF⁻ molecules are thought to be neutralised, suggesting that the self-assembled fibres incorporate a significant amount of still ionised peptide. In Smith *et al.*'s model [4], most of the terminal acid groups are located on the surface of the fibril. We therefore expect the surface of the fibrils to be negatively charged.

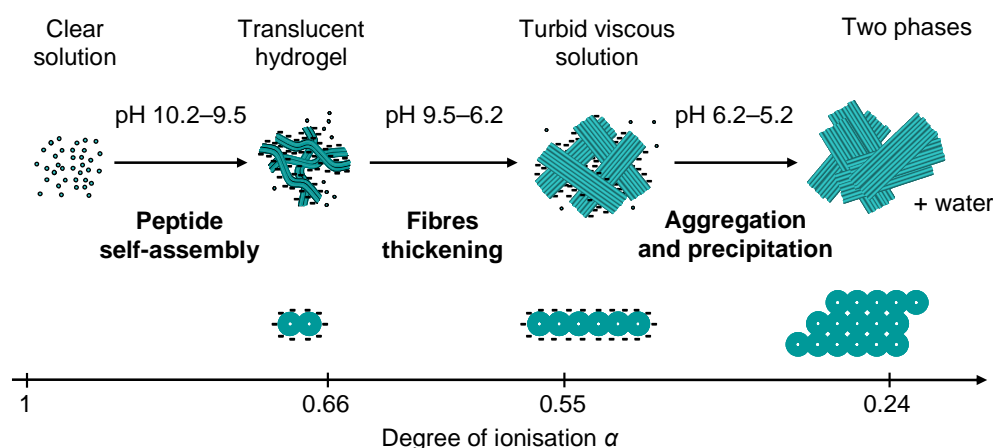


Figure 5.9. Proposed self-assembly mechanism of Fmoc-FF from high to low pH above the critical gelation concentration as a function of the peptide degree of ionisation, α .

Around pH 7.4 (just above the apparent $pK_a 2$ transition), the sample was turbid and a thick viscous solution rather than a weak gel was obtained. As can be seen from Figure 5.8 at

pH \sim 7.4, G' was found to be lower than G'' until a crossover of the moduli was observed beyond 10 rad s^{-1} , confirming that when the pH is decreased the materials become viscous. Both G' and G'' showed a strong frequency dependence between 0.01 and 100 rad s^{-1} . Such rheological behaviour is characteristic of liquid-like materials. From the FT-IR data, it is apparent that β -sheets are still present at pH \sim 7.4 both in the hydrate (Figure 5.4) and the dried state of the hydrogels (Appendix C). The area of the peaks at 1625 and 1687 cm^{-1} at pH \sim 9.0 and \sim 7.4 are comparable, suggesting the presence of a comparable overall amount of β -sheets at both pH values. TEM micrographs at pH 7.4 revealed the presence of large, flat ribbons resulting from the lateral association of many fibrils (Figure 5.5 C) similar to the ones observed by Smith *et al.* [4].

The structural characteristics highlighted by FT-IR and TEM were confirmed by WAXS. Figure 5.7 shows that although the sample preparation method was changed, the same pattern as reported in our previous work (Figure 5.2) was obtained at this pH, suggesting that the structural arrangement of the self-assembled structures was related to the degree of ionisation of the molecules rather than the gel state of the samples. An intense Bragg peak was detected at 2.5 nm^{-1} , corresponding to a repeat distance of 25.6 \AA and was again attributed to the individual fibril diameter. The presence of higher orders of this reflection confirmed that the flat ribbons observed by TEM resulted from the lamellar organisation of fibrils into flat ribbons. The peak attributed to the spacing between β -strands was also observed at 14.6 nm^{-1} , corresponding to a repeat distance of 4.3 \AA .

As pH is reduced from \sim 9.0 to \sim 7.4 the ionisation degree of Fmoc-FF decreases. It is assumed that further neutralisation of the charges enables lateral interactions between fibrils (Figure 5.9). As shown by the diagonal section of the titration curves between the two apparent $\text{p}K_a$ transitions, more molecules are gradually protonated, allowing new fibre-fibre contacts (Figure 4.5 A). Fibre thickening results in the formation of large flat ribbons through lateral hydrophobic interactions. The reason of this apparent one-dimensional aggregation of the fibrils is not clear but suggests the presence of specific directional interfibre interactions. These ribbons are expected to be highly rigid and would therefore not entangle easily and form hydrogels but form liquid-like nematic structures.

Around pH 4.2 (below the 'shifted' apparent $\text{p}K_a$ 2) precipitate formation was observed. The TEM micrograph revealed the presence of rigid rod-like elongated objects at pH 4.7 (Figure 5.5 D). The lateral dimension of these objects is similar to the one of the flat ribbon observed at higher pH, suggesting that they probably derive from them. It is thought that

during the apparent pK_a 2 transition, all the remaining Fmoc-FF⁻ molecules are neutralised. Further assembly of the ribbons occurs as the ionisation degree of the peptide decreases further. This hypothesis is confirmed by infrared spectroscopy since the band associated with ionised carboxyl groups is no longer detected at $\sim 1592\text{ cm}^{-1}$ (Figure 5.4). As a result, these larger rigid rod-like structures, probably corresponding to aggregated ribbons, are formed and precipitate out of solution. Once the process is complete, the pH of the sample decreases again. Below the apparent pK_a 2 transition, a fully separated two-phase system is obtained with a clear liquid phase, corresponding to water, and a solid phase, corresponding to the precipitated rod-like objects containing the peptides (Figure 5.9).

WAXS experiments were also performed at $\text{pH} \sim 4.2$ and showed a similar scattering pattern as at $\text{pH} \sim 7.4$, although the intensity of the Bragg peaks, in particular the ratio between the first and second order peaks, was much lower, suggesting a loss of structure (Figure 5.7). This loss of well defined structure was confirmed by FT-IR since the peaks corresponding to antiparallel β -sheets were still observed but the area of the peaks was much smaller (Figure 5.4). On the other hand additional peaks were observed in the amide I region at 1694 and 1649 cm^{-1} . The peak at 1649 cm^{-1} has been assigned in the literature to peptides adopting a random coil conformation. This would suggest that as the ribbons aggregate and precipitate, the peptides lose their antiparallel β -sheet organisation. The spectrum of Fmoc-FF in its dehydrated form (commercial product straight from the manufacturer, i.e. not structured) shows a peak at 1694 cm^{-1} , which is related to the stretching of the carbonyl group of the amide bond too, confirming the loss of peptide organisation (Appendix D). The exact nature of these precipitated aggregated ribbons and their internal structure has not been yet elucidated.

5.3.1.3. Concentration Study

Similar results to those described above for the 10 mmol L^{-1} sample were obtained for the 5 and 1 mmol L^{-1} samples. For instance, Figure 5.10 A shows that although the area of the peaks was much smaller at 5 mmol L^{-1} than at 10 mmol L^{-1} , the infrared data were overall similar. Above and below the apparent pK_a 1 transition ($\text{pH} 9.2$ and 6.8 respectively), peaks characteristic of antiparallel β -sheets were observed at 1687 and 1625 cm^{-1} . As the pH was lowered to 4.3 , the intensity of these peaks decreased and additional peaks were detected at 1694 and 1649 cm^{-1} . TEM micrographs also revealed the same type of structures as at 10 mmol L^{-1} with thin flexible fibres of $\sim 6\text{ nm}$ in width present at $\text{pH} 9.3$

(Figure 5.10 B), large flat ribbons at pH 7.6 (Figure 5.10 C) and aggregated ribbons at pH 4.1 (Figure 5.10 D).

Although the signal-to-noise ratio was much reduced at 1 mmol L^{-1} , FT-IR spectra presented similar features as at 10 and 5 mmol L^{-1} . The only major difference between the two lower concentrations studied was their macroscopic appearance: while for the 5 mmol L^{-1} sample a weak gel was also obtained just below the apparent $pK_a 1$ transition, for the 1 mmol L^{-1} sample a viscous solution was obtained, suggesting that for this system the critical gelation concentration lies between 1 and 5 mmol L^{-1} .

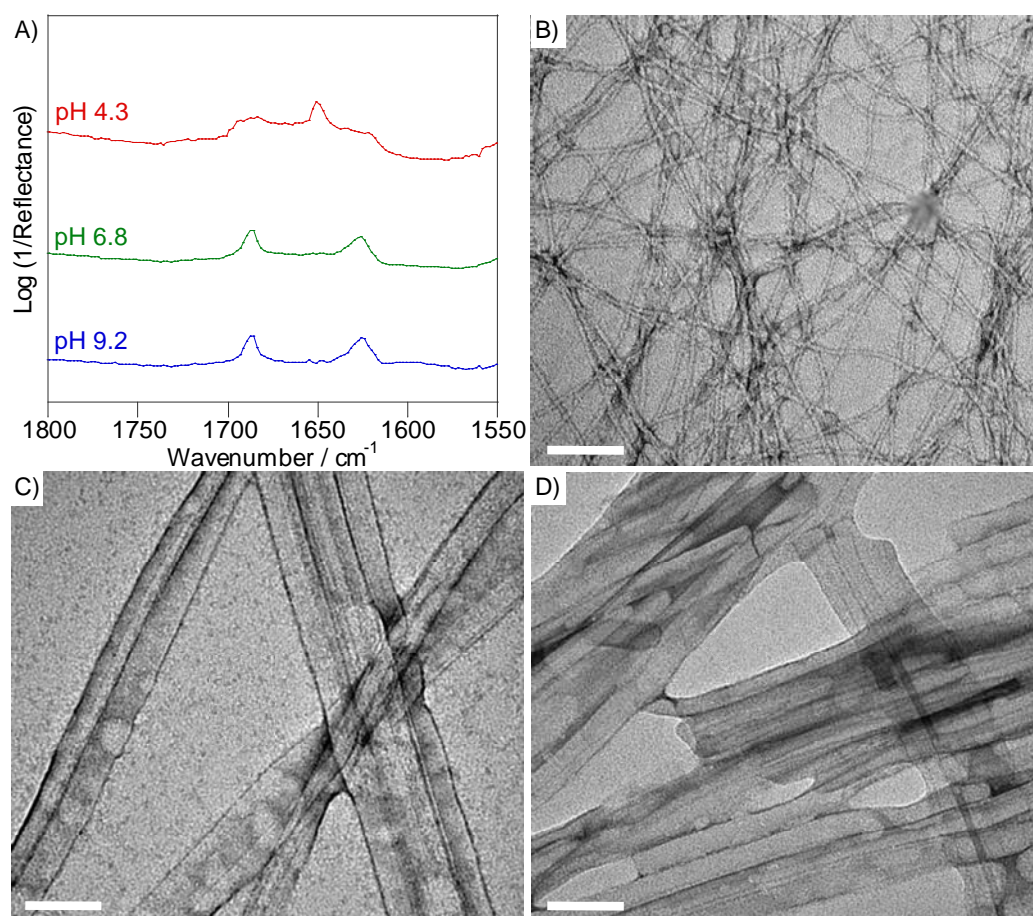


Figure 5.10. A) FT-IR spectra of Fmoc-FF samples at 5 mmol L^{-1} prepared in D_2O at pH 9.2 (below apparent $pK_a 1$) and pH 6.8 and 4.3 (above and below apparent $pK_a 2$ respectively). TEM micrographs of Fmoc-FF samples at 5 mmol L^{-1} B) at pH 9.3 (below apparent $pK_a 1$), C) at pH 7.6 (above apparent $pK_a 2$) and D) at pH 4.1 (below apparent $pK_a 2$). Scale bars represent 100 nm.

Figure 5.11 shows the dynamic frequency sweep of Fmoc-FF hydrogels at 5 mM above the apparent $pK_a 1$ transition (pH 8.9). G' was higher than G'' between 0.01 and 100 rad s^{-1} confirming the material was elastic rather than viscous. As expected, at this concentration the gels were not as strong as at 10 mmol L^{-1} , resulting in G' values in the order of 0.1 Pa. The difference between the two moduli being relatively small added to the fact that they

displayed weak frequency dependence only up to $\sim 1 \text{ rad s}^{-1}$ confirmed the weakness of the hydrogels. At higher frequency ($> 1 \text{ rad s}^{-1}$) a crossover of the moduli was observed, suggesting that the shear stress applied was no longer in the linear regime for such weak gels.

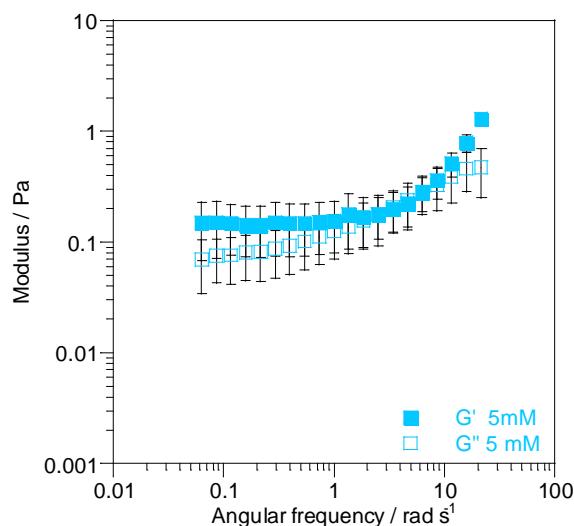


Figure 5.11. Dynamic frequency sweep of Fmoc-FF hydrogels at 5 mmol L^{-1} (pH 8.9).

5.3.1.4. Summary

We have shown that Fmoc-FF molecules self-assemble upon lowering pH (Figure 5.9). Although the modified peptides self-organised into antiparallel β -sheets within the pH range investigated, they showed different structural behaviours depending on the pH. At high pH, most of the molecules were ionised and in solution; therefore, almost no self-assembly was observed. The first ‘shifted’ apparent pK_a transition, at pH 10.2–9.5 corresponded to the self-assembly of molecules into paired fibrils. Above the critical gelation concentration, the fibres entangled, resulting in the formation of a three dimensional network and a hydrogel. The gradual neutralisation of the peptide molecules between pH 9.5 and 6.2 resulted in the lateral self-assembly of fibres through hydrophobic interactions and in the formation of large rigid ribbons. The second ‘shifted’ apparent pK_a transition observed at pH 6.2–5.2 was shown to be related to further aggregation of the ribbons and their precipitation out of solution. Precipitation was associated with a loss of the antiparallel β -sheet conformation adopted by the peptides. Finally, below the apparent pK_a 2 transition, almost all Fmoc-FF⁻ molecules were neutralised and phase separation occurred.

This study provides further understanding of the self-assembly mechanism of aromatic short peptide derivatives. The methodology used here will be exploited in the following

sections to understand the self-assembly behaviour of the other systems of this set of peptide derivatives: Fmoc-FG, Fmoc-GG and Fmoc-GF.

5.3.2. Fluorescent Molecular Behaviour

Fmoc groups were previously found to play a key role in the self-assembly mechanism of Fmoc-FF, enabling the molecules to interact with each other through π - π stacking. In order to monitor the environment of Fmoc-FF, Fmoc-FG, Fmoc-GG and Fmoc-GF fluorenyl moieties as a function of pH, fluorescence spectroscopy was used. The set of Fmoc-dipeptides was studied at 10 mmol L^{-1} in different pH conditions. In order to allow the detection of the molecules in their monomeric state, the systems were also investigated in conditions that were not favourable to self-assembly, i.e. at low concentration (0.1 mmol L^{-1}) above their apparent pK_a transition (pH 8.4–9.1). All the fluorescence spectra were normalised so that the intensity of the emission maximum was set to 1 (see Appendix E for the non-normalised spectra). As shown in Figure 5.12, the four systems of interest displayed common features.

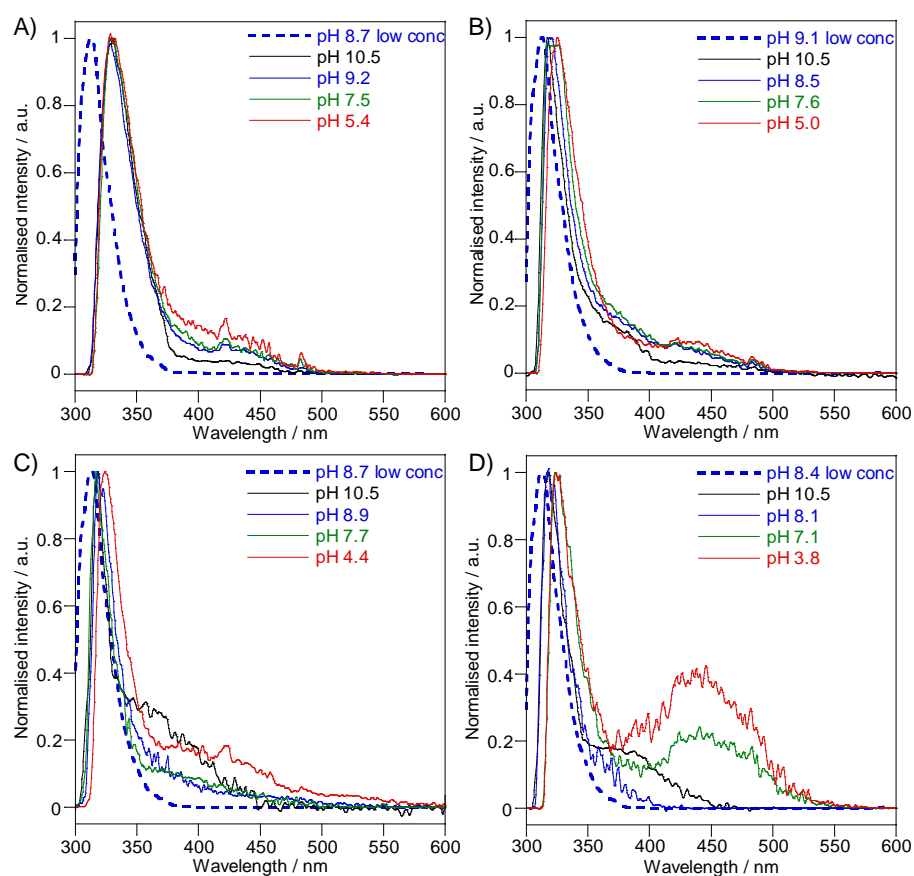


Figure 5.12. Normalised fluorescence emission spectra of **A)** Fmoc-FF, **B)** Fmoc-FG, **C)** Fmoc-GG and **D)** Fmoc-GF samples at 10 mmol L^{-1} at pH 10.5 starting point of the ‘titration’ experiments and at different pH values above and below their respective apparent pK_a and at low concentration (0.1 mmol L^{-1}) above their apparent pK_a (dotted lines).

At low concentration and above their theoretical pK_a values, the molecules were expected to be in solution in all cases. The emission maximum observed at ~ 313 nm for all samples (blue dotted line) was therefore ascribed to monomers of Fmoc groups.

Above the critical gelation concentration and at all pH conditions tested, a fluorescence peak was detected with a maximum centred at 317–330 nm. The emergence of this red shift with respect to the monomer peak at ~ 313 nm is indicative of excimers (excited dimers) of fluorenes. The presence of this band even at pH 10.5 showed that the molecules were not entirely isolated as most of them were probably dimerised by π -stacking of their Fmoc moieties at this stage.

Upon lowering pH, the excimer peak was found to shift from 317 to 325 nm for Fmoc-FG, Fmoc-GG and Fmoc-GF (Figure 5.12 B, C & D). This behaviour could either be attributed to a pH effect on the fluorescence wavelengths [18] or reflect a more efficient overlapping of the fluorenyl groups [19]. However the excimer peak for Fmoc-FF was found to be shifted to the same extent at all pH conditions tested (Figure 5.12 A). This feature provides further support for the hypothesis that more efficient overlapping of the aromatic moieties is at the origin of the enhanced red shifts observed for the three other systems. However, as can be seen in Figure 5.13 the red shifts detected for these three systems were not as marked as for Fmoc-FF in any conditions (even at low pH), suggesting that the most efficient π -stacking conditions were obtained for Fmoc-FF molecules. This behaviour could be related to the presence of the bulky phenylalanine aromatic side chains, which contributes to rigidify the molecules and is thought to favour the stability of the excimers.

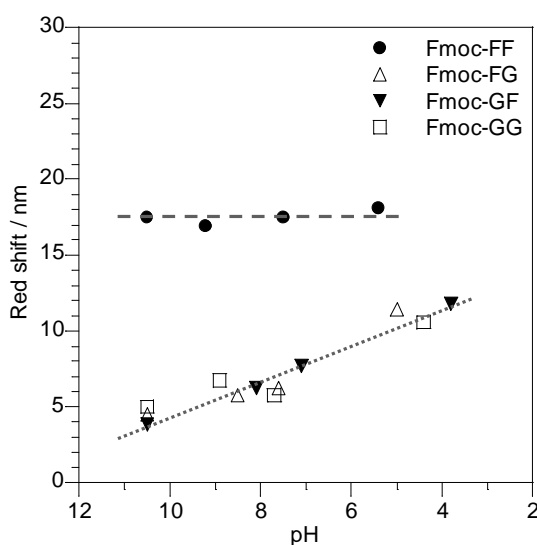


Figure 5.13. Red shift of the excimer peak with respect to the monomer peak as a function of pH for Fmoc-FF, Fmoc-FG, Fmoc-GG and Fmoc-GF samples at 10 mmol L^{-1} .

Emission spectra of fluorene-type moieties arranged in a parallel manner have previously been reported to be shifted towards higher wavelengths compared to their antiparallel analogues [20]. Hence the shoulder observed at ~ 370 nm for Fmoc-FG, Fmoc-GG and Fmoc-GF suggests that a small population of the Fmoc-dipeptides overlapped in a parallel fashion [19]. The higher stability of the antiparallel arrangement was supported by molecular dynamics simulations in which fluorenyl groups arranged in an antiparallel manner were found to be more energetically favourable than those arranged in a parallel fashion [21]. At pH 10.5 i.e. in the presence of NaOH only, the shoulder indicative of parallel Fmoc groups was found to be particularly marked compared to what was observed after addition of HCl. Interestingly, this shoulder was not observed for Fmoc-FF and was more pronounced for Fmoc-GG and Fmoc-GF than for Fmoc-FG, suggesting that ability of these molecules to form parallel dimers is related to their flexibility. Indeed, introduction of a glycine residue next to the fluorenyl moiety enhances the flexibility of the molecules. As can be seen from Figure 5.14 in which the two types of arrangements are shown, the steric hindrance due to the presence of phenyl ring(s) and electrostatic repulsions related to the presence of a negative charge at the carboxyl end make a parallel arrangement of the molecules not favourable. The introduction of glycine next to the Fmoc group probably confers enough flexibility to the molecule tail to allow some level of parallel arrangement, although as can be seen from the fluorescence spectra the antiparallel arrangement was favoured in all cases.

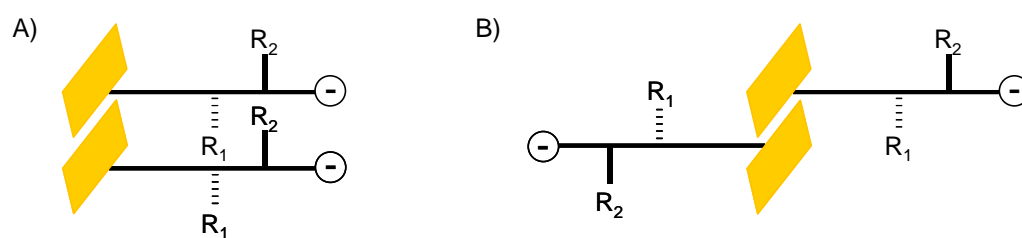


Figure 5.14. Schematic representation of Fmoc-dipeptides π -stacking in **A)** a parallel and **B)** an antiparallel manner.

At lower pH the shoulder at ~ 370 nm was no longer observed for all samples. As shown for Fmoc-FF and as will be seen in the following sections for Fmoc-FG, Fmoc-GG and Fmoc-GF, self-assembly is observed upon lowering pH. It is likely that self-assembly locks the molecules in their most stable conformation i.e. in an antiparallel arrangement. This hypothesis suggests that antiparallel dimers probably correspond to the base building blocks of the supramolecular structures observed.

As the pH was lowered from 10.5 to acidic conditions, a broad photoluminescence peak centred at 425–445 nm indicative of multiple aromatic groups (Fmoc and/or phenyl rings) stacked through π -interactions, was also detected [19]. The presence of this peak suggests that at lower pH, as the peptide derivatives become mainly un-ionised, electrostatic repulsion between the molecules is reduced, favouring their packing into extensive aggregates. As shown in Figure 5.12 D, the photoluminescence peak was found to be relatively intense for Fmoc-GF at pH values of 7.1 and 3.8. Photoluminescence bands have been reported to be particularly intense in some proteins where the fluorophores were located in highly protected environments [22]. This behaviour suggests that Fmoc groups could be buried deeper within the self-assembled structures formed by Fmoc-GF than in those formed by the other Fmoc-dipeptides. Indeed, as will be discussed in the following sections, Fmoc-GF self-assemblies were remarkably different from those formed by the other systems.

As shown above for Fmoc-FF, most notably by TEM, lowering the pH led to an increase of the level of organisation within the self-assembled structures, resulting in the formation of larger molecular self-assemblies. This behaviour was confirmed here as a red shift of the emission peak was observed, as well as an increase in photoluminescence intensity compared to the spectrum of the solubilised molecules [23]. As these two features were also observed for Fmoc-FG, Fmoc-GG and Fmoc-GF, a study as a function of pH should reveal the same trend for these systems – that is the formation of self-assembled structures and enhancement of their level of organisation upon lowering pH.

As observed in Chapter 4 the ‘titration’ of Fmoc-FG, Fmoc-GG and Fmoc-GF is characterised by only one transition as opposed to Fmoc-FF for which the self-assembly process was associated with two pH transitions. In order to relate the ionisation behaviour of these three systems to their self-assembly properties, structural characterisation of the samples has been undertaken using the same methodology at different pHs: 10.5, the starting point of the ‘titration’; above and below the apparent pK_a transition.

5.3.3. Fmoc-FG

5.3.3.1. pH Study

At pH 10.5 all Fmoc-FG molecules are thought to be fully ionised. As mentioned in Chapter 4, solutions became clear only after the samples were heated. This behaviour suggests structures in the size range of visible light wavelength were formed at room temperature and were only dissolved at high temperature. TEM micrographs show the

presence of twisted ribbons with average pitch and width of 213 ± 17 nm and 34.8 ± 4.1 nm respectively under these pH conditions (Figure 5.15 A). Although the handedness of these chiral objects cannot be determined due to the sample preparation and observation conditions used, we can assume that resulting from the self-assembly of L-peptide derivatives the supramolecular structures were left-handed [24]. As indicated by the broad band centred at 1598 cm^{-1} in the infrared spectrum (Figure 5.16), the terminal carboxylic groups are ionised at this pH. The presence of self-assembled structures at pH 10.5 is consistent with the non-normalised fluorescence spectra (Appendix E) since the emission maximum at ~ 313 nm was significantly more intense for this system than for the other Fmoc-dipeptides which did not self-assemble at this pH.

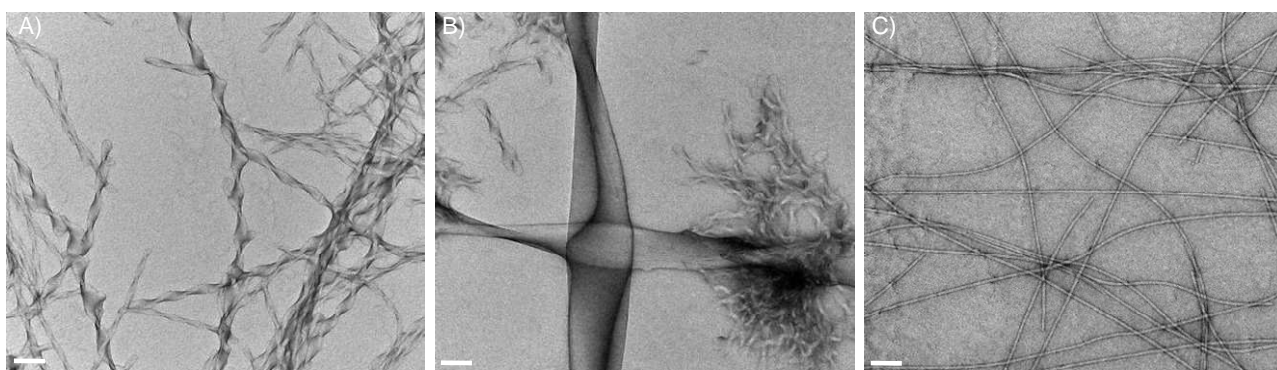


Figure 5.15. TEM micrographs of Fmoc-FG samples at 10 mmol L^{-1} **A)** at pH 10.5 starting point of the ‘titration’ experiments, **B)** at pH 8.6 and 7.6 (above the apparent pK_a) and **C)** pH 5.0 (below the apparent pK_a). Scale bars represent 100 nm.

Although glycine does not have the propensity to favour β -sheet formation, the Fmoc-FG molecules could possibly arrange in antiparallel β -sheets at the molecular level as weak peaks at 1690 and 1623 cm^{-1} were detected by FT-IR (Figure 5.16).

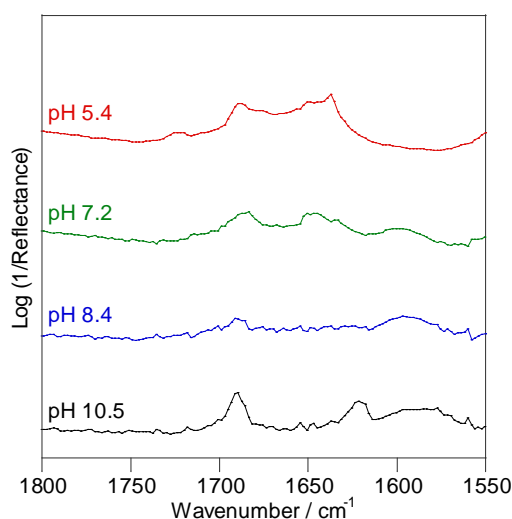


Figure 5.16. FT-IR spectra of Fmoc-FG samples at 10 mmol L^{-1} prepared in D_2O at pH 10.5 starting point of the ‘titration’ experiment, pH 8.4 and 7.2 (above the apparent pK_a) and pH 5.4 (below the apparent pK_a).

Upon addition of HCl (above the apparent pK_a), turbid solutions were obtained after being left overnight at 4 °C. From the dynamic frequency sweep in Figure 5.17, we can see that at pH 7.6 the viscous modulus (G'') was higher than the elastic modulus (G') until a crossover of the moduli was observed beyond 10 rad s^{-1} . Additionally, both moduli were frequency dependent between 0.01 and 100 rad s^{-1} , confirming that the material was liquid-like.

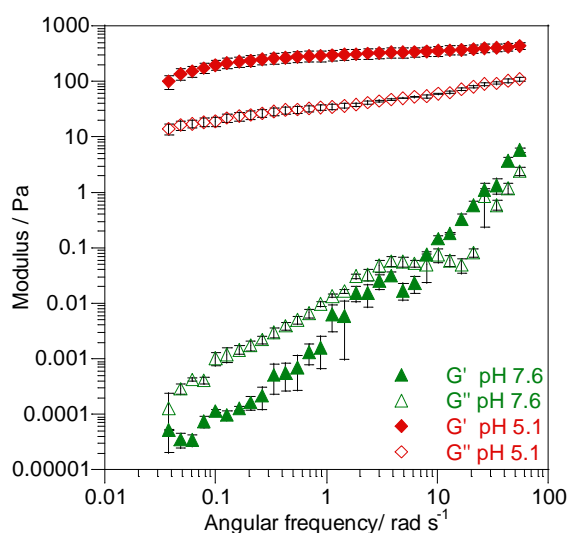


Figure 5.17. Dynamic frequency sweep of Fmoc-FG samples at 10 mmol L^{-1} at pH 7.6 and 5.1 (above and below the apparent respectively).

At pH 9.0–7.2 the twisted ribbons observed at higher pH in absence of HCl were still visible in the TEM micrographs (Figure 5.15 B). In addition, larger twisted ribbons with pitch and width in the range of 1565–3920 nm and 214–384 nm respectively were also observed. The infrared peaks characteristic of antiparallel β -sheets (at 1687 and 1638 cm^{-1}) were barely detectable at pH 8.4, however they were observed at pH 7.2 (Figure 5.16). An additional band, which could be attributed to random coils also started to appear at 1649 cm^{-1} at pH 7.2. The formation of self-assembled structures with different molecular conformations is associated with the apparent pK_a transition observed for this sample (Chapter 4). As shown in Figure 5.17, in this pH range WAXS reflection peaks were observed at 2.0 and 9.9 nm^{-1} , corresponding to repeat distances of 31.1 and 6.4 Å. Although the size of the structures observed by TEM were substantially different at pH \sim 9.0 and 7.6, the Bragg peaks observed in the scattering pattern were at the same positions at both pH values, suggesting that the periodicities detected were likely to be related to repeat units within the self-assembled structures (Figure 5.18). The distances between the β -strands (\sim 4.3 Å) and the pairs of Fmoc groups along the diagonal axis of the fibres

($\sim 7.6 \text{ \AA}$) that were detected for Fmoc-FF system were not observed here since the reflection peak at 6.4 \AA was not in the range of any of these two features.

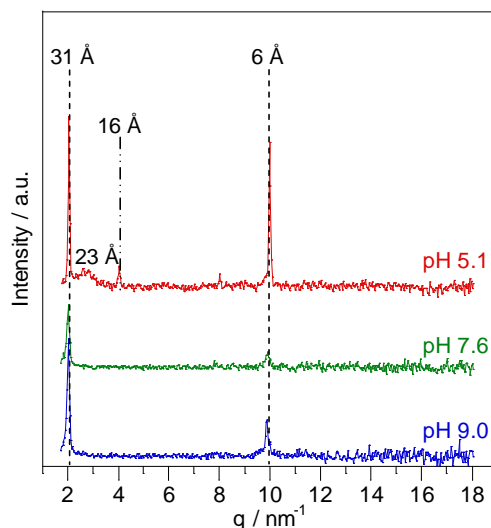


Figure 5.18. WAXS spectra of Fmoc-FG samples at 10 mmol L^{-1} dried at pH 9.0 and 7.6 (above the apparent pK_a) and pH 5.1 (below the apparent pK_a).

Just below the apparent pK_a , clear hydrogels were obtained upon heating. Once cooled down the hydrogels formed were found to be relatively stable provided that the samples had been heated long enough beforehand. Indeed, Fmoc-FG hydrogels formed upon dilution of organic solutions into water were found not to be stable over time and precipitated after a few hours, showing the importance of the heating step in the gel formation for this system [25]. The gel-like nature of the sample at pH 4.7 was confirmed by rheology (Figure 5.17). The elastic modulus ($G' \sim 100\text{--}400 \text{ Pa}$) was about ten times higher than the viscous modulus, confirming the material was elastic rather than viscous. Additionally both G' and G'' depended weakly on frequency between 0.01 and 100 rad s^{-1} . This behaviour, characteristic of entangled polymer networks, was in agreement with the morphology of the structures observed by TEM. As shown in Figure 5.14 C, the presence of an extended entangled network composed of thin fibres with a width of $8.6 \pm 0.5 \text{ nm}$ was revealed. From the infrared data, it is apparent that the peaks at 1649 cm^{-1} and at 1687 and 1638 cm^{-1} characteristic of random coils and antiparallel β -sheets respectively were still present (Figure 5.16). An additional peak was observed at. As expected, the band at 1598 cm^{-1} characteristic of ionised carboxylate groups was no longer detected. As can be seen from Figure 5.18, the Bragg peaks of high intensity detected at 31.1 and 6.4 \AA at higher pH were still present, with comparable ratios at pH 5.1. This observation suggests a common feature exists in the molecular arrangement of the self-assembled structures over the range of pH conditions tested. The various twisted and straight ribbons and fibres

observed above and below the apparent pK_a transition may all result from the same basic unit periodically repeated down the long axis of the structures. Additional reflections were detected at pH 5.1 with a broad peak at 23.3 Å ($q = 2.7 \text{ nm}^{-1}$) and another peak at 15.5 Å ($q = 4.1 \text{ nm}^{-1}$) that were both of low intensity. Unlike for Fmoc-FF, no Bragg peaks corresponding to higher order reflections were detected, suggesting the absence of well defined lamellar organisation. This difference could be due to the structures formed resulting from lateral growth, rather than lateral self-assembly of individual fibrils into larger bundles of fibres (below the apparent pK_a transition). Such behaviour was confirmed by TEM since lateral association was not observed.

5.3.3.2. Temperature Study at pH ~ 4.5

As mentioned in Chapter 4, Fmoc-FG hydrogels were found to form during the heating step, suggesting an increase in the mechanical properties of the materials with increasing temperature. To monitor this evolution, rheological measurements were undertaken below the apparent pK_a transition, from room temperature (25 °C) up to 80 °C while the gels were forming in the rheometer.

Samples were prepared as described in Chapter 3 up to the heating step – that is they were not heated. To prevent self-assembly to occur, all samples were thoroughly sonicated prior to experiment. The temperature variations usually occurring during sample preparation were mimicked as closely as possible: the solutions were heated from 25 to 80 °C at a rate of 10 °C min^{-1} . The temperature was then kept at 80 °C for 2.5 min before being reduced to 4 °C over a period of one minute. Samples were finally kept at 4 °C for 8.5 min. Figure 5.19 shows the viscoelastic behaviour of Fmoc-FG upon heating and subsequent cooling. G' was always higher than G'' for the duration of the measurement, even before heating. This behaviour suggests that self-assembly occurred at 25 °C. However, the Fmoc-FG samples exhibited G' and G'' of the same order of magnitude and displayed relatively low G' values ($< 1 \text{ Pa}$) between 25 and 55 °C, indicating viscous solutions rather than gels were formed at the start of the experiment. As the temperature rose from 55 to 80 °C, G' and G'' increased by three and four orders of magnitude respectively, resulting in G' values about one order of magnitude higher than G'' values. Stable storage ($G' \sim 1950 \pm 150 \text{ Pa}$) and loss moduli values were observed as the sample was cooled down to 40 °C. This feature indicated that a relatively strong stable gel-like material was formed, which is in agreement with the visual observations made during hydrogel preparation. Upon lowering temperature further to 25 °C an abrupt decrease in G' and G'' to ~ 6 and 3 Pa respectively was observed.

Formation of Fmoc-FG hydrogels *in situ* (i.e. in the rheometer) revealed an overall increase of one order of magnitude in both G' and G'' between the beginning of the measurement at 25 °C and the end of the experiment at 4 °C. Interestingly, the heating and cooling curves showed a hysteresis phenomenon. Although as expected, the viscoelastic properties of the material increased with temperature up to greater G' values than those obtained for pre-formed hydrogels, they also remained temperature dependent as this parameter was lowered. Final values of storage modulus at 25 °C were found to be ~ 10 times lower compared to those obtained for pre-formed hydrogels. This difference in moduli could be due to the samples being prepared in distinct ways. Pre-formed gels were cooled down in the test tube unperturbed before the samples were subjected to rheological measurements. In contrast, gels prepared *in situ* were sheared in the rheometer as they were cooled down, resulting in the disruption of the gel. Consequently the gel broke into lumps as observed at the end of the experiment, which led to lower G' values.

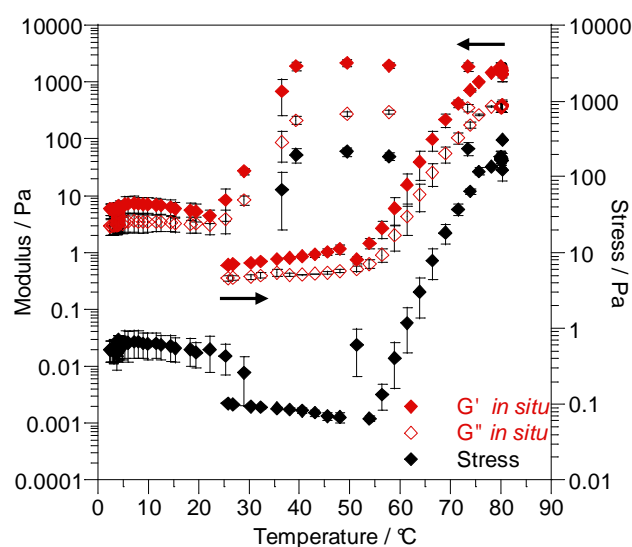


Figure 5.19. Dynamic temperature sweep at constant strain of 0.01 of Fmoc-FG samples (10 mmol L^{-1}) as a function of temperature (from 25 °C to 80 °C to 4 °C).

A TEM micrograph of a non-heated sample is shown in Figure 5.20 A. The fibres observed before and after heating (Figure 5.15 C) were found to be similar in both cases. As shown in Figure 5.20 B, infrared spectra of non-heated and heated samples were found to be similar too at this pH. This behaviour suggests the heating step does not alter the morphological and structural properties of the self-assembled objects. On the other hand, the homogeneity of the samples was improved – the samples became clear and transparent upon heating rather than being cloudy. This behaviour could either be due to the presence of aggregates or be related to solubility issues following addition of HCl. The latter interpretation is favoured; indeed, no clusters of aggregated fibres were observed by TEM.

It is therefore likely that addition of acid led to the precipitation of some Fmoc-FG molecules. During the heating step these molecules were re-dissolved and locked in the self-assembled structures, resulting in an increase in moduli and a more stable hydrogel upon cooling. Although the drop in moduli observed when the sample was cooled down is related to a shearing effect, it also suggests a change in the fibre properties which is not yet fully understood.

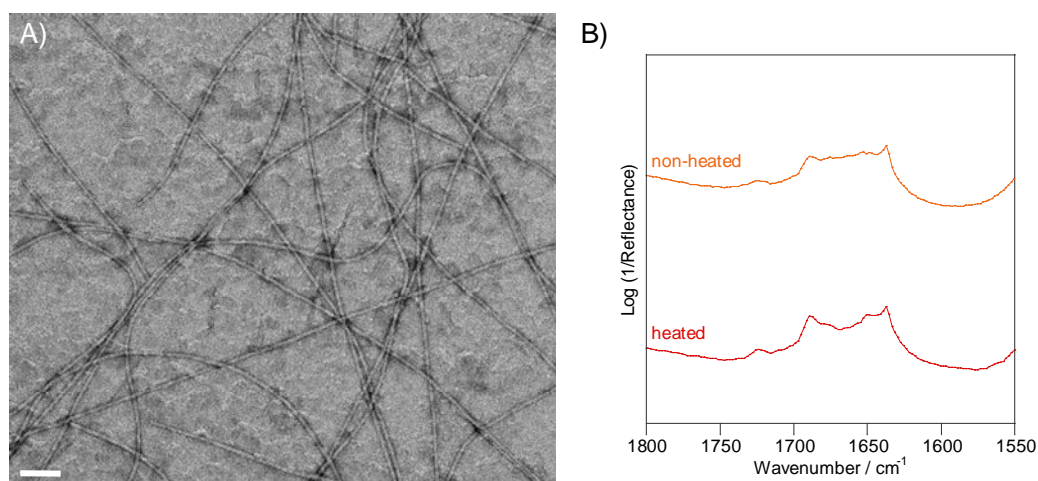


Figure 5.20. A) TEM micrograph of a non-heated Fmoc-FG sample at 10 mmol L^{-1} below the apparent pK_a transition. Scale bar represents 100 nm . B) FT-IR spectra of non-heated and heated Fmoc-FG samples at 10 mmol L^{-1} prepared in D_2O below the apparent pK_a transition.

5.3.4. Fmoc-GG pH study

At pH 10.5 the absence of structure on the TEM micrographs (Figure 5.21 A) and of significant peaks in the amide I region of the FT-IR spectrum (Figure 5.22) suggested that the molecules were not self-assembled. As expected, Fmoc-GG was ionised at this pH, which was confirmed by FT-IR with the presence a broad band at $\sim 1594 \text{ cm}^{-1}$.

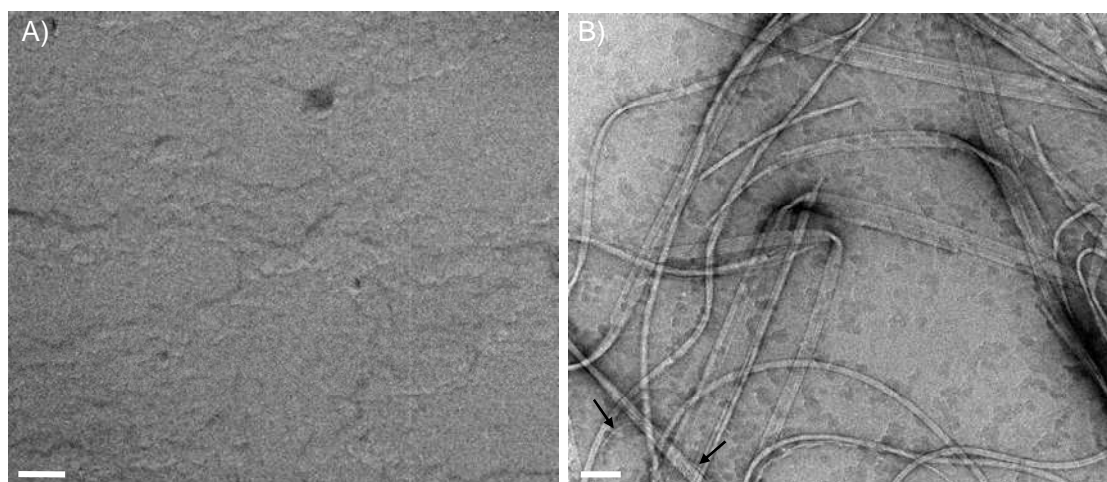


Figure 5.21. TEM micrographs of Fmoc-GG samples at 10 mmol L^{-1} A) at pH 10.5–7.3 (above the apparent pK_a) and B) pH 4.8 (below the apparent pK_a). Scale bars represent 100 nm .

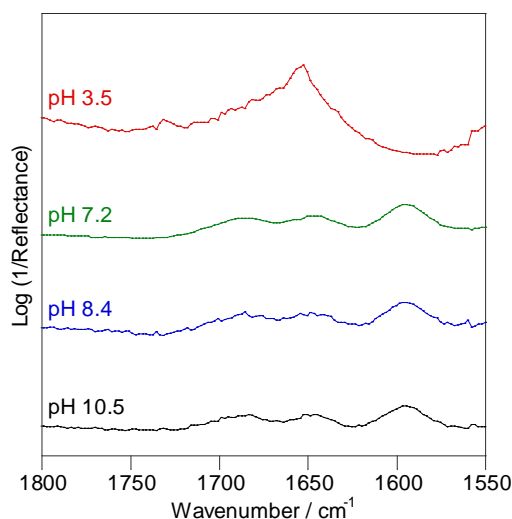


Figure 5.22. FT-IR spectra of Fmoc-GG samples at 10 mmol L^{-1} prepared in D_2O at pH 10.5 starting point of the 'titration' experiment, pH 8.4 and 7.2 (above the apparent pK_a) and pH 3.5 (below the apparent pK_a).

When the pH was reduced to 9.0–7.2 (above the apparent pK_a) clear solutions were still obtained. TEM (Figure 5.21 A) and infrared (Figure 5.22) data remained similar, showing that Fmoc-GG molecules were still in solution. As can be seen from Figure 5.23, the rheological spectra showed a strong frequency dependence of both G' and G'' between 0.01 and 100 rad s^{-1} , which is also typical for liquid-like materials.

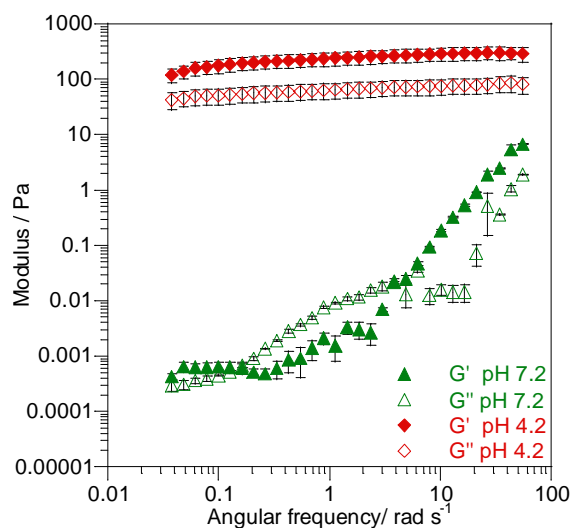


Figure 5.23. Dynamic frequency sweep of Fmoc-GG samples at 10 mmol L^{-1} at pH 7.2 and 4.2 (above and below the apparent respectively).

As shown in Figure 5.24, diffraction peaks of relatively low intensity were observed by WAXS. The presence of these Bragg peaks suggests a lamellar packing pattern characteristic of crystalline structures with a d spacing of 29.9 \AA ($q = 2.1 \text{ nm}^{-1}$) and up to six higher order reflections were detected. Since no structures were observed by TEM in these pH conditions, it is believed that the peaks arose from the formation of crystals

during the sample drying process. An additional reflection peak was detected at 25.3 \AA ($q = 2.5 \text{ nm}^{-1}$), which could correspond to a repeat distance present down the long axis of the structures.

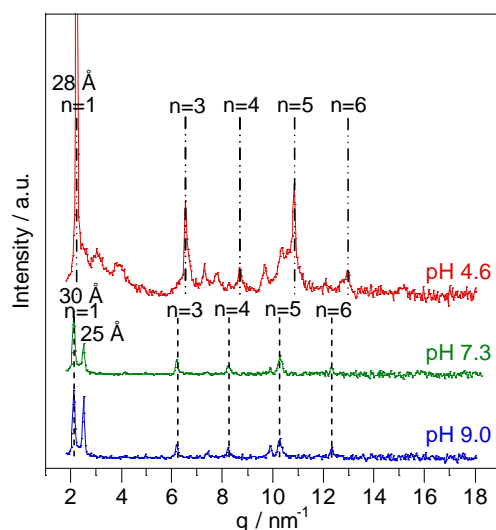


Figure 5.24. WAXS spectra of Fmoc-GG samples at 10 mmol L^{-1} dried at pH 9.0 and 7.3 (above the apparent pK_a) and pH 4.6 (below the apparent pK_a).

When the pH was reduced further below the apparent pK_a , cloudy hydrogels were formed. As can be seen from Figure 5.23, at pH 4.2 G' was higher than G'' between 0.01 and 100 rad s^{-1} , with both moduli displaying little frequency dependence, confirming the gel-like nature of the sample. Like for Fmoc-FG hydrogels, G' values were in the range of 100–400 Pa, which shows Fmoc-FG and Fmoc-GG hydrogels were stronger compared to the Fmoc-FF hydrogels reported in Section 5.3.1 (0.5–5 Pa) [26]. The rheological behaviour of Fmoc-GG was consistent with the entangled fibrillar network observed by TEM at pH 4.6 as flat ribbons of various widths were found to form from fibril units of $\sim 3 \text{ nm}$ in width (arrows in Figure 5.21 B). As can be seen from the micrograph, an increase in the number of fibrils per ribbon resulted in the straightening of the self-assembled objects. FT-IR spectroscopy confirmed the absence of ionised Fmoc-GG species at this pH with the disappearance of the band at $\sim 1594 \text{ cm}^{-1}$. The infrared spectrum of the sample also displayed a peak at $\sim 1653 \text{ cm}^{-1}$, indicating the peptide tail of the molecules possibly adopted a random coil conformation (Figure 5.22). Fmoc-GG hydrogels were found not to be particularly stable as precipitation of the samples started to occur after gel formation at $4 \text{ }^\circ\text{C}$ and was accelerated at room temperature. Figure 5.25 shows a TEM micrograph of Fmoc-GG at pH ~ 4.6 left at room temperature for one week. The large structures observed were assumed to correspond to crystals, which would be in agreement with the scattering pattern obtained at this pH (Figure 5.24). Since the samples

used for WAXS experiments were obtained by a slow drying process at room temperature, crystallisation was observed in the scattering pattern. The series of Bragg peaks ascribed to a lamellar type organisation observed at higher pH was still present, however a slight shift in size was observed since the series was characterised by a d spacing of 28.2 Å ($q = 2.2 \text{ nm}^{-1}$) and up to six higher order reflections. This series is thought to arise from the Fmoc-GG self-assembly into ribbons of fibres. However since the hydrogel state is metastable, the system tends to return to the more stable precipitated state by expelling water, resulting in smaller repeat distances.

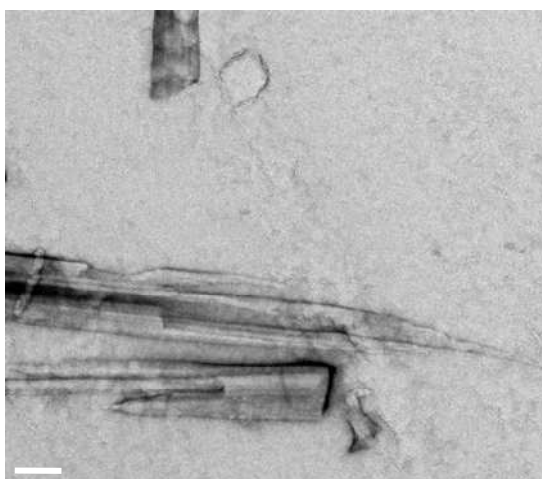


Figure 5.25. TEM micrographs of Fmoc-GG hydrogel at 10 mmol L^{-1} precipitating slowly after one week. Scale bars represent 100 nm.

5.3.5. Fmoc-GF pH study

At pH 10.5, clear solutions were obtained from Fmoc-GF. As can be seen from the TEM micrograph (Figure 5.26 A) no self-assembly was formed, which was confirmed by FT-IR with the absence of peak in the amide I region (Figure 5.27).

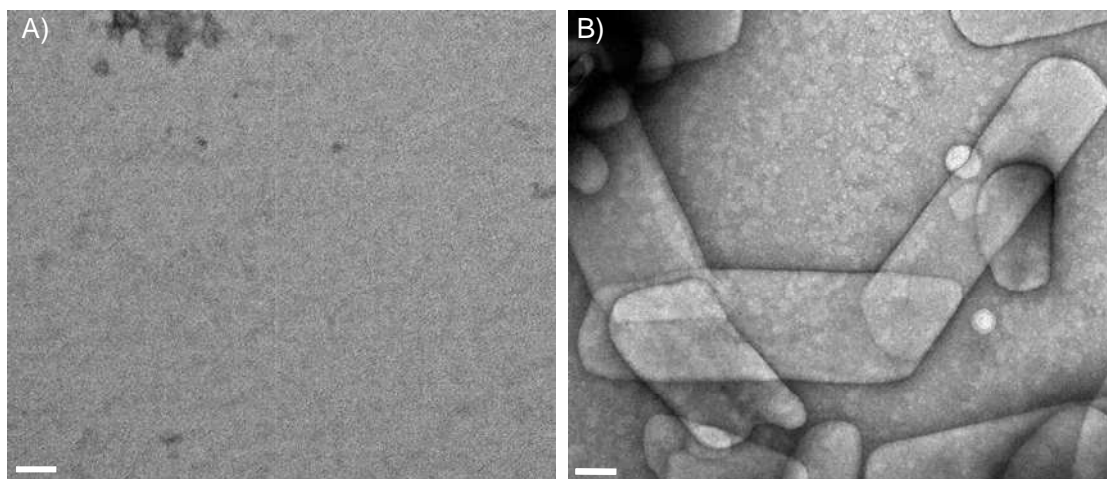


Figure 5.26. TEM micrographs of Fmoc-GF samples at 10 mmol L^{-1} **A)** at pH 10.5 and 8.9 (above the apparent pK_a) and **B)** pH 7.3 and 4.6 (below the apparent pK_a). Scale bars represent 100 nm.

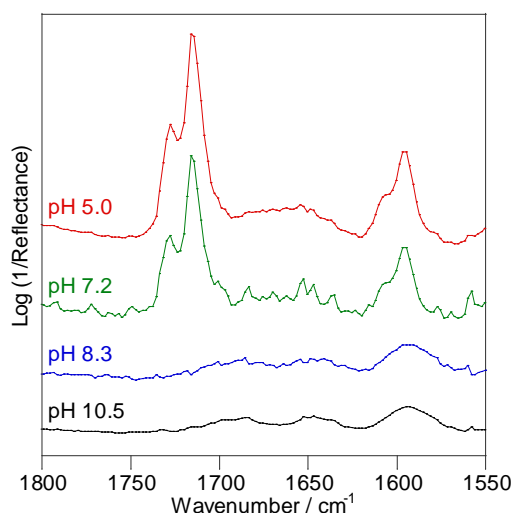


Figure 5.27. FT-IR spectra of Fmoc-GF samples at 10 mmol L^{-1} prepared in D_2O at pH 10.5 starting point of the 'titration' experiment, pH 8.3 and 7.2 (above the apparent pK_a) and pH 5.0 (below the apparent pK_a).

After addition of HCl at pH ~ 8.7 (above the apparent pK_a), clear solutions were still obtained. No significant difference was observed by TEM (Figure 5.26 A) and FT-IR (Figure 5.27) suggesting that self-assembled structures were not formed yet at this stage. As can be seen from Figure 5.28, a weak reflection was observed at $q = 2.2 \text{ nm}^{-1}$, corresponding to a repeat distance of $d = 28.2 \text{ \AA}$.

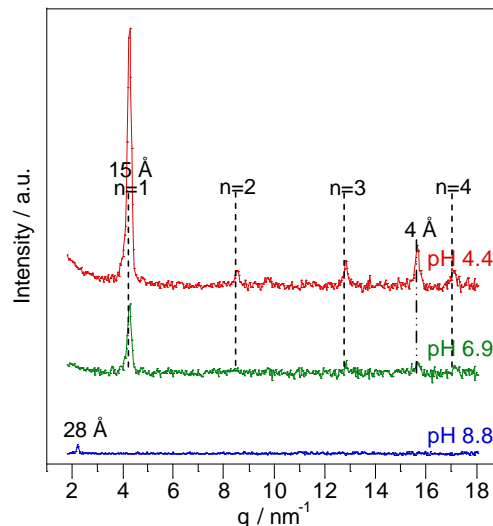


Figure 5.28. WAXS spectra of Fmoc-GF samples at 10 mmol L^{-1} dried at pH 8.8 and 6.9 (above the apparent pK_a) and pH 4 (below the apparent pK_a).

Upon further addition of HCl, milky flocculates indicating the formation of insoluble self-assembled structures were obtained. In contrast with the other Fmoc-dipeptides studied in this Chapter no high aspect ratio architectures were observed. TEM micrographs revealed the presence of large sheet-like objects of more than 200 nm in width (Figure 5.26 B). These structures were too short to entangle with each others, so no 3D networks enabling solvent trapping could be formed, which explains why hydrogels were not formed at any

pH conditions with Fmoc-GF system. Complementary analyses of the self-assembled objects were undertaken by atomic force microscopy (AFM). Although the quality of the micrographs obtained was not good due to sample preparation issues related to the technique, measurements were carried out on the observed structures (Appendix F). Rough estimations of the thickness of the sheets were obtained by measuring the difference in height between the top of the objects and the mica surface, which provided values of ~ 50 nm, enabling it to be concluded that the sheets were constituted of multilayers of peptide derivatives. The formation of non-gelling structures was also observed from Fmoc-GF by Gazit *et al.*, however the self-assemblies were identified as tubular by the authors. It is likely that this difference resulted from distinct methods of preparation since Gazit's samples were obtained upon dilution of organic solutions of peptide derivatives into water [25]. At pH 7.3–4.4 (below the apparent pK_a transition), absorption bands were observed in the infrared spectrum (Figure 5.27), indicating that at this stage self-assembly of Fmoc-GF has occurred, which is in agreement with the microscopy results. Although the molecular arrangement is not fully understood yet, the resemblance of the infrared spectra below the apparent pK_a transition and of the peptide powder as received confirmed the peptide tails were not structured in these pH conditions. The presence of the self-assembled structures observed by TEM is in agreement with the WAXS pattern as a series of Bragg peaks of relatively low intensity suggesting a lamellar packing was observed at pH 6.9, near the apparent pK_a transition (Figure 5.28). Just as the spectroscopic signal detected by FT-IR became stronger upon addition of more HCl (pH 5.0, Figure 5.27), the intensity of the Bragg peaks observed by WAXS increased at pH 4.4. As shown in Figure 5.28 the lamellar organisation was confirmed with the presence of reflection peaks at the same q values as at neutral pH, displaying a d spacing of 14.8 \AA ($q = 4.2 \text{ nm}^{-1}$) and up to four higher order reflections. An additional Bragg peak was observed at 15.7 nm^{-1} , corresponding to a repeat distance of 4.0 \AA .

5.3.6. Summary

From fluorescence spectroscopy data, Fmoc-FF, Fmoc-FG, Fmoc-GG and Fmoc-GF molecules were found to essentially dimerise in an antiparallel manner through π -interactions of their fluorenyl groups. Further self-assembly of the base building block dimers was then driven by π -stacking and hydrogen bonding to generate supramolecular structures upon lowering pH. For all the studied systems the apparent pK_a transitions highlighted in Chapter 4 were found to be associated with the formation of distinct self-assembled structures with differing molecular conformations that were amino acid

sequence dependent. Indeed, phenylalanine provides rigidity to the molecules and has the propensity to favour β -sheet formation whereas glycine brings about some level of flexibility, tending to promote random coil conformations.

Due to the C-terminal phenylalanine residue of Fmoc-FF π -stacking with Fmoc dimers, the peptide backbones of the molecules were constrained and rigid enough to allow the formation of antiparallel β -sheets. Replacement of the phenylalanine by a glycine residue in the C-terminal position of Fmoc-FG slightly altered the rigidity of the molecules and the stability of the antiparallel β -sheets. As a result they were found to coexist with random coils at low pH. Introduction of glycine next to the Fmoc group in Fmoc-GF and Fmoc-GG enhanced the flexibility of the molecules' tail, making intermolecular hydrogen bond formation unfavourable and resulting in random coils (for Fmoc-GG) rather than antiparallel β -sheet structures.

Below their (first) apparent pK_a transition, Fmoc-FF, Fmoc-FG and Fmoc-GG formed hydrogels with varying mechanical properties depending on the amino acid sequence, which were associated with entangled fibrillar networks on the microscopic scale. Fmoc-FF and Fmoc-GG both formed fibres of ~ 3 nm in width, which could further self-assemble laterally to adopt a lamellar organisation with d spacings of about 26 and 28 Å respectively. However, Fmoc-GG hydrogels were found to be not particularly stable as they tended to precipitate and crystallise. Despite the ionised state of the molecules above their apparent pK_a , Fmoc-FG peptide derivatives were found to form large twisted ribbons at high pH. Neutralisation of the peptide derivatives resulted in the formation of an entangled network of untwisted fibres of ~ 8.5 nm in width. The hydrogels associated with this transition had the peculiarity of being obtained upon heating. Unlike the other studied systems, Fmoc-FG did not exhibit a lamellar organisation, indicating that the self-assembly mechanism was not based on the lateral association of individual fibres. However, both twisted and untwisted structures were characterised by common repeat distances that were probably related to the conformation of the peptide derivatives within the self-assembled structures. The d spacing of 31 Å is therefore likely to correspond to a periodicity in the long axis of the fibres. Similarly, the d spacing of 25 Å detected for Fmoc-GG could also be related to a repeat unit in the long axis of the fibres.

In contrast, below its apparent pK_a Fmoc-GF was characterised by the presence of large sheet-like structures related to the formation of non-gelling flocculates. The formation of such structures confirms fluorescence spectroscopy data in which a strong photoluminescence band characteristic of extensive aggregates was detected. From the

TEM observations, it is unlikely that these structures resulted from the lateral self-assembly of smaller fibrils. Although the parameters that control the preferential growth direction of the sheets have not yet been elucidated, it is clear from the WAXS pattern that these supramolecular objects result from a lamellar organisation with a d spacing of $\sim 15 \text{ \AA}$.

5.4. CONCLUSION

Like Fmoc-FF molecules, Fmoc-FG, Fmoc-GG and Fmoc-GF peptide derivatives also self-assembled upon lowering pH. Study of the different systems as a function of pH revealed the dramatic pK_a shifts characterising the four systems of interest in this chapter were related to significantly different structural behaviours. The peptide derivatives typically showed self-assembling behaviour below their apparent pK_a following a mechanism that was either gradual (two-transition feature) for Fmoc-FF or more abrupt (one-transition feature) for Fmoc-GG and Fmoc-GF. Despite its one-transition feature, Fmoc-FG did not follow the exact same trend as the other systems. Self-assembly also occurred above the apparent pK_a , however the transition coincided with structural and morphological changes.

By varying the two amino acids of the Fmoc-dipeptides, microscopic objects displaying various morphologies were formed. Entangled networks of different types of fibres related to hydrogel formation were formed for Fmoc-FF, Fmoc-FG and Fmoc-GG whereas sheet-like structures associated with precipitation was observed for Fmoc-GF.

Although for the four systems the new sample preparation method did not seem to affect the structural properties of the aggregates formed, the stability of the samples was found to be altered in the case of Fmoc-GG.

5.5. REFERENCES

1. Ulijn, R.V., Moore, B.D., Janssen, A.E.M., *et al.*, *A single aqueous reference equilibrium constant for amide synthesis–hydrolysis*. *Journal of the Chemical Society, Perkin Transactions 2*, **2002**, 1024-1028.
2. Jayawarna, V., Ali, M., Jowitt, T.A., *et al.*, *Nanostructured hydrogels for three-dimensional cell culture through self-assembly of fluorenylmethoxycarbonyl-dipeptides*. *Advanced Materials*, **2006**, 18 (5), 611-614.
3. Adams, D.J., Butler, M.F., Frith, W.J., *et al.*, *A new method for maintaining homogeneity during liquid–hydrogel transitions using low molecular weight hydrogelators*. *Soft Matter*, **2009**, 5 (9), 1856-1862.
4. Smith, A.M., Williams, R.J., Tang, C., *et al.*, *Fmoc-diphenylalanine self assembles to a hydrogel via a novel architecture based on π - π interlocked β -sheets*. *Advanced Materials*, **2008**, 20 (1), 37-41.
5. Stryer, L., *Biochemistry*. 4th ed. **1995**, New York: Freeman.
6. Urry, D.W., Peng, S.Q., Parker, T.M., *et al.*, *Relative significance of electrostatic- and hydrophobic-induced pKa shifts in a model protein: the aspartic acid residue*. *Angewandte Chemie International Edition in English*, **1993**, 32 (10), 1440-1442.
7. Kanicky, J.R., Poniatowski, A.F., Mehta, N.R., *et al.*, *Cooperativity among molecules at interfaces in relation to various technological processes: effect of chain length on the pKa of fatty acid salt solutions*. *Langmuir*, **2000**, 16 (1), 172-177.
8. Mahler, A., Reches, M., Rechter, M., *et al.*, *Rigid, self-assembled hydrogel composed of a modified aromatic dipeptide*. *Advanced Materials*, **2006**, 18 (11), 1365-1370.
9. Das, A.K., Collins, R.F., and Ulijn, R.V., *Exploiting enzymatic (reversed) hydrolysis in directed self-assembly of peptide nanostructures*. *Small*, **2008**, 4 (2), 279-287.
10. Jayawarna, V., Richardson, S.M., Hirst, A.R., *et al.*, *Introducing chemical functionality in Fmoc-peptide gels for cell culture*. *Acta Biomaterialia*, **2009**, 5 (3), 934-943.
11. Zhou, M., Smith, A.M., Das, A.K., *et al.*, *Self-assembled peptide-based hydrogels as scaffolds for anchorage-dependent cells*. *Biomaterials*, **2009**, 30 (13), 2523-2530.
12. Kim, U.-J., Park, J., Li, C., *et al.*, *Structure and properties of silk hydrogels*. *Biomacromolecules*, **2004**, 5 (3), 786-792.
13. Blake, C. and Serpell, L., *Synchrotron X-ray studies suggest that the core of the transthyretin amyloid fibril is a continuous β -sheet helix*. *Structure*, **1996**, 4 (8), 989-998.
14. Barth, A. and Zscherp, C., *What vibrations tell about proteins*. *Quarterly Reviews of Biophysics*, **2002**, 35 (4), 369-430.
15. Bellamy, L.J., *The infra-red spectra of complex molecules*. 3rd ed. Vol. 1. **1975**, London: Chapman and Hall.

16. Schneider, J.P., Pochan, D.J., Ozbas, B., *et al.*, *Responsive hydrogels from the intramolecular folding and self-assembly of a designed peptide* Journal of the American Chemical Society, **2002**, *124* (50), 15030-15037.
17. Rapaport, H., Grisar, H., and Silberstein, T., *Hydrogel scaffolds of amphiphilic and acidic β -sheet peptides*. Advanced Functional Materials, **2008**, *18* (19), 2889-2896.
18. Fink, D.W. and Koehler, W.R., *pH effects on fluorescence of umbelliferone*. Analytical Chemistry, **1970**, *42* (9), 990-993.
19. Yang, Z., Gu, H., Zhang, Y., *et al.*, *Small molecule hydrogels based on a class of antiinflammatory agents*. Chemical Communications, **2004** (2), 208-209.
20. Schweitzer, D., Hauser, K.H., and Haenel, M.W., *Transannular interaction in [2.2]phanes: [2.2](4,4')Diphenylphane and [2.2](2,7) fluorenophane*. Chemical Physics, **1978**, *29* (1-2), 181-185.
21. Shaik, M.S., *Personnal communication*. **2009**, Calculations based on molecular dynamics simulations in a cubic cell where water and peptide derivatives were modeled using TIP3P and AMBER force field respectively.
22. Lakowicz, J.R., *Principles of fluorescence spectroscopy*. 3rd ed. **2006**, Boston: Springer.
23. Wang, W., Han, J.J., Wang, L.-Q., *et al.*, *Dynamic π - π stacked molecular assemblies emit from green to red colors*. Nano Letters, **2003**, *3* (4), 455-458.
24. Fishwick, C.W.G., Beevers, A.J., Carrick, L.M., *et al.*, *Structures of helical β -tapes and twisted ribbons: the role of side-chain interactions on twist and bend behavior*. Nano Letters, **2003**, *3* (11), 1475-1479.
25. Orbach, R., Adler-Abramovich, L., Zigerson, S., *et al.*, *Self-assembled Fmoc-peptides as a platform for the formation of nanostructures and hydrogels*. Biomacromolecules, **2009**, *10* (9), 2646-2651.
26. Tang, C., Smith, A.M., Collins, R.F., *et al.*, *Fmoc-diphenylalanine self-assembly mechanism induces apparent pKa shifts*. Langmuir, **2009**, *25* (16), 9447-9453.

Effect of Hydrophobic Alkyl Chains in the Self-Assembly of Fmoc-Dipeptides

6.1. ABSTRACT

The self-assembly process of Fmoc-dipeptides possessing aromatic side chains was found to be pH dependent. In order to understand the importance of the aromatic moieties on the self-assembly mechanism, similar systems possessing alkyl side chains were investigated. ‘Titrations’ of Fmoc-LL, Fmoc-LG and Fmoc-GL also revealed apparent pK_a shifts above their theoretical pK_a^{th} . Using Fourier transform infrared (FT-IR) and fluorescence spectroscopy, transmission electron microscopy (TEM), wide-angle X-ray scattering (WAXS), and oscillatory rheology, these transitions were shown to coincide with significant structural changes. Common features were observed between the leucine-based systems and their phenylalanine-based homologues, providing additional clues towards the design rules for the preparation of hydrogels with tailored properties. Fmoc-LL hydrogels were characterised by relatively weak mechanical properties in a similar manner to Fmoc-FF. Fmoc-FG and Fmoc-LG both exhibited supramolecular chirality and formed gels upon heating. As for Fmoc-GF, Fmoc-GL was found to self-assemble into structures incompatible with hydrogel formation. On the other hand, no lamellar organisation was detected for the leucine-based Fmoc-dipeptides, contrarily to what was observed for their phenylalanine homologues.

6.2. INTRODUCTION AND OBJECTIVES

Fmoc-dipeptides based on the pairing of phenylalanine and glycine were shown to exhibit dramatic pK_a shifts that were found to be related to significant structural modifications. In order to measure the impact of the aromatic side chains on the self-assembling behaviour of the studied systems, phenylalanine was replaced by leucine (Figure 6.1), the alkyl side chain of which has the same hydrophobicity as the phenyl side chain of phenylalanine (Table 2.2). Such type of substitution has previously been shown not to alter the ability of the molecules to self-assemble into higher order structures [1]. Additionally, formation of hydrogels from leucine-based Fmoc-peptides by pH change and by enzymatic reaction has

been reported in the literature. No hydrogels were formed from Fmoc-GL [2,3]. Under specific conditions, Fmoc-LG was found to generate fibrillar networks forming hydrogels, whether the pH was adjusted with HCl [2] or sugar precursors of acid [4]. Fmoc-LL hydrogels could be generated by hydrolysis of the corresponding ester. Interestingly, distinct morphologies (nanotubes or nanofibres) were obtained depending on the route used to synthesise the Fmoc-LL-OMe precursor [5].

Despite these studies, there is still insufficient data about the structural characterisation and mechanical properties of the gels formed. Employing the same pH controlled procedure as used in Chapter 5, here we will study the Fmoc-LL, Fmoc-LG and Fmoc-GL ionisation behaviour in the first instance. The full physico-chemical characterisation of the systems will then be investigated.

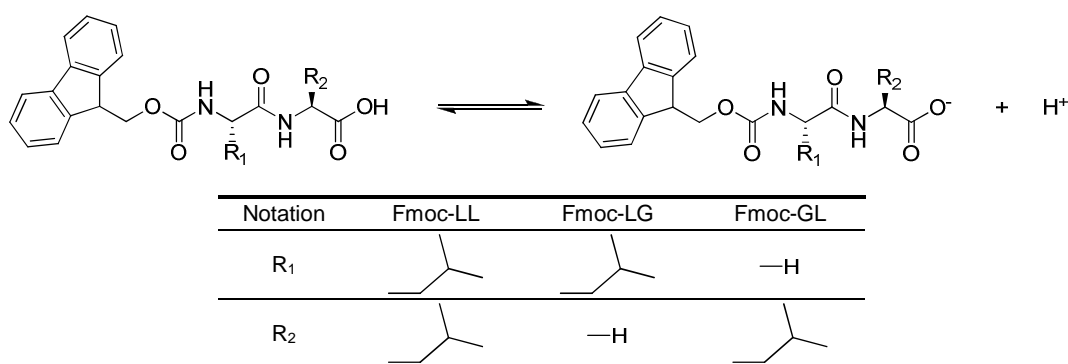


Figure 6.1. Equilibrium between Fmoc-dipeptide neutral (acid) and ionised (conjugated base) forms and notation.

6.3. RESULTS AND DISCUSSION

6.3.1. Solution Behaviour

To investigate the ionisation behaviour of Fmoc-LL, Fmoc-LG and Fmoc-GL, ‘titrations’ were undertaken at varying concentrations at 1, 5, 10 and 20 mmol L⁻¹. At all concentrations tested the peptide derivatives were found to be fully dissolved upon addition of NaOH to pH 10.5. HCl was then added and variation of the samples’ pH was measured as shown in Figure 6.2. The same procedure was applied to water as a control.

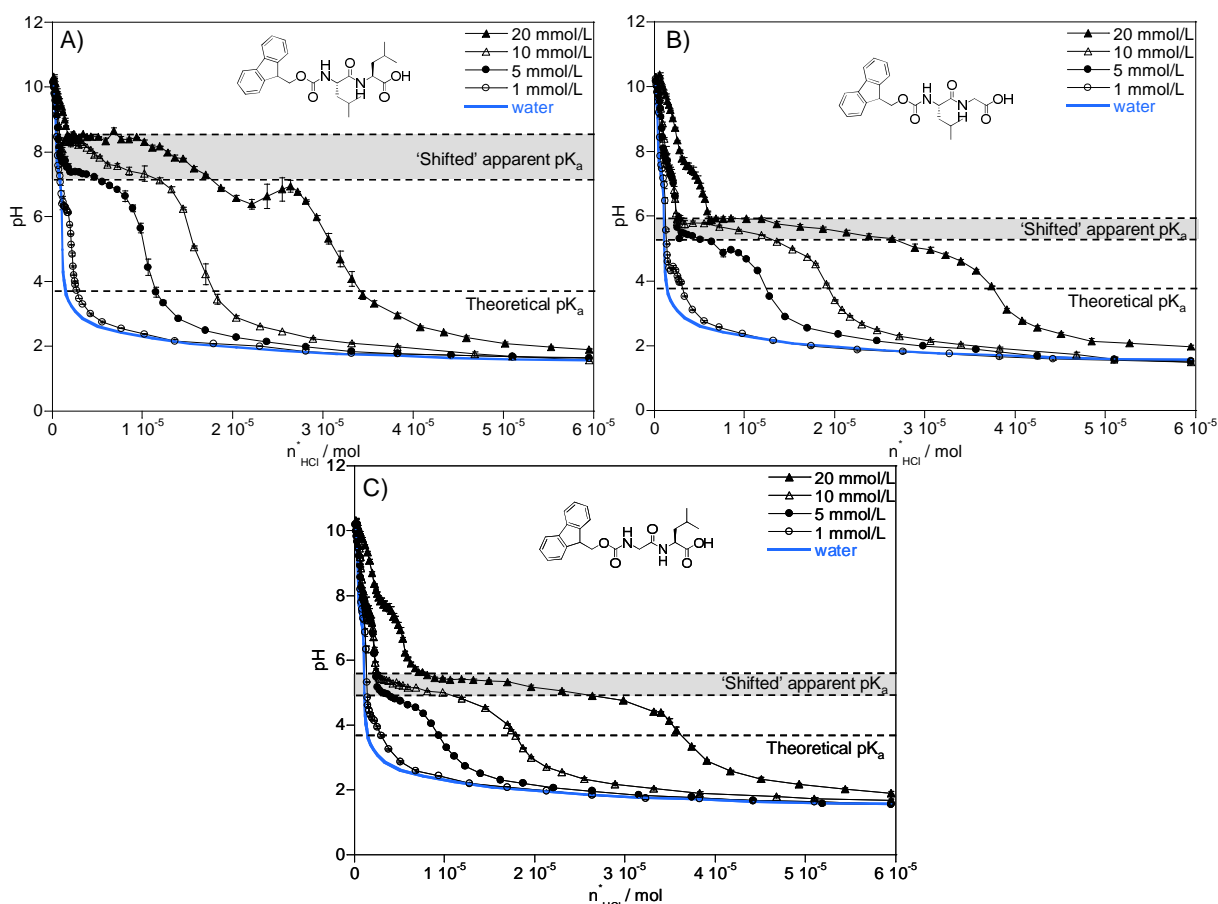


Figure 6.2. ‘Titration’ curves (pH vs. moles of added HCl) of water and **A)** Fmoc-LL, **B)** Fmoc-LG and **C)** Fmoc-GL samples at 1, 5, 10 and 20 mmol L^{-1} . The theoretical pK_a values of the Fmoc-dipeptides were assessed using SPARC web calculator (<http://ibmlc2.chem.uga.edu/sparc>).

At pH 10.5, Fmoc-LL was fully dissolved at all concentrations studied and clear solutions were obtained in all cases. As shown in Figure 6.2 A, the pH of all solutions progressively decreased upon addition of HCl and became slightly cloudy. Once a pH of about 8.5, 7.6, 7.4 and 6.4 was reached for 20, 10, 5 and 1 mmol L^{-1} samples respectively, the specimen started to become cloudier and their pH values were found to remain relatively constant. After the transition, the pH started to drop for all the samples. An increase in turbidity was observed in particular for 10 and 20 mmol L^{-1} samples, which started to become more viscous. However the pH of the 20 mmol L^{-1} sample was found to augment slightly before dropping again. Although the origin of such augmentation has not yet been investigated, the feature was reproducible and also observed for 30 mmol L^{-1} samples (data not shown). Upon further addition of HCl, decrease in pH was accompanied by the formation of a precipitate. At pH \sim 2.1, phase separation occurred with the emergence of a clear liquid phase at the top and a precipitate at the bottom of the test tube and the ‘titration’ curves started to merge with the water curve.

At all concentrations tested Fmoc-LG peptides fully dissolved at pH 10.5 following addition of NaOH. The pH of the solutions was then gradually lowered as HCl was added. As depicted in Figure 6.2 B, a shoulder corresponding to the neutralisation of NaOH excess contained in water was observed on all ‘titration’ curves at a pH of ~ 8.0. Again this feature was common to all Fmoc-dipeptides studied but was only visible when the apparent pK_a transition did not occur in the same pH range. For 20, 10 and 5 mmol L⁻¹ samples, the pH became constant at values of about 5.9, 5.8 and 5.3 respectively while the samples became cloudy. The turbidity of the samples increased along the transition and was found to be more apparent for the most concentrated samples (10 and 20 mmol L⁻¹). After the transition, the samples’ pH decreased again while precipitation occurred at pH ~ 3.0 for 20, 10 and 5 mmol L⁻¹ samples. At 1 mmol L⁻¹ the solution remained clear throughout the experiment, although a transition was observed at lower pH value of ~ 4.4. As the pH decreased further all the ‘titration’ curves started to merge with the control curve.

Fmoc-GL followed the same overall trend as Fmoc-LG. At pH 10.5 the peptide derivatives were found to be soluble at all concentrations studied. A decrease in the samples’ pH (Figure 6.2 C) and an increase in their turbidity were observed upon addition of HCl. The shoulder related to neutralisation of the excess of NaOH present in solution was observed at pH ~ 8.0. The pH of the samples became constant at values of about 5.4, 5.1, 5.0 and 4.3 for 20, 10, 5 and 1 mmol L⁻¹ samples respectively. Once the transition was complete the samples’ pH dropped again. However as the samples precipitated in the form of a solid mass constituted of insoluble peptide derivatives, they became less turbid. Towards the end of the ‘titrations’ the liquid phase became almost clear at all concentrations tested and the samples’ curves were found to merge with the water curve.

Only one apparent pK_a transition was observed for Fmoc-LL, Fmoc-LG and Fmoc-GL. Like for the phenylalanine-based Fmoc-dipeptides, this set of peptide derivatives are weak acids and are presumably all ionised at pH 10.5. Again, the degree of ionisation of the molecules can be estimated using the equation introduced in Chapter 4:

$$\alpha = 1 - \frac{n_{HCl}}{n_{Fmoc-dipeptide-COOH}} \quad \text{Equation 6.1}$$

Figure 6.3 shows the degree of ionisation of the three Fmoc-dipeptides above and below their respective apparent pK_a that is at pH 8.5 and 7.0 for Fmoc-LL and pH 8.5 and 5.0 for Fmoc-LG and Fmoc-GL. n_{HCl} was plotted against $n_{Fmoc-dipeptide-COOH}$ at each stage and α was inferred from the slope of the fitted linear curves. Before the transition arose (pH 8.5),

97%, 95% and 96% of Fmoc-LL, Fmoc-LG and Fmoc-GL respectively were in their ionised form. Neutralisation of the molecules probably just started during the pK_a transition (and must have continued as the pH was decreased further) as about half of them were still in their ionised form just below their apparent pK_a (59%, 40% and 53% of Fmoc-LL, Fmoc-LG and Fmoc-GL respectively).

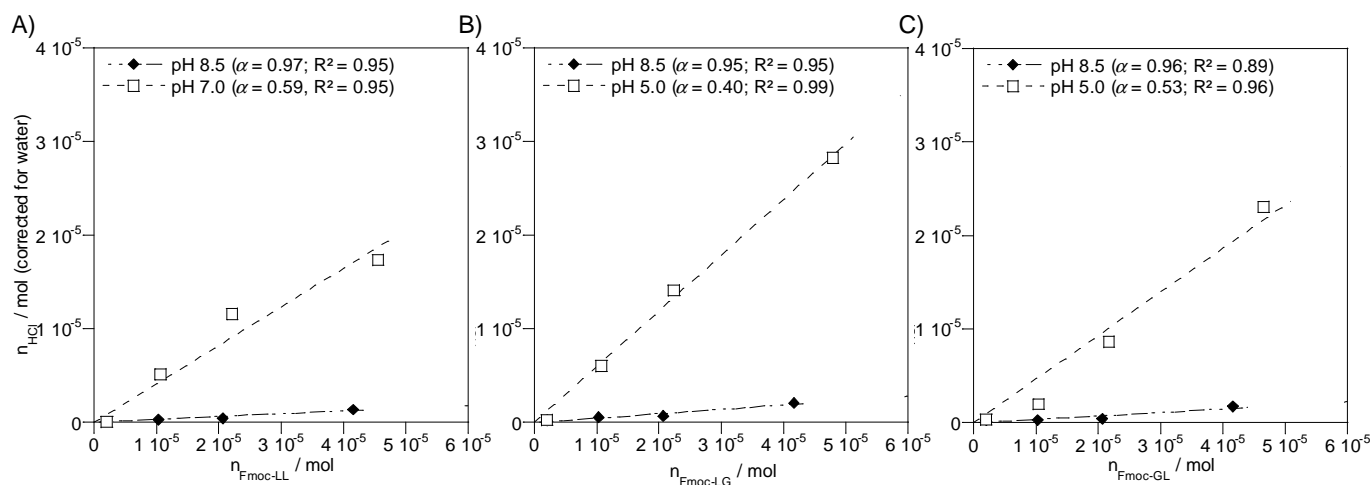


Figure 6.3. n_{HCl} (moles of HCl added corrected for moles of HCl needed to titrate water) vs. $n_{Fmoc-dipeptide-COOH}$ (moles of Fmoc derivative present in the sample) for the 1, 5, 10 and 20 $mmol L^{-1}$ samples of **A)** Fmoc-LL at pH values of 8.5 and 7.0, **B)** Fmoc-LG at pH values of 8.5 and 5.0 and **C)** Fmoc-GL at pH values of 8.5 and 5.0. Inset: Degree of ionisation α derived from the slope of the fitted linear curves.

The apparent pK_a transitions became more marked and occurred at higher pH values as the concentrations of peptide derivatives increased. However beyond 5–10 $mmol L^{-1}$ the pH at which the transition appeared, no longer depended on the Fmoc-dipeptide concentration (Figure 6.4 A). The pK_a transitions of the Fmoc-dipeptides were all shifted towards higher values compared to their theoretical pK_a^{th} , as recently reported in the literature [6]. Fmoc-LL ($pK_a^{th} = 3.79$), Fmoc-LG ($pK_a^{th} = 3.82$) and Fmoc-GL ($pK_a^{th} = 3.79$) displayed pK_a shifts of about 4.3, 2.0 and 1.5 pH units on average respectively at 10 $mmol L^{-1}$. As illustrated in Figure 6.4 B, the shifted pK_a values were also found to arise at high pH for molecules possessing high Log P values* (e.g. Fmoc-LL) and at lower pH for molecules characterised by lower Log P values (e.g. Fmoc-GL), indicating that the transition pH was related to the relative hydrophobicity of the Fmoc-dipeptides and confirming the results published by Adams *et al* [6]. Although free leucine is characterised by a higher pK_a than free phenylalanine, the pK_a transition for the leucine-based Fmoc-dipeptides was found to occur at lower pH than for their phenylalanine-based homologues, suggesting an effect of the side chain nature on the transition pH.

* Log P values were determined using ACD/Labs v. 12.01/ChemSketch.

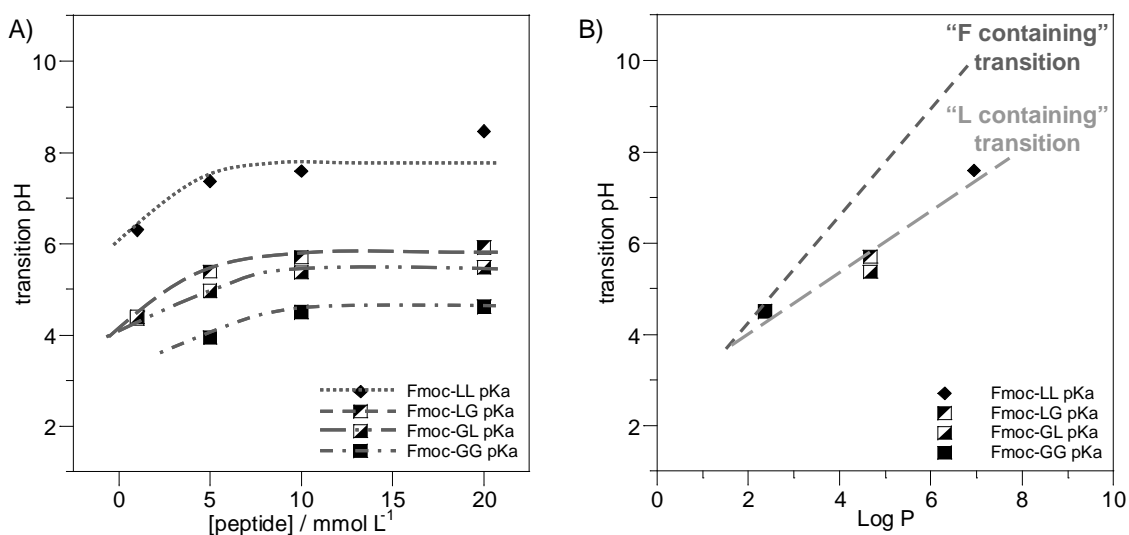


Figure 6.4. A) Transition pH values versus concentration of the Fmoc-dipeptides studied (1, 5, 10 and 20 mmol L⁻¹). B) Transition pH values versus Log P values of the Fmoc-dipeptides at 10 mmol L⁻¹.

Due to the slight increase in pH observed below the apparent pK_a transition for Fmoc-LL at 20 mmol L⁻¹, the pH drop following the pK_a transition was found to be gradual but did not reveal a two-transition feature as shown by Fmoc-FF. Like Fmoc-FG and Fmoc-GF, Fmoc-LG and Fmoc-GL were characterised by a one-transition feature.

The behaviour in solution of the leucine-based Fmoc-dipeptides revealed similarities with what was observed for phenylalanine-based Fmoc-dipeptides since the pH at which the pK_a transition occurred increased with the hydrophobicity of the molecules. It can therefore be assumed that the difference in behaviour underlines the effect of the nature of the amino acid side chains (i.e. aromatic or aliphatic).

Equations 6.2 and 6.3, corresponding to the fitted linear curves of the phenylalanine- and leucine-based system transitions respectively, could potentially be used to estimate the apparent pK_a values of other phenylalanine and leucine containing Fmoc-peptides. However further investigations will be needed in order to validate this hypothesis.

$$\text{Transition pH} = 1.86 + 1.18 \log P \quad \text{Equation 6.2}$$

$$\text{Transition pH} = 2.65 + 0.67 \log P \quad \text{Equation 6.3}$$

6.3.2. Fluorescent Molecular Behaviour

Phenyl rings of the amino acids side chains were found to participate in the intermolecular interactions between phenylalanine-based Fmoc-dipeptides. In order to assess whether the peptide derivatives π -stacked in a different manner due to the lack of aromatic moieties or if the alkyl chains were likely to interfere in the overlapping of the Fmoc groups, fluorescence spectroscopy was used to monitor the environment of the Fmoc-LL, Fmoc-

LG and Fmoc-GL fluorenyl moieties. Measurements were carried out on 10 mmol L^{-1} samples as a function of pH and at 0.1 mmol L^{-1} at pH ~ 8.6 . All the fluorescence spectra were normalised so that the intensity of the emission maximum was set to 1 (see Appendix E for the non-normalised spectra). As shown in Figure 6.5, the three systems of interest displayed common features.

At low concentration (0.1 mmol L^{-1}) and above the apparent pK_a (pH ~ 8.6) of all the Fmoc-dipeptides studied, clear solutions were obtained. In these conditions all molecules should be in their ionised form. Hence the emission maximum observed at $\sim 313 \text{ nm}$ for all samples was ascribed to Fmoc group monomers.

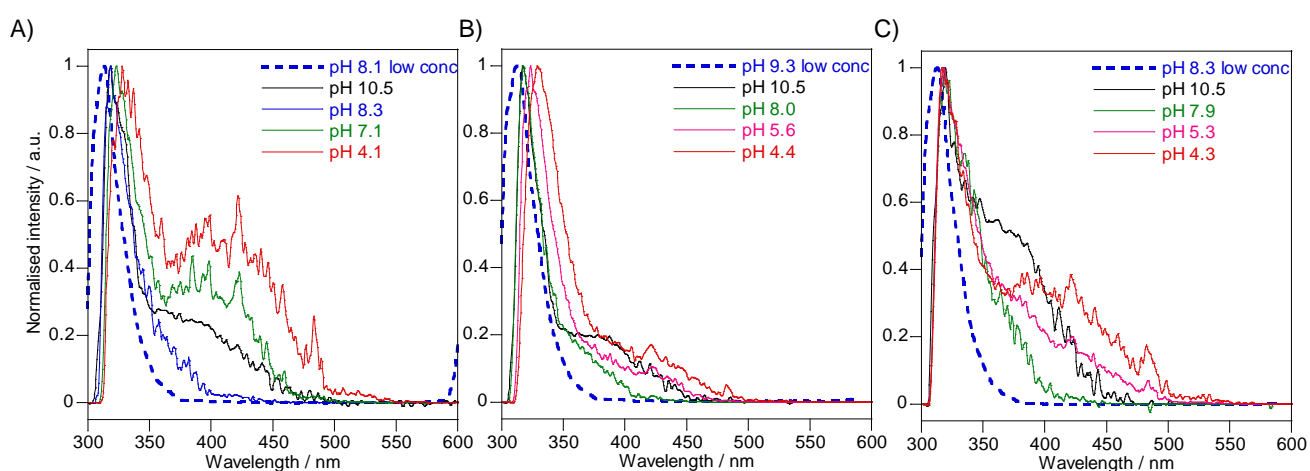


Figure 6.5. Normalised fluorescence emission spectra of **A)** Fmoc-LL, **B)** Fmoc-LG and **C)** Fmoc-GL samples at 10 mmol L^{-1} at pH 10.5 starting point of the ‘titration’ experiments and at different pH values above and below their respective apparent pK_a and at low concentration (0.1 mmol L^{-1}) above their apparent pK_a (dotted lines).

At 10 mmol L^{-1} (i.e. above the critical gelation concentration of the three systems) an emission maximum presumably related to antiparallel Fmoc excimers was observed at 317–330 nm at all pH conditions tested. The presence of this peak at pH 10.5 indicated that interactions between the Fmoc-dipeptides occurred even at high pH, forming base dimer units, probably at the origin of the structures formed at lower pH. As the pH was reduced this band was found to shift from 317 nm towards 330 nm for Fmoc-LL and Fmoc-LG, showing that the Fmoc groups constituting the dimers were overlapping in a more efficient manner. On the other hand, the excimer peak for Fmoc-GL was found to be shifted to the same extent at all pH conditions, suggesting the dimers formed were not stabilised further by lowering the pH (Figure 6.6). This behaviour could be due to the presence of glycine next to the Fmoc group, which enhanced the molecules flexibility and would disfavour the stability of the excimers.

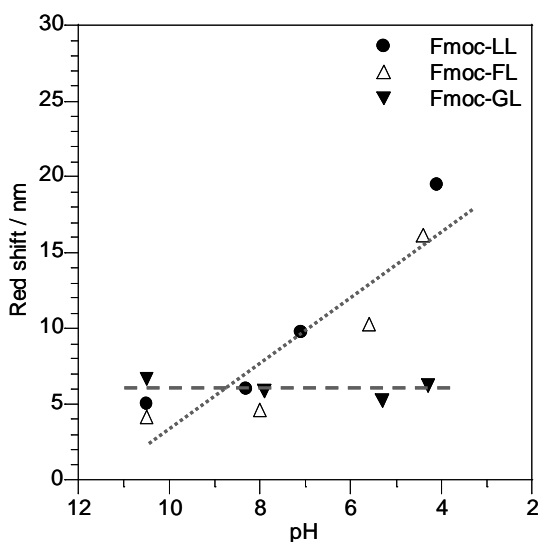


Figure 6.6. Red shift of the excimer peak with respect to the monomer peak as a function of pH for Fmoc-LL, Fmoc-LG and Fmoc-GL samples at 10 mmol L^{-1} .

A shoulder centred at 370–375 nm likely indicative of Fmoc excimers arranged in a parallel manner was also detected [7,8]. This band was found to be particularly marked at pH 10.5 than in any other pH conditions tested and was more pronounced for Fmoc-GL than for Fmoc-LL and Fmoc-LG. This difference could be related to the flexibility of the molecule brought about by the introduction of glycine adjacent to the Fmoc group, which leads to an increased flexibility of the Fmoc-GL peptide tail compared to the two other systems. Steric hindrance arising from the leucine aliphatic side chain and the electrostatic repulsions caused by the carboxylate group were therefore reduced. As a result, some level of parallel arrangement was allowed although as suggested by Figure 6.5 the antiparallel conformation was favoured for all systems. The shoulder ascribed to parallel dimers was no longer observed at lower pH, which could be due to self-assembly occurring, which locks the molecules into the supramolecular structures as described later in this chapter. Interestingly, this shoulder was found to be overall more or equally marked for the leucine-based Fmoc-dipeptides than for their phenylalanine-based homologues. This behaviour is in agreement with the effect of the molecular flexibility on parallel dimerisation since the leucine aliphatic side chain confers more flexibility to the molecule tail than the phenyl ring of the phenylalanine side chain.

An extensive emission band was observed at $\sim 421 \text{ nm}$ at or below pH values of 7.1, 5.6 and 5.3 for Fmoc-LL, Fmoc-LG and Fmoc-GL respectively, which is in all cases below the apparent $\text{p}K_{\text{a}}$ transition. As previously mentioned this photoluminescence peak is characteristic of the π - π stacking of multiple fluorenyl moieties and indicates the presence of higher order aggregates [8]. This behaviour is consistent with the hypothesis that self-

assembled structures are formed below the shifted pK_a . As shown in Figure 6.5 A, the photoluminescence emission was particularly intense for Fmoc-LL. Detection of a photoluminescence band in these conditions implies the fluorenyl groups could be packed in hydrophobic clusters away from the solvent in the aggregates formed [9].

The fluorescence study of leucine-based Fmoc-dipeptides revealed that like in phenylalanine-based Fmoc-dipeptides, the fluorenyl moieties were preferentially arranged in antiparallel dimers. However at high pH, when molecules are mainly ionised, parallel dimerisation can be also allowed. Again, lowering of the pH appeared to enhance the overlapping of the Fmoc-LL and Fmoc-LG molecules, possibly due to the presence of fewer ionised entities in solution causing fewer electrostatic repulsions and hence favouring the formation of higher order aggregates (Figure 5.14). Like Fmoc-FG, Fmoc-GG and Fmoc-GF, the molecular structures of Fmoc-LL, Fmoc-LG and Fmoc-GL also presented a degree of flexibility. The dimers formed by these systems were therefore found to be less stable (feature associated with a pH dependence of the antiparallel excimer peak) compared to those resulting from the association of the more rigid Fmoc-FF molecules. Introduction of a glycine residue next to the Fmoc moiety contributed to an enhancement in the flexibility of the molecules. As a consequence, Fmoc-GL formed the least stable dimers of the Fmoc-dipeptides studied as shown by the weak red shift of the excimer peak with respect to the monomer peak.

Based on the behaviour in solution and the one-transition feature displayed by this set of Fmoc-dipeptides, hydrogels were formed from these systems under specific conditions. The mechanical properties of these scaffolds were assessed using oscillatory and the systems were characterised as a function of pH using TEM, FT-IR and WAXS.

6.3.3. Fmoc-LL pH study

At pH 10.5, clear solutions constituted of ionised Fmoc-LL were obtained. This observation was confirmed by FT-IR (Figure 6.7) with the band at $\sim 1589\text{ cm}^{-1}$ characteristic of carboxylate. As can be seen from the TEM micrograph in Figure 6.8 A and the absence of significant peak in the amide I region (Figure 6.7), no self-assembled structures were formed in these conditions.

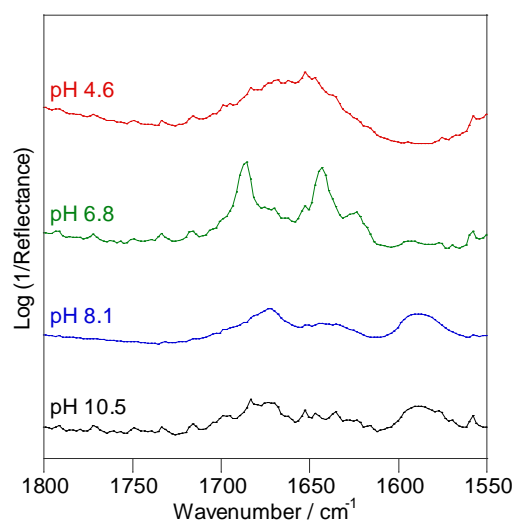


Figure 6.7. FT-IR spectra of Fmoc-LL samples at 10 mmol L^{-1} prepared in D_2O at pH 10.5 starting point of the 'titration' experiment, pH 8.1 (above the apparent pK_a), pH 6.8 and 4.6 (below the apparent pK_a).

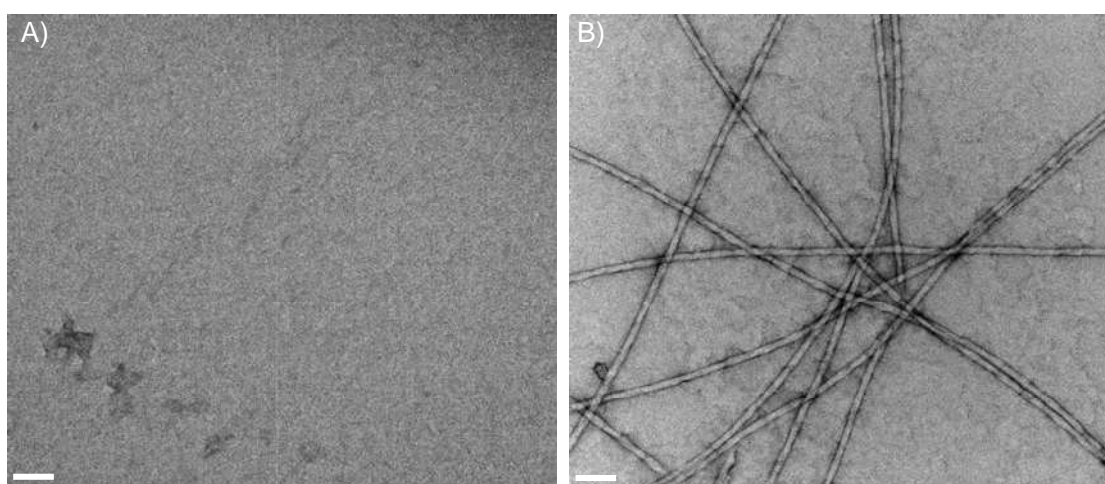


Figure 6.8. TEM micrographs of Fmoc-LL samples at 10 mmol L^{-1} **A)** at pH 10.5 and 8.0 (above the apparent pK_a) and **B)** at pH 6.8 and 4.3 (below the apparent pK_a). Scale bars represent 100 nm.

Addition of HCl led to gradual protonation of the peptide derivatives. After a slight reduction of the samples' pH, clear solutions were obtained. The molecules remained mostly ionised (as indicated by the presence of the band at $\sim 1589 \text{ cm}^{-1}$ in the infrared spectrum). Self-assembly did not occur at pH 8.0 (i.e. $\alpha \leq 0.97$) as shown by TEM (Figure 6.8 A) and FT-IR (Figure 6.7).

As shown in Figure 6.9 the absence of organised structure above the apparent pK_a was consistent with the WAXS data as no Bragg peaks were detected at pH 8.2.

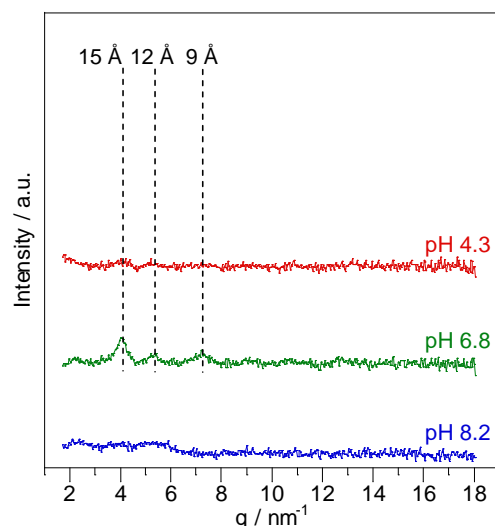


Figure 6.9. WAXS spectra of Fmoc-LL samples at 10 mmol L^{-1} dried at pH 8.2 (above the apparent pK_a) and pH 6.6 and 4.3 (below the apparent pK_a).

The liquid-like nature of the sample was confirmed by oscillatory rheology. As illustrated in Figure 6.10 at pH 8.5, the elastic modulus G' was found to be lower than the viscous modulus G'' until a crossover of the moduli was observed around 10 rad s^{-1} . Both G' and G'' showed strong frequency dependence between 0.01 and 100 rad s^{-1} , which is indicative of liquid-like materials.

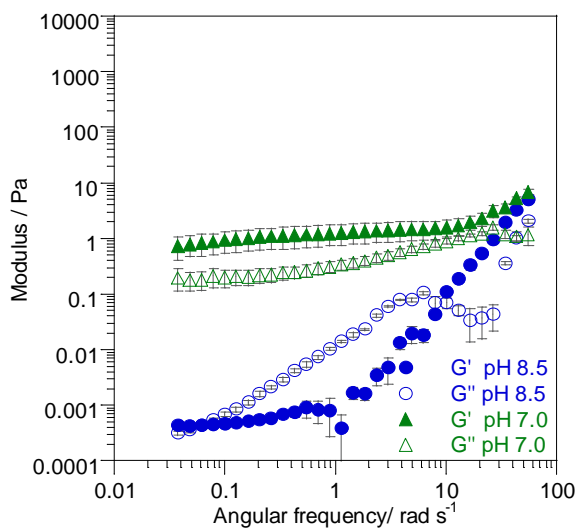


Figure 6.10. Dynamic frequency sweep of Fmoc-LL samples at 10 mmol L^{-1} at pH 8.5. and 7.0 (above and below the apparent respectively).

Further addition of HCl led to the formation of translucent self-supported hydrogels below the apparent pK_a . As can be seen from Figure 6.10 at pH 7.0, G' was higher than G'' between 0.01 and 100 rad s^{-1} , with both moduli displaying weak frequency dependence, confirming the gel-like nature of the sample. G' values were in the range of 0.7 – 5 Pa , showing the hydrogels formed by Fmoc-LL were weak. The entangled fibrillar network observed by TEM at pH 6.8 was consistent with the rheological behaviour of the system.

As can be seen in Figure 6.8 B, fibres of $\sim 15.7 \pm 0.7$ nm in width were formed. A topology of this type with a comparable size has been reported for Fmoc-LL hydrogels formed through hydrolysis of the corresponding ester. Das *et al.* showed that the morphology and dimensions of the self-assembled structures obtained varied depending on the route via which they were prepared. Tubular (15.2 ± 1.1 nm in width) and fibrillar (12.0 ± 2.5 nm in width) structures were generated when the corresponding ester were synthesised by conventional solution phase methodology and by solid-solid reactions respectively [5]. FT-IR also confirmed the formation of self-assembled structures at this pH since peaks were detected in the amide I region. Figure 6.7 reveals the presence of bands at 1687 and 1624 cm^{-1} characteristic of antiparallel β -sheets, which is in agreement with the results of Das *et al.* In addition, the peak at 1643 cm^{-1} showed the coexistence of random coils. As shown by WAXS in Figure 6.9, broad reflection peaks were detected at 4.1 , 5.3 and 7.2 nm^{-1} , corresponding to distance of 15.4 , 11.9 and 8.7 Å. These Bragg peaks indicated the structures formed did not result from lateral self-assembly, hence no lamellar organisation was observed.

When the pH was reduced to 4.3, milky flocculates suggesting the formation of insoluble self-assembled structures were obtained. As shown in Figure 6.8 B, nanofibres were still observed by TEM. However at this pH a large signal comparable to the spectrum of Fmoc-LL in its dehydrated form (commercial product straight from the manufacturer) was detected by FT-IR, confirming the peptide derivatives were precipitating out of solution (for more details about FT-IR spectrum of the commercially available Fmoc-LL, see Appendix D). The WAXS pattern in Figure 6.9 displayed a drop in intensity indicating a loss of structure that was probably provoked by the precipitate state of the sample.

Although Fmoc-LL was characterised by only one $\text{p}K_{\text{a}}$ transition, similarities with the Fmoc-FF system were observed. In both cases, the hydrogels formed exhibited similar G' values and indicated that the gels were weak. On the microscopic scale these gels were associated with the presence of entangled fibrillar networks, however no lateral association of the fibres characteristic of a lamellar organisation was observed for Fmoc-LL. Despite the absence of interactions between Fmoc groups and the amino acid side chain, which was found to rigidify the peptide backbone of Fmoc-FF system favouring the formation of antiparallel β -sheets, such conformation was detected for Fmoc-LL under specific conditions.

6.3.4. Fmoc-LG

6.3.4.1. pH Study

At pH 10.5, clear solutions were obtained from Fmoc-LG and no structures were observed at the microscale (Figure 6.11 A). As expected, no significant band other than the broad one at $\sim 1597\text{ cm}^{-1}$ was detected by FT-IR, confirming the ionised state of the molecules (Figure 6.12).

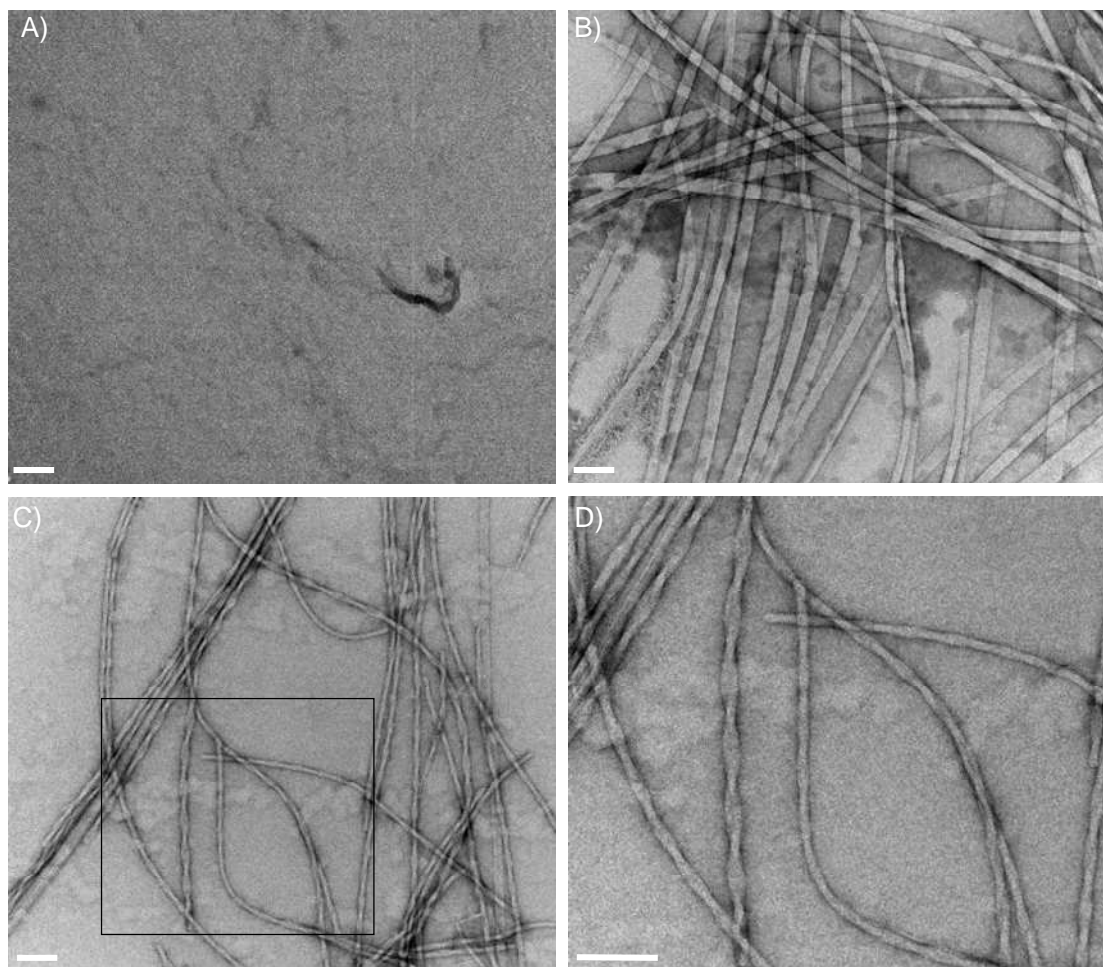


Figure 6.11. TEM micrographs of Fmoc-LG samples at 10 mmol L^{-1} **A)** at pH 10.5 starting point of the ‘titration’ experiment, **B)** at pH 7.6 (above the apparent pK_a), and **C)** at pH 5.6 and 4.3 (below the apparent pK_a). **D)** Close up of the box in C. Scale bars represent 100 nm.

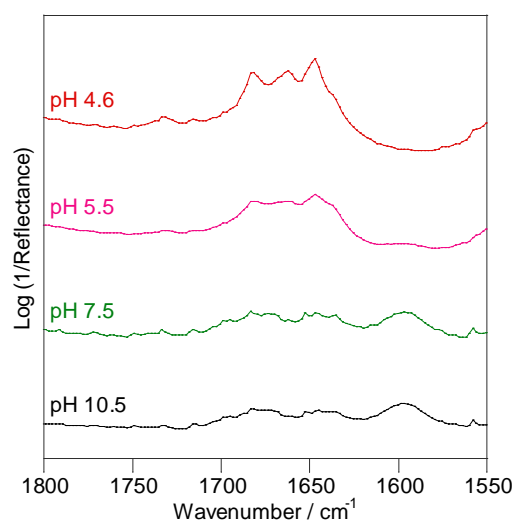


Figure 6.12. FT-IR spectra of Fmoc-LG samples at 10 mmol L^{-1} prepared in D_2O at pH 10.5 starting point of the 'titration' experiment, pH 7.5 (above the apparent pK_a), pH 5.5 and 4.6 (below the apparent pK_a).

When the pH was reduced (above the apparent pK_a) clear solutions containing a small portion of precipitate were obtained at pH 7.6. At this same pH, infrared data remained similar as in the presence of NaOH only, suggesting that most of the molecules were still in solution (Figure 6.12). However relatively straight ribbons of $24.0 \pm 1.7 \text{ nm}$ in width were observed by TEM in a few windows of the grid (Figure 6.11 B). These self-assembled structures were likely to constitute the precipitated fraction of the sample. As can be seen from the WAXS data at pH 7.7 (Figure 6.13), a lamellar packing pattern with a d spacing of 29.0 \AA ($q = 2.2 \text{ nm}^{-1}$) and up to five higher order reflections was detected. This feature indicated that the straight ribbons observed by TEM resulted from the lateral association of fibrillar structures.

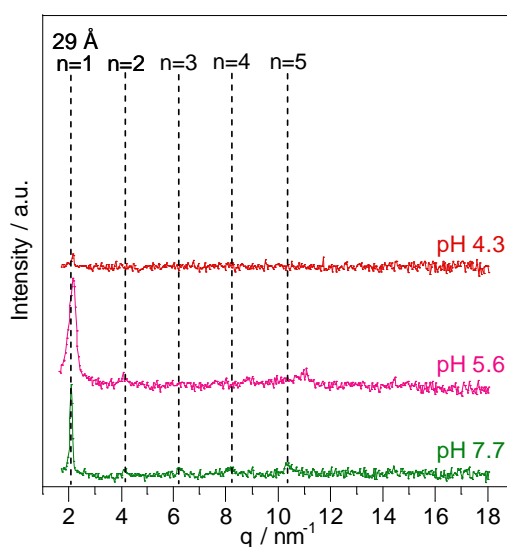


Figure 6.13. WAXS spectra of Fmoc-LG samples at 10 mmol L^{-1} dried at pH 7.6 (above the apparent pK_a) and pH 5.8 and 4.1 (below the apparent pK_a).

From the frequency sweep in Figure 6.14, we can see that at pH 7.6 G' was mainly lower than G'' and both moduli were frequency dependent between 0.01 and 100 rad s^{-1} , confirming that the material was liquid.

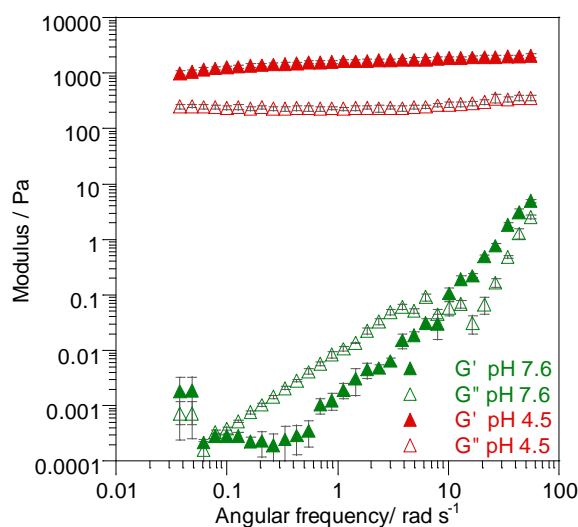


Figure 6.14. Dynamic frequency sweep of Fmoc-LG samples at 10 mmol L^{-1} at pH 7.6 and 4.5 (above and below the apparent pK_a respectively).

At pH ~ 5.5 (below the apparent pK_a) viscous solutions were obtained. As shown in Figure 6.12, the disappearance of the band at $\sim 1597 \text{ cm}^{-1}$ was observed, indicating that the molecules were protonated at this stage. Peaks were barely detected in the amide I region of the infrared spectrum, suggesting that the system went through a transition and a different type of structure formed. At this same pH, twisted ribbons with average pitch and width of $149.2 \pm 20.3 \text{ nm}$ and $13.5 \pm 0.9 \text{ nm}$ respectively were observed on the TEM micrographs (Figure 6.11 C), which is in agreement with the FT-IR data. These structures were found to coexist with a few flat ribbons of $21.3 \pm 1.0 \text{ nm}$ in width, remaining from the previous pH stage. At this same pH, the reflection at 29.0 \AA ($q = 2.2 \text{ nm}^{-1}$) corresponding to a periodic unit present in the straight ribbons was still detected, however the intensity of the five higher order reflections was attenuated (Figure 6.13). This attenuation could be due to the presence of the coexisting twisted ribbons.

As the pH was lowered further to ~ 4.3 , translucent hydrogels were formed. Like the Fmoc-FG hydrogels studied in Chapter 5, these samples were found to gel during the heating step at $80 \text{ }^\circ\text{C}$ and to be relatively stable upon cooling to $4 \text{ }^\circ\text{C}$ and room temperature (should the gels have been completely formed at high temperature). As shown in Figure 6.14, a typical gel spectrum was obtained, confirming the gel-like nature of the sample. G' values (1000–2080 Pa) were about one order of magnitude higher than G'' values and both moduli were slightly frequency dependent between 0.01 and 100 rad s^{-1} ,

which suggested the presence of an entangled fibrillar network. Higher values of G' have been reported for Fmoc-LG hydrogels obtained by pH change (5900 Pa) [4]. Such difference is likely to be related to the method of preparation of the samples. As hypothesised in Chapter 4, non-heated samples resulted in stiffer materials constituted of kinetically trapped aggregates. Besides, the hydrogels were prepared at a slightly higher concentration ($\sim 15 \text{ mmol L}^{-1}$). The entangled nature of the system was consistent with the type of microstructures observed by TEM as the presence of twisted ribbons, similar to those formed at $\text{pH} \sim 5.5$, was noted (Figure 6.11 C). The relative reduction of the proportion of flat ribbons compared to that of the twisted ribbons led to a significant decrease in intensity of the Bragg peak at 2.2 nm^{-1} (i.e. $d = 29.0 \text{ \AA}$). As can be seen from the FT-IR spectrum (Figure 6.12), the peaks centred at 1717, 1687 and 1652 cm^{-1} were more resolved at $\text{pH} \sim 4.3$ than at $\text{pH} \sim 5.5$. These peaks were related to the stretching of the carbonyl functions in the Fmoc group and the un-ionised carboxylic acid, and to the amine of the amide bond respectively. It is likely that these peaks were related to the presence of the twisted ribbons.

The Fmoc-LG and the Fmoc-FG systems were characterised by common features. Both were found to form stable hydrogels upon heating and exhibited structural and morphological changes, including supramolecular chirality with the sol-gel transition. For both systems, the self-assembled structures did not exhibit any lamellar organisation. On the other hand, replacement of the phenylalanine by a leucine residue altered the relative rigidity of the molecule, preventing them from creating intermolecular hydrogen bonding that would stabilise the structures into β -sheets. As a result, this conformation was not detected at any pH conditions.

6.3.4.2. Temperature Study at $\text{pH} \sim 4.7$

Surprisingly, Fmoc-LG hydrogel formation appeared to be temperature dependent (in the same manner as Fmoc-FG, as seen in Chapter 5). The mechanical properties of the system were therefore monitored below the apparent $\text{p}K_{\text{a}}$, as a function of temperature during *in situ* (in the rheometer) gel formation.

Sequential addition of NaOH and HCl was undertaken as described in Chapter 3. Following this the samples were not heated but thoroughly sonicated. They were then subjected to the following temperature variations: from 25 to $80 \text{ }^{\circ}\text{C}$ at a rate of $10 \text{ }^{\circ}\text{C min}^{-1}$, 2.5 min at $80 \text{ }^{\circ}\text{C}$, 1 min from 80 to $4 \text{ }^{\circ}\text{C}$ and 8.5 min at $4 \text{ }^{\circ}\text{C}$. The temperature-dependent mechanical spectrum of Fmoc-LG is presented in Figure 6.15. G' values were found to be

higher (about one order of magnitude) than the G'' values at all temperatures, including at room temperature (at the beginning of the experiment). This observation suggests that self-assembly occurred at 25 °C before the samples were heated. The lack of stiffness of the sample was however confirmed by the relatively low G' values displayed by the solutions between 25 and 50 °C. Both moduli increased by about three orders of magnitude as the temperature was raised further, reaching a maximum G' value of ~ 3000 Pa at 80 °C (i.e. close to the G' values obtained for the corresponding pre-formed gels). G' and G'' values were then found to decrease of about one order of magnitude ($G' \sim 320 \pm 65$ Pa) when the samples were kept at 80 °C and to remain relatively constant as the samples were cooled down between 70 and 4 °C. The heating-cooling sequence between 25 and 4 °C resulted in an overall increase of about one order of magnitude in both G' and G'' . As observed for Fmoc-FG, Fmoc-LG pre-formed hydrogels displayed storage modulus values that were about ten times higher than those obtained for the systems heated *in situ*. The decrease in G' was attributed to the samples being damaged while they were cooled down in the rheometer during the measurement.

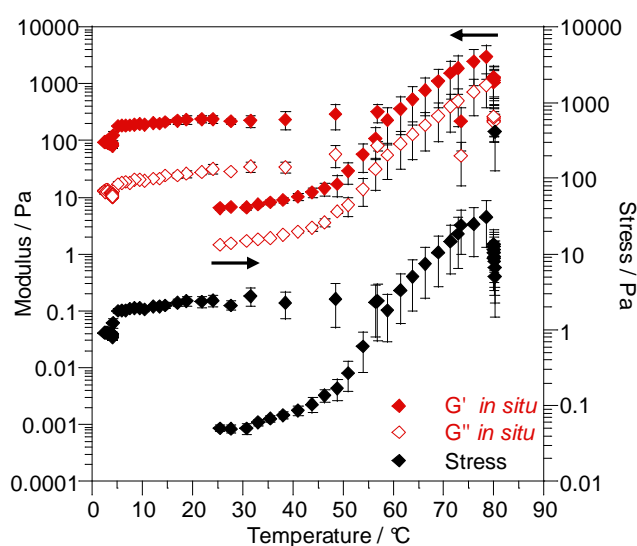


Figure 6.15. Dynamic temperature sweep at constant strain of 0.01 of Fmoc-LG samples at 10 mmol L^{-1} as a function of temperature (from 25 °C to 80 °C to 4 °C).

A TEM micrograph of a non-heated sample is shown in Figure 6.16 A. Although the microstructures formed from non-heated samples looked less regular than those obtained from heated samples (Figure 6.11 C), the coexistence of twisted and flat ribbons was observed in both cases. FT-IR analyses of the samples were undertaken in both conditions. Spectral signatures of the specimen were found to be comparable in the amide I region although absorption bands were not as well defined for the non-heated samples (Figure 6.16 B). The heating step was therefore shown to improve the homogeneity of the

samples without altering the molecular arrangement within the self-assembled structures and their topography.

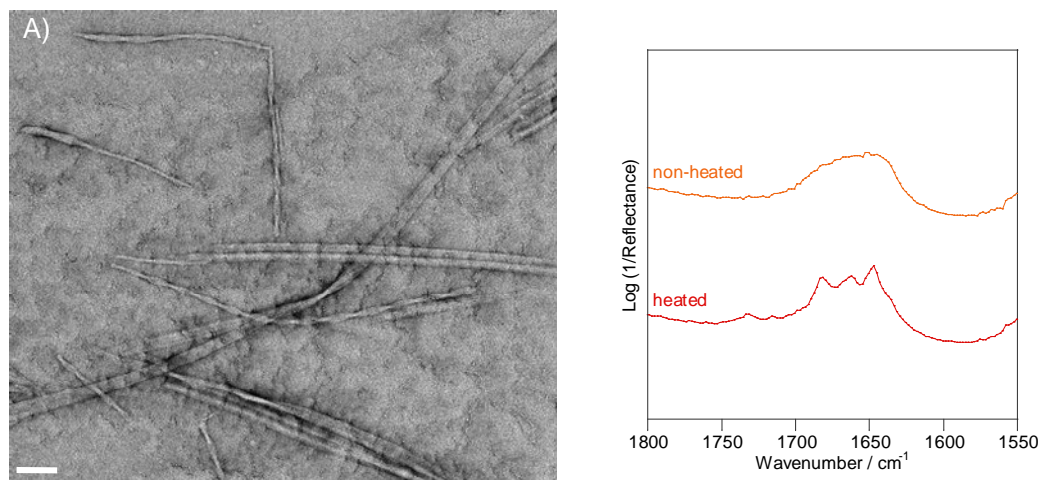


Figure 6.16. A) TEM micrograph of a non-heated Fmoc-LG sample at 10 mmol L^{-1} below the apparent pK_a transition. Scale bar represents 100 nm. B) FT-IR spectra of non-heated and heated Fmoc-LG samples at 10 mmol L^{-1} prepared in D_2O below the apparent pK_a transition.

6.3.5. Fmoc-GL pH study

As expected, no self-assembly has occurred at pH 10.5: clear solutions were obtained from Fmoc-GL molecules and no microstructures were observed in the TEM micrographs (Figure 6.17 A).

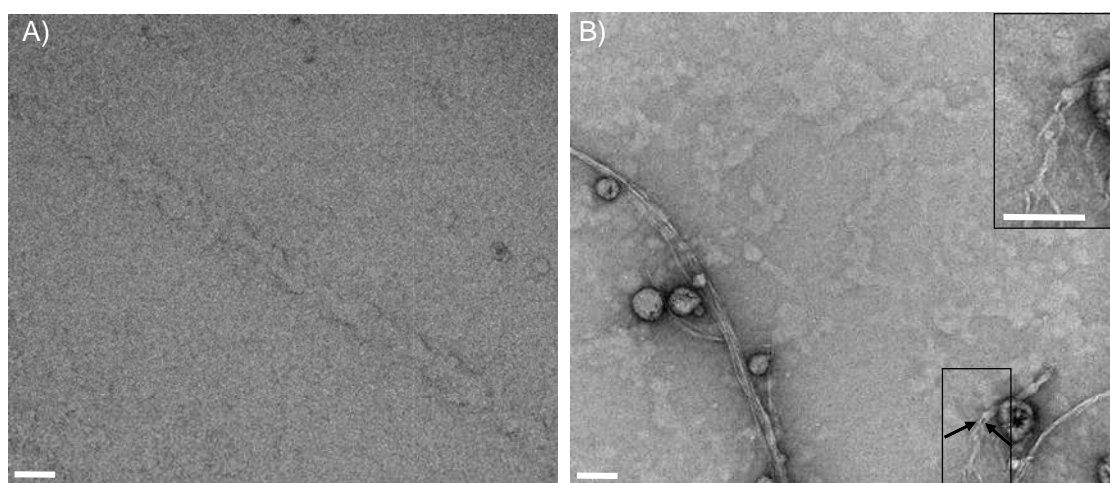


Figure 6.17. TEM micrographs of Fmoc-GL samples at 10 mmol L^{-1} A) at pH 10.5–5.7 (above the apparent pK_a) and B) at pH 4.2 (below the apparent pK_a) – the right hand side inset corresponds to a close up of the box. Scale bars represent 100 nm.

As shown by FT-IR in Figure 6.18, the infrared spectrum was noisy, however no significant peak was detected in the amide I region, confirming that no particular structure was formed in these conditions.

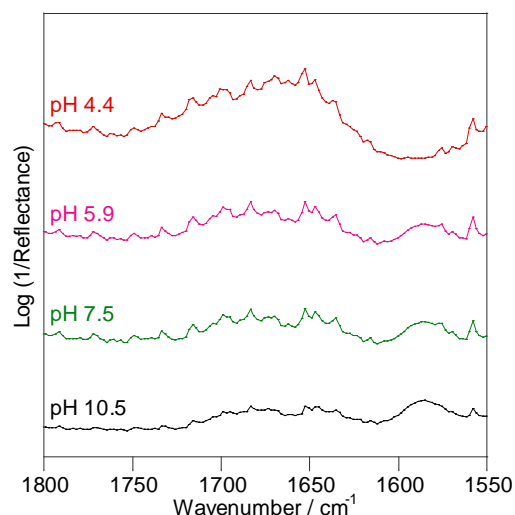


Figure 6.18. FT-IR spectra of Fmoc-GL samples at 10 mmol L^{-1} prepared in D_2O at pH 10.5 starting point of the 'titration' experiment, pH 7.5 and 5.9 (above the apparent pK_a) and pH 4.4 (below the apparent pK_a).

After addition of HCl to produce pH 7.5 (above the apparent pK_a), small amounts of precipitate were observed in the clear solutions. However, TEM (Figure 6.17 A) and FT-IR spectroscopy (Figure 6.18) remained the same as at pH 10.5 showing that the molecules were mostly not self-assembled yet in solution at this pH. WAXS data revealed the presence of a weak Bragg peak at 23.2 \AA ($q = 2.7 \text{ nm}^{-1}$) that could be related to the periodicity of the molecular arrangement within the precipitated matter (Figure 6.19).

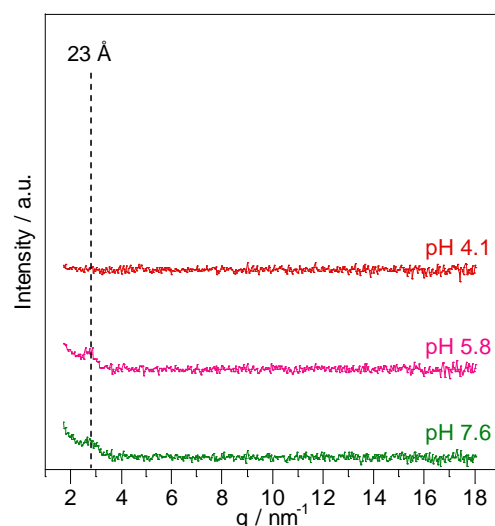


Figure 6.19. WAXS spectra of Fmoc-GL samples at 10 mmol L^{-1} dried at pH 7.6 and 5.8 (above the apparent pK_a) and pH 4.1 (below the apparent pK_a).

After further addition of HCl to pH ~ 5.8 (still above the apparent pK_a) clear solutions with small amounts of precipitate were still obtained. No significant structural changes were noted since TEM (Figure 6.17 A), FT-IR (Figure 6.18) and WAXS (Figure 6.19) data remained overall identical.

At pH 4.1 (below the apparent pK_a), turbid solutions containing small amounts of precipitates were obtained, however no particular scattering pattern was detected by WAXS (Figure 6.19). This behaviour could be due to the sample precipitating out of solution at this pH, which led to the loss of the scattering pattern. As shown in Figure 6.18, the precipitated state of the sample was in agreement with the FT-IR data since the spectrum obtained at pH 4.4 was similar to the one of Fmoc-GL in its dehydrated form, exhibiting a large band centred around 1652 cm^{-1} (for more details about the commercial Fmoc-GL spectrum, see Appendix D). In contrast with the other Fmoc-dipeptides studied in this Chapter no high aspect ratio architectures were observed. Observations of the insoluble material by TEM (Figure 6.17 B) revealed the coexistence of spherical irregular aggregates (ranging from approximately 25 to 90 nm in diameter) and sparse ribbons that were both unable to form a solvent trapping 3D network. The extremities of the ribbons were found to split into narrower ribbons or fibres of $3.9 \pm 0.6\text{ nm}$ in width, providing indications on the formation process of such supramolecular structures. Similar morphological behaviour has previously been reported for peptide amphiphiles as a mechanistic evidence of the lateral self-assembly of ribbons into larger ribbons [10].

As for Fmoc-GF, self-assembly of Fmoc-GL below its apparent pK_a transition was not accompanied by hydrogel formation because of the inability of the structures generated to trap solvent, resulting in the system precipitating. Unlike Fmoc-GF, Fmoc-GL formed spherical objects and sparse ribbons rather than sheet-like structures. Consequently no lamellar organisation was detected. In both cases, the presence of the glycine adjacent to the Fmoc moiety enhanced the flexibility of the peptide tail, which unfavoured β -sheet formation.

6.3.6. Summary

The behaviour of Fmoc-LL, Fmoc-LG and Fmoc-GL in solution revealed that each system was characterised by one apparent pK_a transition, which in all cases has been shown to be associated with structural and morphological changes that were peptide sequence dependent.

Based on fluorescence spectroscopy data, all three systems were all found to be ordered through their Fmoc groups, which were mainly π -stacked into antiparallel dimers that were thought to correspond to the base unit of the self-assembled supramolecular structures generated as the pH was reduced. On the other hand Fmoc-LL peptide tail was found to arrange in β -sheets below the apparent pK_a although leucine does not have the propensity

to favour such conformation. The coexistence of random coils was also detected. As expected, Fmoc-LG and Fmoc-GL did not form β -sheets in any conditions due to the flexibility of the molecules brought about by both leucine and glycine.

Although the Fmoc-LG molecules were ionised above the apparent pK_a straight ribbons were observed at the microscopic scale. Neutralisation of the peptide derivatives induced the formation of an entangled network of twisted ribbons. Stable hydrogels associated with this phenomenon were obtained upon heating. The self-assembly of Fmoc-LL into an entangled network of fibres of ~ 15.7 nm in width also led to hydrogel formation, however the modulus values were lower than Fmoc-LG gels. In contrast, Fmoc-GF self-assembled into spherical objects and sparse ribbons, which were incompatible with hydrogel formation, leading to precipitation of the system. The absence of a regular scattering pattern – in agreement with the TEM observations – showed that in most cases (with the exception of Fmoc-LG) the leucine-based Fmoc-dipeptides did not exhibit any lamellar organisation. The d spacings detected by WAXS were therefore ascribed to periodic units down the long axis of the structures rather than lateral association.

6.4. CONCLUSION

Similar behaviours were observed between the leucine-based Fmoc-dipeptides and their phenylalanine-based homologues. Fmoc-LL, Fmoc-LG and Fmoc-GL peptide derivatives were each characterised by a single shifted pK_a transition. Study of the systems as a function of pH showed this transition coincided with molecular self-assembly or structural and morphological changes. Again, the structural properties of the systems were found to be dependent on the peptide sequence. Entangled fibrillar networks associated with hydrogel formation were formed for Fmoc-LL and Fmoc-LG whereas the nature of the architectures generated for Fmoc-GL favoured precipitation rather than hydrogel formation.

6.5. REFERENCES

1. de Groot, N.S., Parella, T., Aviles, F.X., *et al.*, *Ile-Phe dipeptide self-assembly: clues to amyloid formation*. *Biophysical Journal*, **2007**, 92 (5), 1732-1741.
2. Jayawarna, V., Ali, M., Jowitt, T.A., *et al.*, *Nanostructured hydrogels for three-dimensional cell culture through self-assembly of fluorenylmethoxycarbonyl-dipeptides*. *Advanced Materials*, **2006**, 18 (5), 611-614.
3. Smith, A.M., Collins, R.F., Ulijn, R.V., *et al.*, *Raman optical activity of an achiral element in a chiral environment*. *Journal of Raman Spectroscopy*, **2009**.
4. Adams, D.J., Butler, M.F., Frith, W.J., *et al.*, *A new method for maintaining homogeneity during liquid-hydrogel transitions using low molecular weight hydrogelators*. *Soft Matter*, **2009**, 5 (9), 1856-1862.
5. Das, A.K., Collins, R.F., and Ulijn, R.V., *Exploiting enzymatic (reversed) hydrolysis in directed self-assembly of peptide nanostructures*. *Small*, **2008**, 4 (2), 279-287.
6. Adams, D.J., Mullen, L.M., Berta, M., *et al.*, *Relationship between molecular structure, gelation behaviour and gel properties of Fmoc-dipeptides*. *Soft Matter*, **2010**, 6, 1971-1980.
7. Schweitzer, D., Hausser, K.H., and Haenel, M.W., *Transannular interaction in [2.2]phanes: [2.2](4,4')Diphenylophane and [2.2](2,7) fluorenophane*. *Chemical Physics*, **1978**, 29 (1-2), 181-185.
8. Yang, Z., Gu, H., Zhang, Y., *et al.*, *Small molecule hydrogels based on a class of antiinflammatory agents*. *Chemical Communications*, **2004** (2), 208-209.
9. Lakowicz, J.R., *Principles of fluorescence spectroscopy*. 3rd ed. **2006**, Boston: Springer.
10. Cui, H., Muraoka, T., Cheetham, A.G., *et al.*, *Self-assembly of giant peptide nanobelts*. *Nano Letters*, **2009**, 9 (3), 945-951.

Conclusions and Future Work

7.1. CONCLUSIONS

The strategy adopted in this project consisted in using dipeptides that were modified with aromatic ligands to drive the self-assembly of the molecules through π -interactions and hydrogen bonding. Combinations of glycine with hydrophobic aromatic (phenylalanine) or non-aromatic (leucine) residues were exploited in order to stabilise and reinforce the structures formed. Despite the distinct chemical structures of these two amino acids, similarities were found in the self-assembling behaviour of the Fmoc-dipeptides based on them. In all cases the supramolecular structures obtained under specific conditions were formed from base dimer units of Fmoc-dipeptides π -stacking in an antiparallel manner, as demonstrated by fluorescence spectroscopy.

As shown for the Fmoc-FF gelling system, aromatic amino acids in the peptide sequence were found to participate in the stabilisation of the self-assembled structures. The rigidity brought about by the phenyl rings was shown to support both the stacking of the Fmoc groups and the antiparallel β -sheet arrangement of the peptide components. Replacement of the phenylalanine residues by leucines (amino acids having the same hydrophobicity) also led to hydrogel formation. Antiparallel β -sheet supramolecular structures were also detected for Fmoc-LL. Although the molecular arrangement of the peptide derivatives in the self-assembled structures is not fully understood yet, it is apparent that hydrophobic effects involving the amino acid alkyl side chains also contributed to the self-assembly mechanism. Additionally, Fmoc-FF and Fmoc-LL hydrogels were characterised by relatively poor mechanical properties in comparison with the other systems studied.

Fmoc-FG and Fmoc-LG showed the peculiarity to form hydrogels upon heating below their respective apparent pK_a . In both cases, self-assembly was observed above the shifted pK_a transition, however the sol-gel transition coincided with morphological changes involving chiral and non-chiral structures as illustrated by the straight and twisted ribbons observed at the microscopic level.

Introduction of a glycine residue adjacent to the Fmoc group (leaving the hydrophobic amino acid in the C-terminal position of the peptide component) provided flexibility to the systems (Fmoc-GF and Fmoc-GL), preventing molecular self-assembly to generate high aspect ratio architectures and giving rise to non-gelling samples.

On the other end, Fmoc-derivatives composed of glycine exclusively were able to form hydrogels. Due to their inherent flexibility, the Fmoc-GG molecules were less constrained and were more able to adopt spatial conformations that would favour self-assembly. However the resulting hydrogels were found not to be stable.

As summarised in Table 7.1 the hydrogels formed exhibited different mechanical properties and morphologies depending on the system. With the exception of Fmoc-FG, the phenylalanine-based Fmoc-dipeptides tended to form one-dimensional lamellar aggregates whereas their leucine-based homologues did not (with the exception of Fmoc-LG). However the fibres resulting from the self-assembly of the leucine-based systems were generally found to be wider than those formed from the phenylalanine-based systems. Such behaviour suggested the π -interactions in which amino acids with aromatic side chains were involved enabled a tight packing of the molecules, which resulted in narrow structures. On the other hand, the hydrophobic interactions in which amino acids possessing alkyl side chains led to a looser packing of the peptide derivatives, resulting in the formation of larger fibres.

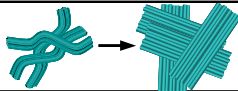

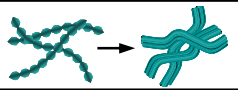
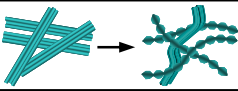
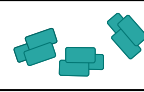


Entry	System	Log P	Apparent pK_a	Phase	G' / Pa	Morphology
1	Fmoc-FF	6.77	10.2–9.5 6.2–5.2	Gel	0.5–5	
2	Fmoc-LL	6.95	6.4–8.5	Gel	0.7–5	
3	Fmoc-FG	4.58	7.3–6.3	Gel (high T)	100–400	
4	Fmoc-LG	4.66	5.3–5.9	Gel (high T)	1000–2080	
5	Fmoc-GF	4.56	7.6–7.0	Precipitate	–	
6	Fmoc-GL	4.66	5.4–4.3	Precipitate	–	
7	Fmoc-GG	2.37	4.8–4.0	Gel	100–400	

Table 7.1. Summary of the main characteristics of the studied Fmoc-dipeptides.

^a Macroscopic aspect below the apparent pK_a .

^b Average width of the fibrillar units.

7.2. FUTURE WORK

Overall trends on the behaviour of Fmoc-dipeptides composed of hydrophobic amino acids were drawn from the results of this project. Additional investigations using fluorescence spectroscopy at specific pH conditions should allow a better understanding of the influence of positioning of the hydrophobic amino acid within the peptide sequence on the self-assembly behaviour of the molecules.

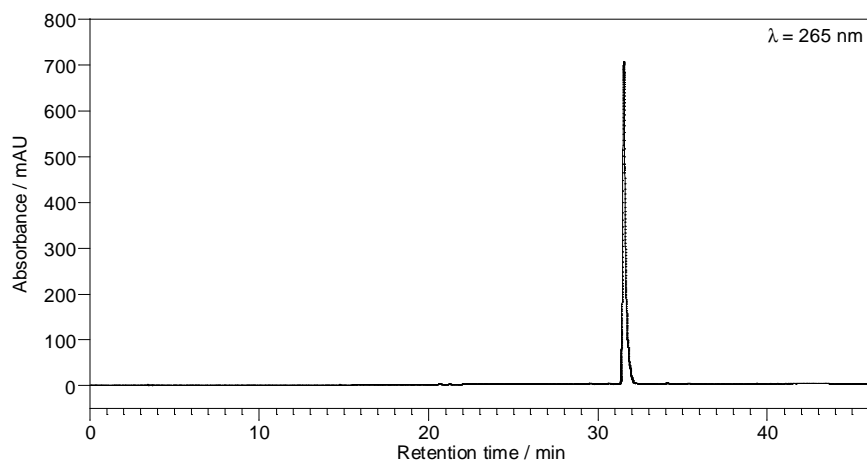
In order to generalise the hypotheses ventured, our investigations will need to be extended to other phenylalanine and leucine containing Fmoc-dipeptides. In particular further work will allow verification of the use of the proposed equations to estimate the apparent pK_a values of such systems.

Further research might focus on the effect of the N-terminal aromatic ligand. For example, dipeptides modified with naphthalene (Nap) and benzyloxycarbonyl (Cbz) groups have been studied previously, however the literature suffers from a lack of documentation regarding the gelation properties and structural characterisation of the self-assembled architectures.

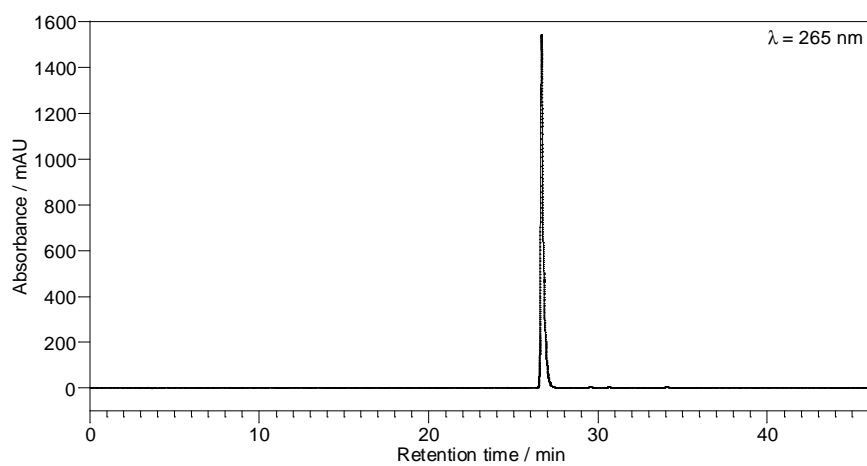
Although kinetic effects have not been investigated in this work, it is believed that aging effects would lead to stiffer structures, presenting improved mechanical properties. Fmoc-FG and Fmoc-LG for instance were found to be particularly stable with time, including at room temperature, and should hence be good candidates for this type of investigation. Additionally, under specific conditions these two systems led to the formation of twisted ribbons, the pitch of which was too large to be detected by WAXS. Using small angle X-ray scattering (SAXS) it should be possible to determine such characteristics.

Appendices

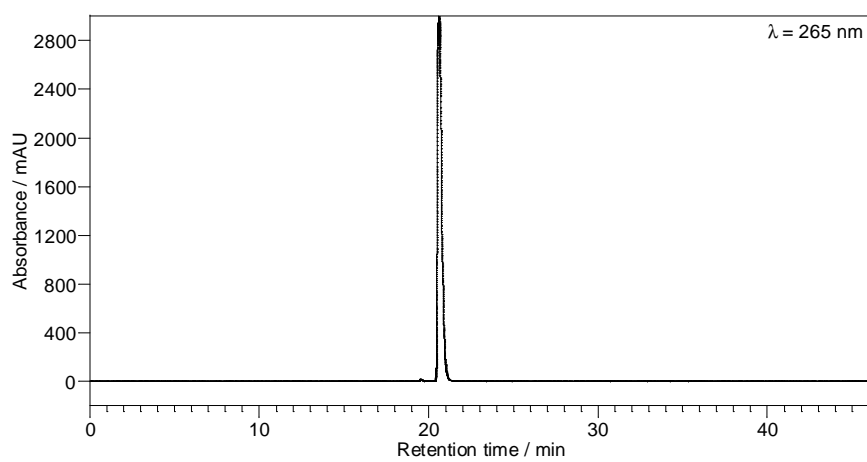
Appendix A: HPLC Chromatograms of Commercial Fmoc-Dipeptides



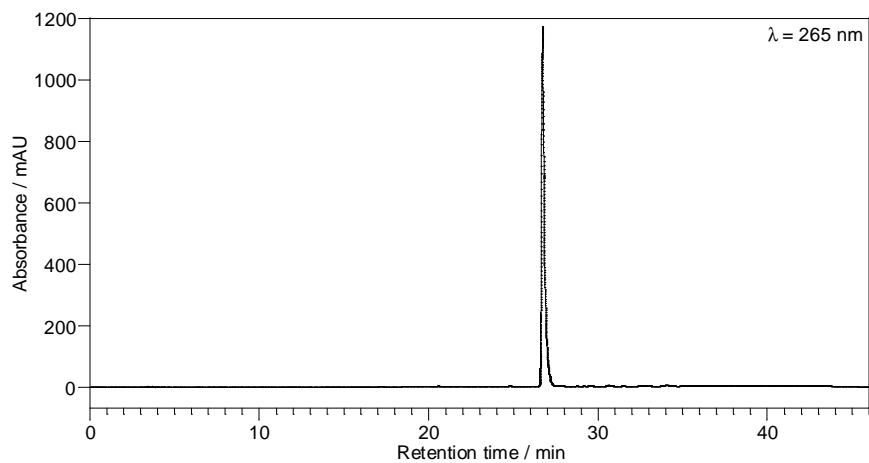
HPLC chromatogram of Fmoc-FF.



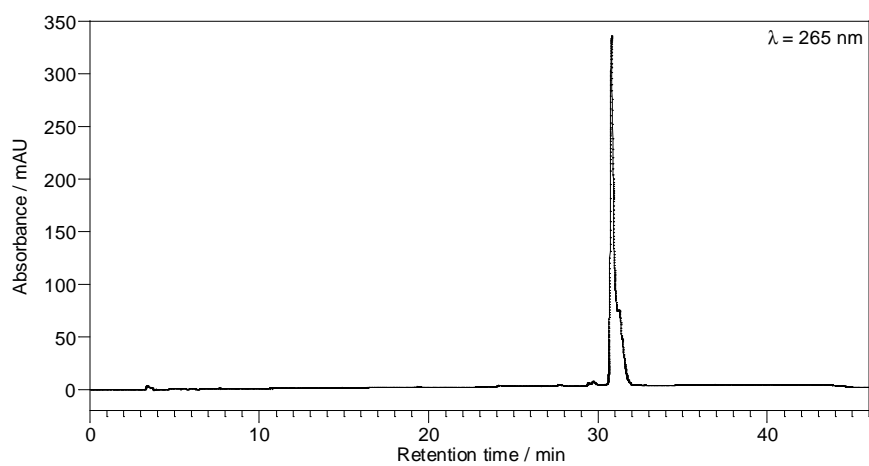
HPLC chromatogram of Fmoc-FG.



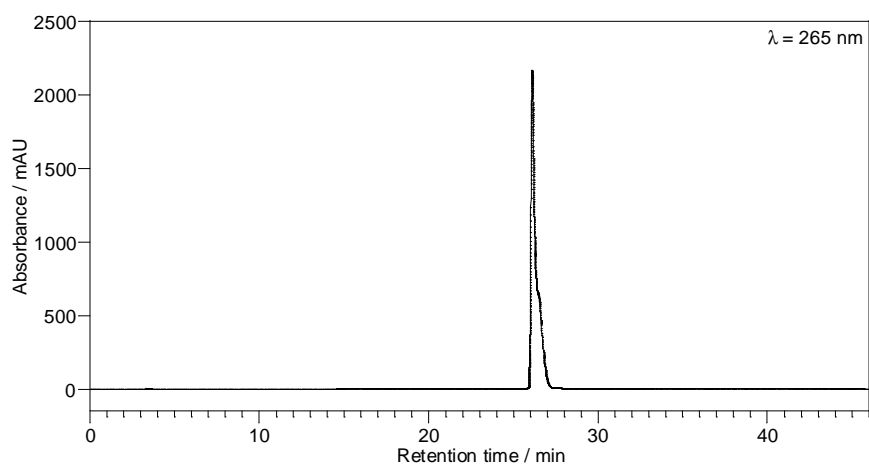
HPLC chromatogram of Fmoc-GG.



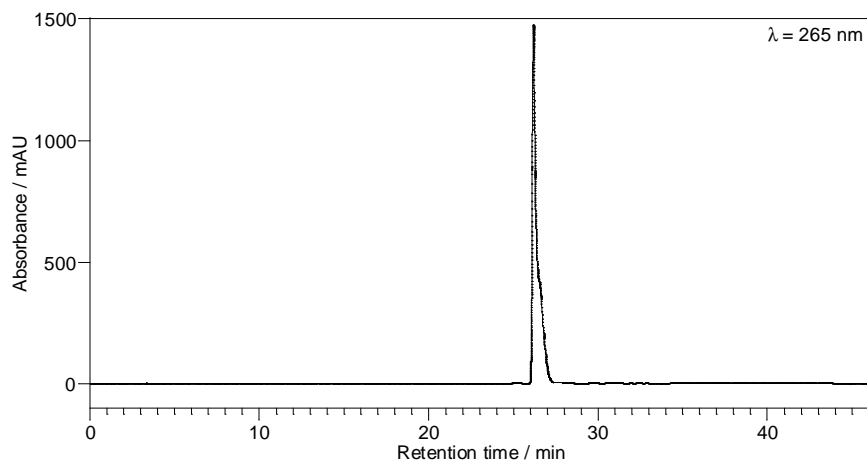
HPLC chromatogram of Fmoc-GF.



HPLC chromatogram of Fmoc-LL.

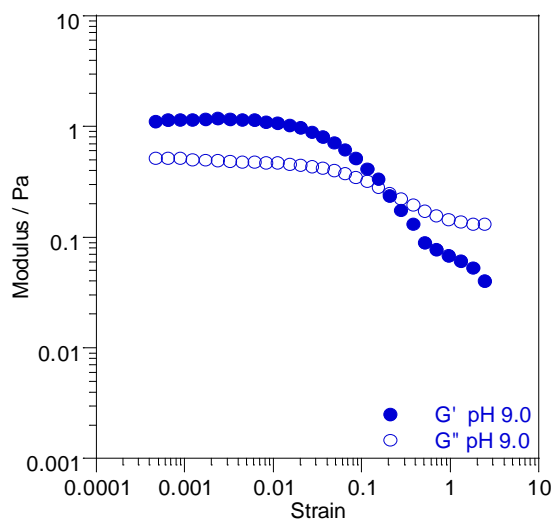


HPLC chromatogram of Fmoc-LG.

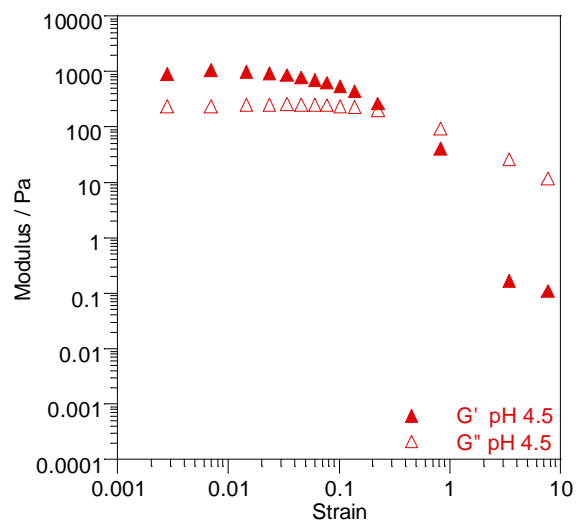


HPLC chromatogram of Fmoc-GL.

Appendix B: Dynamic Amplitude Sweeps of Fmoc-Dipeptide Hydrogels

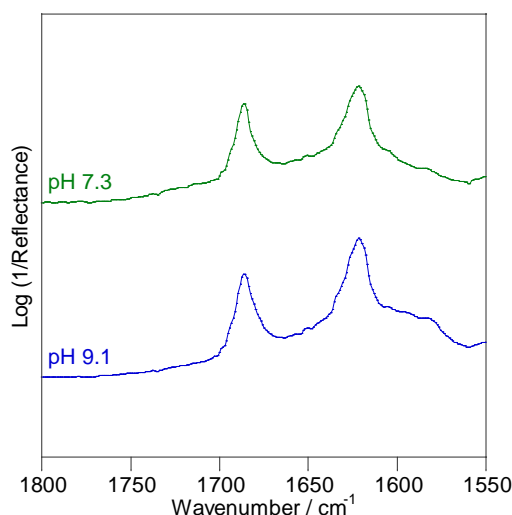


Dynamic amplitude sweep at constant frequency of 6.3 rad s^{-1} of an Fmoc-FF gel at 10 mmol L^{-1} at pH 9.0.



Dynamic amplitude sweep at constant frequency of 6.3 rad s^{-1} of an Fmoc-LG gel at 10 mmol L^{-1} at pH 4.5.

Appendix C: FT-IR Spectra of Thin Films of Fmoc-FF



FT-IR spectra of Fmoc-FF samples at 10 mmol L^{-1} dried at pH 9.1 (below apparent $pK_a 1$) and pH 7.3 (above apparent $pK_a 2$).

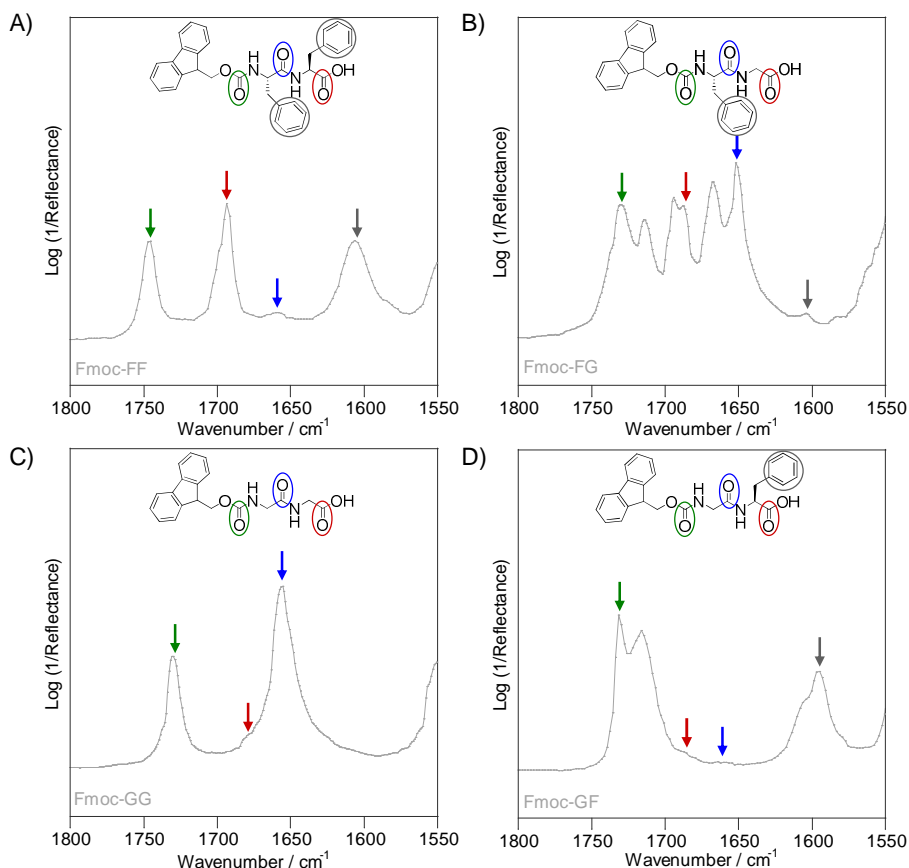
Appendix D: FT-IR Spectra of Commercial Fmoc-Dipeptides

The doublet centred at $\sim 1600 \text{ cm}^{-1}$ is related to benzene ring (phenylalanine side chain) stretching [1]. Absorption bands commonly fluctuate widely in intensity in this region of the spectrum. As a result, this doublet can be weak as it is the case for Fmoc-FG, or can appear as a weak shoulder on the high frequency side of a peak like it was observed for Fmoc-GF. As expected, these bands were absent from the Fmoc-GG spectrum.

In short peptides the carbonyl group of un-ionised carboxylic acids is usually characterised by a weak band at $\sim 1680 \text{ cm}^{-1}$. However ionisation of the acid results in the disappearance of this band [1]. Consequently the peak corresponding to this function can be observed in the spectra of the dehydrated commercial Fmoc-dipeptides and at low pH but not around and above the apparent pK_a of the systems.

The bond linking the Fmoc moiety to the dipeptides is in the form of the group R-NH-CO-OR, which is also called urethane. In secondary urethanes the carbonyl group has been reported to absorb in the range of $1739\text{--}1705 \text{ cm}^{-1}$ [1]. Hence, the peak detected at $\sim 1730 \text{ cm}^{-1}$ for Fmoc-FG, Fmoc-GG and Fmoc-GF corresponds to the carbonyl of the Fmoc group. Although it is off-range, the band at $\sim 1746 \text{ cm}^{-1}$ on the Fmoc-FF spectrum was also attributed to the Fmoc carbonyl as the peak could be shifted to higher frequencies due to the presence of steric effects caused by the phenyl group. C=O stretching vibrations are indeed known to vary as a function of the angle α defined by the axes of the C=O and C-X bonds, X being the nearest substituent of the carbonyl group [2].

As expected, the carbonyl group of the peptide bond absorbs at $\sim 1655 \text{ cm}^{-1}$ [1].

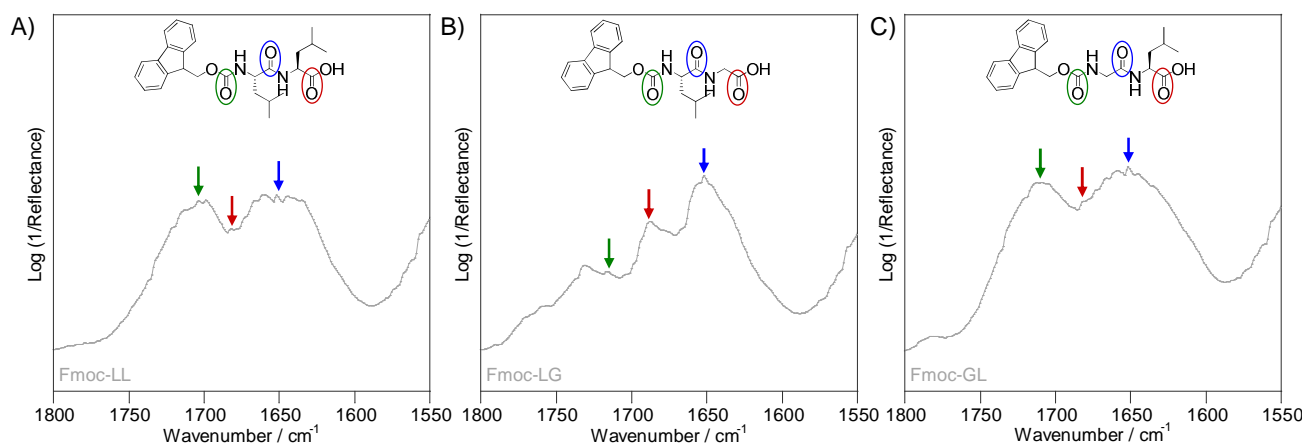


FT-IR spectra of **A) Fmoc-FF**, **B) Fmoc-FG**, **C) Fmoc-GG** and **D) Fmoc-GF**.

The peaks observed at about 1682 cm^{-1} , 1687 cm^{-1} and 1681 cm^{-1} for commercial Fmoc-LL, Fmoc-FG and Fmoc-GL respectively are attributed to the carbonyl group of their un-ionised carboxylic acids as these functions typically absorb at $\sim 1680\text{ cm}^{-1}$ in short peptides [1].

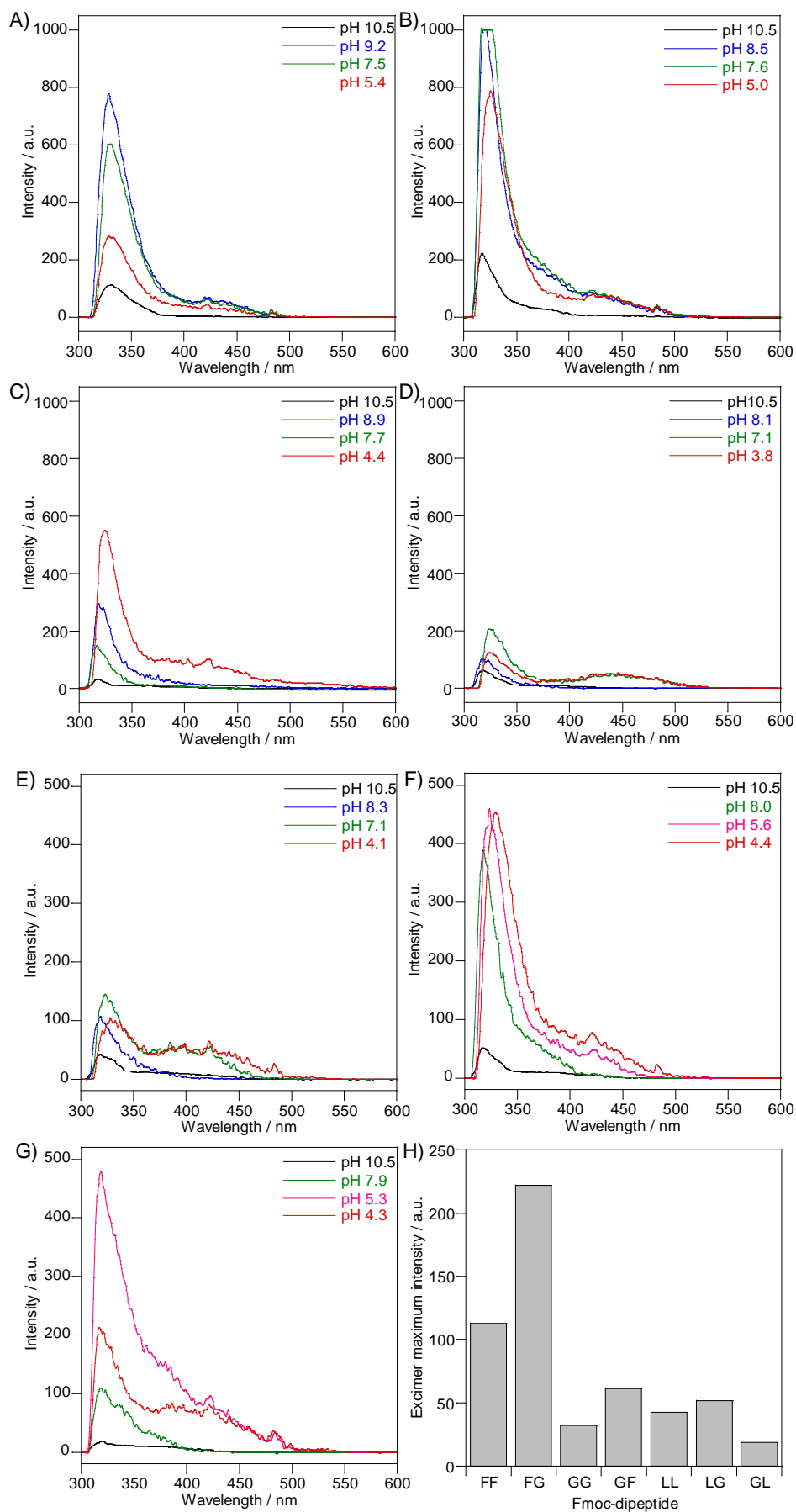
Carbonyl groups of secondary urethanes usually absorb in the range of $1739\text{--}1705\text{ cm}^{-1}$ [1]. The peaks detected at $\sim 1708\text{ cm}^{-1}$ for Fmoc-LL, $\sim 1717\text{ cm}^{-1}$ for Fmoc-LG and $\sim 1710\text{ cm}^{-1}$ for Fmoc-GL are therefore ascribed to the carbonyl function upstream of the dipeptides.

As observed for Fmoc-LL, Fmoc-LG and Fmoc-GL the band at $\sim 1652\text{ cm}^{-1}$ corresponds to the carbonyl of amide bonds linking amino acids as these groups commonly display stretching bands at $\sim 1655\text{ cm}^{-1}$ (amide I band) [1].



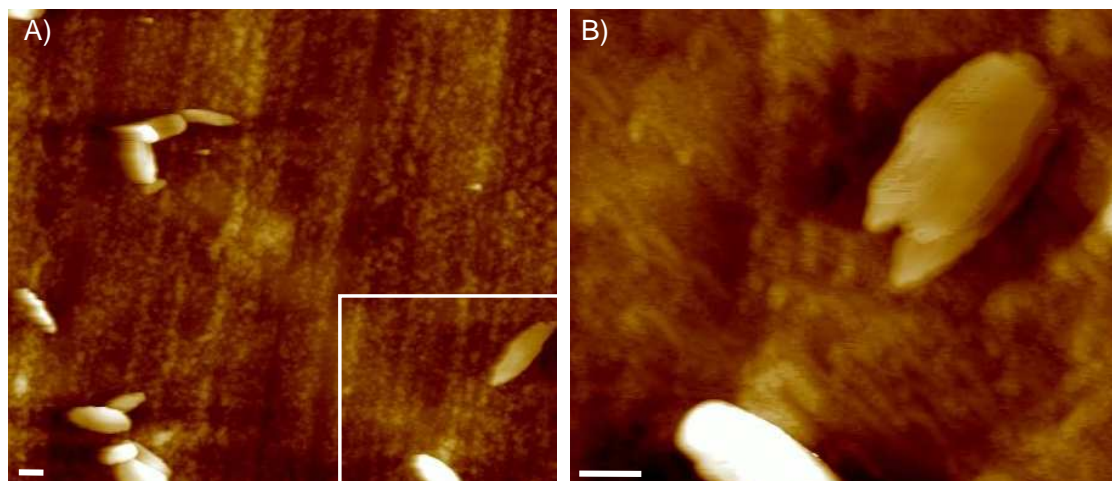
FT-IR spectra of **A) Fmoc-LL**, **B) Fmoc-LG** and **C) Fmoc-GL**.

Appendix E: Fluorescence Spectra of Fmoc-Dipeptides



Fluorescence spectroscopy spectra of **A)** Fmoc-FF, **B)** Fmoc-FG, **C)** Fmoc-GG, **D)** Fmoc-GF, **E)** Fmoc-LL, **F)** Fmoc-LG and **G)** Fmoc-GL. **H)** Excimer maximum intensity at pH 10.5 for the studied Fmoc-dipeptides.

Appendix F: AFM Micrographs of Fmoc-GF



A) AFM height micrograph of Fmoc-FG (10 mmol L^{-1}) at pH 5.6. The sample was prepared following the TEM preparation procedure and imaged using a Veeco Multimode atomic force microscope equipped with a Nanoscope IIIa controller and an 'E' scanner. The uneven surface is due to carbon coating. **B)** Observation at higher magnification of the selected area in A. Scale bars represent 200 nm.

1. Bellamy, L.J., *The infra-red spectra of complex molecules*. 3rd ed. Vol. 1. **1975**, London: Chapman and Hall.
2. Bellamy, L.J., *The infrared spectra of complex molecules: advances in infrared group frequencies*. 2nd ed. Vol. 2. **1980**, London: Chapman and Hall.